SCUOLA DI DOTTORATO
UNIVERSITÀ DEGLI STUDI DI MILANO-BICOCCA

Department of Environmental and Earth Science

PhD program: **Chemical, Geological and Environmental Science** Cycle: **XXXVII**

Curriculum in: **Terrestrial and Marine Environmental Sciences**

INTEGRATION OF GROUND AND REMOTE OBSERVATIONS FOR THE ANALYSIS OF FOREST FUNCTIONALITY AND BIODIVERSITY

Surname: **Savinelli** Name: **Beatrice**

Registration number: 893263

Tutore / Tutor: Dr. Andrea FRANZETTI

Supervisor: Micol ROSSINI, Emilio PADOA-SCHIOPPA

Coordinatore / Coordinator: Marco Giovanni MALUSA'

ACADEMIC YEAR: 2024/2025

Contents

Abstract

Forest ecosystems are increasingly threatened by climate change-related impacts and anthropogenic disturbances, jeopardising their health, biodiversity, and ecosystem functionality. Effective forest monitoring is critical for understanding forest dynamics, guiding conservation strategies, and supporting sustainable management practices. Remote sensing technologies have become essential tools in this context, with satellite and drone-based systems offering unique capabilities for forest assessment. Among these, Sentinel-2 stands out for its high spatial, spectral, and temporal resolution, enabling detailed monitoring of forest dynamics and health. Differently, drones provide high-resolution data at fine spatial scales, allowing for localized studies of forest structure and condition at tree level.

Traditional remote sensing approaches often rely on spectral vegetation indices to derive information related to various aspects of vegetation health status, but these indices lack effectiveness in providing immediate and/or direct evidence of functional and biophysical state of forests. An emerging focus in remote sensing research is the monitoring of plant traits, such as Leaf Area Index (LAI), Canopy Chlorophyll Content (CCC), and Canopy Water Content (CWC). These traits provide a more specific and immediate insights into forest functionality and ecosystem processes, to directly capture the spatio-temporal variation of vegetation structural and physiological characteristics.

By employing advanced remote sensing techniques, this thesis aims to develop and propose innovative remote sensing methods for the effective monitoring of forest functionality and biodiversity.

The analysis can be summarised as follows: (1) reviewing Sentinel-2 time series studies for the quantitative estimation and monitoring of forest stress, synthetising existing methodological approaches, identifying research gaps and suggesting potential improvements (2) developing robust time series analysis methods using daily standardized anomalies of key functional traits to detect and map forest stress distribution, and (3) establishing an integrated multi-sensor drone-based monitoring system for detailed local-scale forest characteristic assessment.

This thesis effectively demonstrated the strength of remote sensing for monitoring forest status over time, providing a scalable, cost-effective alternative to traditional field-based methods, enabling detailed monitoring of forest health and resilience under environmental stressors.

Overall, the results of this thesis identified gaps in existing forest monitoring methodologies and propose innovative solutions to address them. We found that plant traits anomaly serves as a particularly sensitive indicator of drought stress. Moreover, it emerges how species-specific information is critical for accurate forest health assessments.

This work approaches provide new insights into forest ecosystem dynamics, ultimately contributing to improved management practices and conservation strategies.

1. Introduction

Forests are among the most extensive and biodiverse habitats on Earth, covering a wide range of ecosystems, from coastal zones to mountain chains, temperate woodlands and tropical regions. They represent one of the most species-rich habitats globally, hosting an extraordinary variety of flora and fauna (Brockerhoff et al., 2017, Gibson et al., 2011). These ecosystems are fundamental to support life on earth, providing essential ecosystem services such as biomass production, food and water supply, air and water purification, pollination, biodiversity conservation, and the provision of goods crucial for human well-being (Brockerhoff et al., 2017; Krieger et al., 2001). Moreover, forests play a vital role in maintaining global carbon dynamics and regulate climatic and hydrological cycles (Bonan, 2008; Brockerhoff et al., 2017).

Throughout history, human activities have profoundly shaped forest ecosystems, with the rate of change dramatically accelerating in recent times. Deforestation, in particular, has led to a dramatic reduction in global forest cover. Since the beginning of human civilization it is estimated that forest has decreased by approximately one-third from its original extent, from 6 billion to 4 billion hectares (by 2020), half of which was lost during the 20th century alone (FAO, 2020). Nowadays many efforts are in place to stop deforestation, however not only the direct cutting of forests is causing forest loss. Increasing indirect anthropogenic and climate change drivers are profoundly altering trees' physiological processes and health, leading to widespread forest degradation and fragmentation, causing the disruption of the structural and functional integrity of these ecosystems (FAO, 2020; Foley et al., 2007). As a consequence, these changes compromise forests' ability to provide critical ecosystem services, including carbon sequestration, thereby undermining both environmental stability and human well-being (Foley et al., 2007; Chazdon et al., 2008).

Given the critical role that forests play in global dynamics, and the expected rise in future disturbances, there is an urgent need to foster the development of effective technologies and tools for the continuous monitoring of forest status and vigour. Forest monitoring is essential for assessing forest dynamics and conditions, guiding conservation strategies and supporting sustainable management practices to protect these crucial ecosystems (Bustamante et al., 2016).

Traditional methods of forest monitoring relied on field data collection. However, while effective, these are often labour-intensive, time-consuming and costly, limiting their ability to keep pace with the rapid changes occurring in forest ecosystems at a global scale.

Optical remote sensing has emerged as a scalable cost-effective method, offering a practical solution for mapping vegetation parameters and monitoring forest status (Trumbore et al., 2015; Wang and Gamon, 2019). The principle of remote sensing in vegetation monitoring involves using sensors to measure the various wavelengths of electromagnetic radiation reflected or emitted by plants

and their surrounding environment. Each object reflects and absorbs light at distinct wavelengths in a characteristic way, and by analysing these variations, it is possible to characterize the health status of plants and their biophysical properties (Lausch et al., 2016).

Satellite remote sensing is a key tool for forest monitoring due to its wide coverage and consistent data collection capabilities. Among the available technologies, the recently available Sentinel-2 has become increasingly popular due to its intrinsic characteristics, which make it particularly suitable for forest health monitoring. The Sentinel-2 constellation consists of two multispectral satellites: Sentinel-2A, launched in June 2015, and Sentinel-2B, launched in March 2017. Together, they provide an operational capability for delivering high-resolution spatial, spectral, and temporal observations. Sentinel-2 offers imagery with spatial resolutions ranging from 10 to 60 meters across 13 spectral bands, with a revisit time of just 5 days (Drusch et al., 2012). The availability of dense time series multispectral images makes Sentinel-2 data ideal for tracking forest dynamics and health.

In addition to satellites, drones represent as well a valuable tool for forest monitoring, offering high-resolution imagery at finer spatial scales than satellite systems. This enabling detailed assessments of forest structure and health at tree level, being therefore particularly useful for fine-scale localized studies requiring frequent temporal data acquisition (Tang et al., 2015). Furthermore, drones provide significant flexibility through the ability to mount various types of sensors, such as multispectral, hyperspectral, or thermal cameras, facilitating diverse analytical approaches.

Traditionally, spectral vegetation indices have been extensively used to derive information related to various aspects of vegetation health status. Among them, the Normalized Difference Vegetation Index (NDVI) and its derivatives are widely employed due to their effectiveness in assessing productivity and overall plant vigour. While vegetation indices are powerful tools, they predominantly serve as proxies for general vegetation productivity and condition, therefore lacking to directly quantifying the functional and biophysical state of forests (Anderegg et al., 2019; Le et al., 2023). An emerging focus in remote sensing research is the quantification of plant traits, such as Leaf Area Index (LAI), Canopy Chlorophyll Content (CCC), and Canopy Water Content (CWC). The spatio-temporal variation of these traits provides more specific and immediate insights into forest functionality and ecosystem processes, moving beyond greenness metrics to directly capture the structural and physiological characteristics of vegetation (Anderegg et al., 2019; Le et al., 2023; Campos-Taberner et al., 2018).

Remote sensing is increasingly utilized for monitoring forest health, offering the capability to collect large-scale consistent data to track forest dynamics. These technologies provide critical insights into spatial and temporal changes in forest conditions, which are essential for designing effective conservation strategies and targeted forest management plans. Despite its potential, the inherent complexity of remote sensing methodologies presents significant application challenges.

Advancing methodological frameworks in remote sensing is crucial to ensure the consistent acquisition of accurate and reliable data for forest monitoring, that would enable more precise and operational evaluations of forest health, ultimately supporting the development of targeted management plans.

1.1 Objective

The main objective of this thesis is to develop and propose innovative remote sensing methods for the effective monitoring of forest functionality and biodiversity. To achieve this goal, multi-source remote sensing data collected at various temporal and spatial scales have been used. These data were processed and analyzed to extract quantitative information on key plant physiological and functional traits, such as Leaf Area Index (LAI), chlorophyll content, and other relevant metrics. The thesis aims to relate these physiological traits to broader aspects of forest health, including species composition and the impact of environmental factors (e.g. drought). By employing advanced remote sensing techniques, the research seeks to enhance our understanding of how forest ecosystems function and respond to change, ultimately contributing to improved management practices and conservation strategies.

The specific objectives of this research can be summarised as follows:

- to conduct a comprehensive review of Sentinel-2 time series studies for the quantitative estimation and monitoring of forest stress. This systematic review synthesises existing methodological approaches, identifies research gaps, and suggests potential improvements.
- to develop an innovative remote sensing-based methodology to monitor the functional state of forests using the multispectral, high-temporal, and high-spatial resolution imagery provided by Sentinel-2 satellite. To do so we retrieved and validated time series of LAI, CCC and CWC from Sentinel-2 (2017-2022) and analysed them to identify drought-induced anomalies in plant traits and relate these anomalies to species ecology and local environmental conditions.
- to evaluate how drones can enhance forest monitoring by implementing a methodology for retrieving plant functional traits at the individual tree level. This approach integrates LiDAR and multispectral data to provide detailed, high-resolution insights into forest structure, species composition, and ultimately plant status.

1.2 Thesis outline

This Ph.D. thesis is structured in four main sections. It begins with a general introduction, which provides an overview of the research objectives and the broader context of the study. The second

section consists of a comprehensive review summarizing the state of the art in forest monitoring using Sentinel-2 remote sensing technologies. This review presents the current methodologies, identifies existing gaps, and outlines potential advancements in the field.

The third section is composed of two chapters, each corresponding to a scientific paper. Each chapter includes its own introduction, materials and methods, results, discussion, conclusions, and references, presenting the findings in a detailed and structured manner. These chapters focus on proposing two methods for monitoring forest status at two different spatial scales. The first investigates the potential to identify drought anomalies in a temperate mixed forest by deriving high temporal resolution time series of forest traits, focusing on their relationship with forest type and environmental factors. The second scientific paper proposes a workflow for collecting information on forest structure and species composition integrating drone-based LiDAR and multispectral data for cost-effective and accurate monitoring of forest health and change detection.

Finally, the thesis concludes with a comprehensive summary, highlighting the key findings, their implications for forest monitoring, and outlining potential directions for future research. The analyses presented throughout the thesis are based on data collected during intensive field campaigns, providing a solid foundation for the proposed methodologies and their resulting outcomes.

2. Forest stress detection using optical time series from Sentinel-2 images: Systematic literature review

2.1 Introduction

The increasing frequency and intensity of climate change-related disturbances, such as drought and biotic attacks, and anthropogenic disturbances pose significant threats to forest ecosystems globally. These stressors can lead to a decline in forest health, impairing ecosystem functionality and biodiversity. Therefore, it is of primary importance to detect forest stress in order to act before this leads to tree death.

Traditional field surveys, while valuable, are often costly and time-consuming, and can be logistically challenging, especially in remote areas (Dash et al., 2018). This has led to the increasing reliance on remote sensing technologies, which offer a cost-effective solution for assessing and monitoring forest health at large-scale landscapes.

The launch of the Sentinel-2 satellite constellation in 2015 and 2017 marked a significant advancement in this field, providing high-resolution optical imagery that enables the monitoring of forest stress at unprecedented temporal and spatial scales (Trubin et al., 2023; Zhang et al., 2015). Sentinel-2 is equipped with the MultiSpectral Instrument (MSI) that captures data across 13 spectral bands, including visible, near-infrared, and shortwave infrared wavelengths, at varying spatial resolutions of 10, 20, and 60 meters. It has a revisiting period of five days at the equator, making it particularly suitable for monitoring dynamic environmental changes (Hüttnerová et al., 2023; Siirtola & Röning, 2020). Previous studies have demonstrated the effectiveness of remote sensing indices, such as the Normalized Difference Vegetation Index (NDVI), in detecting physiological changes in vegetation associated with water stress and other environmental factors (He et al., 2016). These indices can provide critical insights into plant health, enabling early detection of stress responses that may precede visible decline (Morris et al., 2016; Bell et al., 2018).

Despite the benefits provided by Sentinel-2, its use in monitoring forest stress is still relatively limited when compared to other satellite systems, mainly due to its recent introduction (Xu et al., 2018; Watt et al., 2016). However, the potential for continuous large-scale observation and analysis of forest health is great, especially as the availability of imagery increases, enabling more effective anomaly detection and trend analysis (Grabska et al., 2020; Ding et al., 2023). This review aims to synthesize existing literature on the application of Sentinel-2 imagery for detecting forest stress, focusing on its ability to capture drought-induced changes in plant physiology, biochemistry, and structure over time. By examining the current state of research, we aim to highlight the opportunities and challenges associated with using Sentinel-2 time series for monitoring forest stress.

2.2 Systematic literature review

2.2.1 Identification of relevant literature

In this section, we present the findings of a systematic literature review aimed at providing an overview of how the recently launched S2 satellite has been employed to generate high-resolution time-series imagery for detecting and monitoring changes in tree spectral characteristics associated with forest stress symptoms and vitality decline. Relevant peer-reviewed articles were identified through the Web of Science catalogue (www.webofscience.com). The topic field search was constructed as follows: “Sentinel-2 AND ("time series" OR "time-series") AND (stress OR disturbance OR health) AND forest”. This search yielded a total of 123 publications. The records were screened to include only relevant research articles, excluding reviews.

The inclusion criteria were as follows:

1. studies had to explicitly utilise S2 data for forest monitoring;
2. multiple S2 observations must be employed, enabling time-series analysis of forest spectral characteristic;
3. the research must focus on detecting and monitoring forest stress and status decline over time.

Publications referencing "random forest" algorithms without relevance to forest health were excluded. Additionally, studies emphasizing land cover changes or forest dieback, rather than the detection of forest stress, were not considered. Indeed, the objective of this review is to explore how S2 time-series imagery has been applied to identify pre-mortem spectral indicators of forest stress and vitality declines. Studies that incorporated complementary datasets, such as MODIS and Landsat, alongside S2 data were also included in this review (however the primary source of data must be S2). After applying these rigorous criteria, a substantial number of articles were excluded, resulting in a final selection of 25 studies that met all requirements.

Table 1. Summary of the main characteristics of the included studies: when a study considered more than 10 variables, only the best-performing variables were reported in the table. The studies are categorized based on their methodology.

Author (year)	Forest type/ tree species	Study area location	Period of analysis	N° of S2 images	Target Variables	Stress type	Methodology	Spectral range
Arthur et al. (2024)	Norway spruce forest	Belgium and France	2016-2023	245	SWIRcr	Bark beetle	Anomaly/ change detection	NIR/SWIR
Gomez et al. (2020)	Pine forests	Florida	2015-2019	/	NDVI	Bark beetle	Anomaly/ change detection	Red/NIR
Hislop et al. (2023)	Eucalyptus forest	Australia	2016-2022	/	NBR	Drought and fire	Anomaly/ change detection	NIR/SWIR
Jamali et al. (2024)	Hemi-boreal forest (Scots pine and Norway spruce)	Sweden	2017-2018	113	NDVI, NDWI, NDRS, CCI	Bark beetle	Anomaly/ change detection	Green/Red/NIR/SWIR
Lange et al. (2024)	Norway spruce, Scots pine, European beech and Pedunculate oak	Germany	2016-2022	67	FCA	Forest disturbance	Anomaly/ change detection	Red edge/NIR/SWIR
Low et al. (2020)	Deciduous and coniferous forests	Austria	2017-2019	225	NDVI, GNDVI, RGVI	Forest disturbance	Anomaly/ change detection	Visible/NIR
Marinelli et al. (2023)	Norway spruce forest	Italy	2018-2022	857	NDVI, MSAVI2, NBR, NDRE	Forest disturbance	Anomaly/ change detection	Red/NIR/SWIR

Author (year)	Forest type/ tree species	Study area location	Period of analysis	N° of S2 images	Target Variables	Stress type	Methodology	Spectral range
Müller et al. (2024)	Deciduous and coniferous forest	Sweden	2015-2022	/	NMDI, CIR, PPI	Drought and fire	Anomaly/ change detection	Red/Red-edge/NIR SWIR
Reinosch et al. (2024)	Deciduous and coniferous forest	Germany	2018-2022	13,282	3 spectral bands	Forest disturbance	Anomaly/ change detection	Green/Red/NIR
Bárta et al. (2021)	Norway spruce	Czech Republic	2018	14	9 spectral bands and 6 VIs: NDVI 550/650, NDVI 800/650, NDVI 819/1649, REIP, TCG, TCW	Bark beetle	Machine learning	Visible/Red-edge/NIR SWIR
Brun et al. (2020)	Mix broadleaves and conifeorus	Central Europe	2018-2019	87	NDVI	Drought	Machine learning	Red/NIR
Candotti et al. (2022)	Norway spruce	Italy, Austria, and Slovenia	2017–2020	15	Single Bands and 10 VIs, best performing: NDWI, TCW, NMDI, DWSI	Bark beetle and wind damage detection	Machine learning	Visible/NIR/SWIR Red-edge
Guzman et al. (2023)	Oak	USA	2017-2022	/	Phenological metrics derived from CCI	Wilt deseas	Machine learning	Green/Red
König et al. (2023)	Bohemian Forest Ecosystem,	Czech Republic	2016-2019	662	21 VIs, best performing: CRE, ND1	Bark beetle	Machine learning	Visible/Red-edge/NIR SWIR
Mantas et al. (2022)	Maritime Pine	Portugal	2017- 2020	8	37 VIs, best performing: NDWI, DWSI, NMDI, NDRS	Pine wilt deseas	Machine learning	Red/Green/NIR/SWIR

Author (year)	Forest type/ tree species	Study area location	Period of analysis	N° of S2 images	Target Variables	Stress type	Methodology	Spectral range
Schiller et al. (2024)	Broadleaved and coniferous forests	Germany and Luxembourg	2016–2018	/	10 bands - 10 Vis: CRSWIR, TCD, NDVI, NDMI, NDWI, TCW, NBR, NDMI, MSI, NDRE	Forest disturbance	Machine learning	Visible/Red-edge/NIR /SWIR
Barka et al. (2018)	Norway spruce and beech deciduous	Czech Republic and Slovakia	2015- 2017	/	LAI derived from NDII and TWC, REIP	Forest disturbance	Trend analysis	NIR/SWIR
Binh et al. (2024)	Mangroves	Southern Vietnam	2019–2023	> 300	LAI, Cab, Cw, Cm	Forest disturbance	Trend analysis	Visible/Red-edge/NIR SWIR
De Petris et al. (2021)	Broadleaves with predomnance of pedunculate oak	Italy	2016-2019	221	nVVI	Forest disturbance	Trend analysis	Red/NIR
Descals et al. (2023)	Deciduous forests	Europe	2017–2021	/	NDVI	Drought	Trend analysis	Red/NIR
Mandl and Lang, (2023)	Coniferous forest	Germany	2020	10	DSWI, NDWI, NDMI, TCW, NGRDI, NDRE-3, NDI45, TCG	Bark beetle	Trend analysis	Visible/Red-edge/NIR SWIR
Lastovicka et al. (2020)	Coniferous forest	Slovakia and Czechia	2017-2019	180	NDVI, NDMI, TCG, TCW	Bark beetle	Trend analysis	Visible/NIR/SWIR
Navarro et al. (2019)	Cork oak forest	Portugal	2017-2018	30	NDVI, NDWI, GNDVI, CI, VCI	Forest disturbance	Trend analysis	Visible/Red-edge/NIRSWIR/

Author (year)	Forest type/ tree species	Study area location	Period of analysis	N° of S2 images	Target Variables	Stress type	Methodology	Spectral range
Puletti et al. (2019)	Mediterranean forest tree (broadleaves and coniferous)	Italy	2016-2018	30	NDVI - RENDVI - SRI	Drought	Trend analysis	Visible/Red-edge/NIR
Raza et al. (2024)	Mangroves	Pakistan	2016-2023	8,655	NDVI	Forest disturbance	Trend analysis	Red/NIR

Vegetation index abbreviation: **SWIRcr** = Short wave infrared Continuum Removal vegetation index, **NDVI** = Normalized Difference Vegetation Index, **NBR** = Normalized Burn Ratio index, **NDWI** = Normalized difference water index, **NDRS** = Normalized Distance Red and SWIR, **CCI** = Chlorophyll Carotenoid Index, **FCA** = Forest Condition Anomaly Index, **GNDVI** = Green-NDVI, **RGVI** = Red-Green Vegetation Index, **MSAVI2** = modified soil adjusted vegetation index 2, **NDRE =** normalized difference red edge, **NMDI =** normalized multiband drought index, **CIR =** chlorophyll index red-edge, **PPI** = plant phenology index, **REIP** = Red-edge inflection point, **TCG** = tasseled cap greenness, **TCW** = tasseled cap wetness, **DWSI** = Disease Water Stress Index, **CCI** = Chlorophyll/Carotenoid Index, **CRE =** Chlorophyll Red Edge Index, **ND1** = Normalized Difference Red Edge Index 1, **CRSWIR** = Continuum Removal Shortwave Infrared, **TCD** = Tasselled-Cap Disturbance, **NDMI =** Normalized Difference Moisture Index, **MSI** = Moisture Stress Index, **LAI** = Leaf Area Index, **NDII** = Normalized Difference Infrared Index, **REIP** = Red Edge Inflection Point , **Cab** = Leaf Chlorophyll Content, **Cw** = Leaf Water Thickness, **Cm** = Leaf Dry Matter, **nVVI** = Normalized Vegetation Vigour Index, **NGRDI =** Normalized Difference Green Red Index, **NDRE-3** = Normalized Difference Red-Edge-3 index, **NDI45** = Normalized Difference Index Bands ⅘, **CI** = red-edge chlorophyll indices, **VCI** = vegetation condition index, **RENDVI =** red edge NDVI, **SRI** = simple ratio index

2.2.2 Publication date and Journal

The 25 studies analysed in this review were published between 2018 and 2024, with a notable increase in publications starting in 2023 and peaking in 2024 with eight studies. This upward trend highlights the growing research interest and adoption of Sentinel-2 data for forest stress monitoring. The increment can be attributed to the increasing availability of Sentinel-2 datasets following the launch of Sentinel-2A in 2015 and Sentinel-2B in 2016, coupled with significant advances in automated data processing techniques and methodologies for analysing Sentinel-2 imagery.

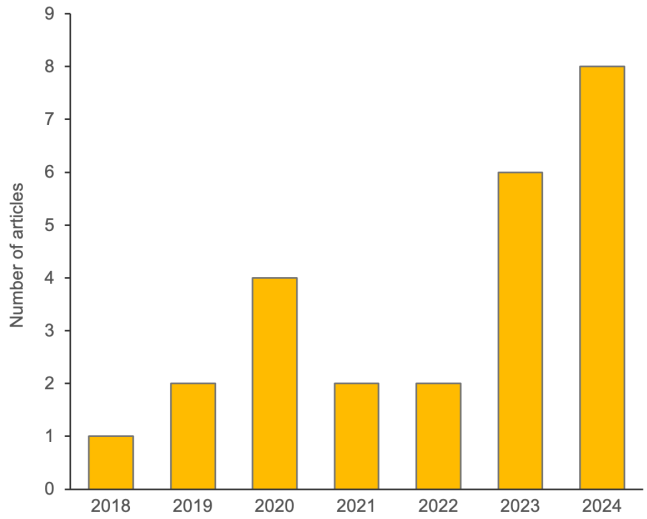

Figure 1. Number of articles published per year

The most common journals publishing papers were: (i) "*Remote Sensing*", with 5 papers and (ii) "*Remote Sensing of Environment*" with 4 papers. Of the remaining 17 publications, 9 appeared in other applied Earth observation and remote sensing journals, 4 in different forestry journals, and 1 each in "*Global change biology*", "*Environmental Monitoring and Assessment*" and "*Frontiers in Environmental Science*".

2.2.3 Location of the study area

Most of the studies (19) were conducted in Europe, with a particular focus on Central Europe (12 articles), primarily analysing coniferous forests dominated by Norway spruce (*Picea abies*). Five studies were located in Southern Europe, including two in Portugal: Mantas et al. (2022) focused on maritime pine (*Pinus pinaster*), while Navarro et al. (2019) analysed cork oak (*Quercus suber*). Three studies were based in Italy, where De Petris et al. (2021) examined mixed mountain forests, Marinelli et al. (2023) studied coniferous forests, and Puletti et al. (2019) investigated Mediterranean forests. In Northern Europe, two studies focused on forests in Sweden. Jamali et al. (2024) analysed hemi-

boreal forests of Scots pine (*Pinus sylvestris*) and Norway spruce, while Müller et al. (2024) studied a mixed forest of pine and broadleaf species. Descals et al. (2023) examined different deciduous and mixed forest in different european locations (specifically deciduous and mixed in Brun et al., 2020). Outside Europe, two studies were conducted in Asia, including one in Vietnam (Binh et al., 2024) and one in Pakistan (Raza at al., 2024), both analyzing mangrove forests. Additionally, one study in Australia (Hislop et al., 2023) focused on eucalyptus forests, and two studies in the USA explored oak (Guzman et al., 2023) and pine forests (Gomez et al., 2020).

2.2.4 Number of S2 images analysed and inter or intra annual time series

Not all studies explicitly reported the number of S2 images analysed (i,e. Barka et al., 2018; Descals et al., 2023; Hislop et al., 2023; Müller et al., 2024; and Schiller et al., 2024). However, these studies employed multi-year S2 observations, ensuring that comprehensive time-series analyses were conducted, despite the lack of specific image counts.

For studies that specified the number of Sentinel-2 images analysed, the range varied significantly, from 8 images (Mantas et al., 2022) to 13,282 images (Reinosch et al., 2024). We chose not to exclude any articles based on the number of images analysed, as setting a minimum threshold for time-series observations would be arbitrary. Additionally, given the already limited number of studies meeting our criteria, we prioritized inclusivity to ensure a comprehensive review. The majority of studies included in this review adopted a multi-year approach to stress analysis, enabling a more comprehensive understanding of temporal dynamics and interannual variability in forest health. However, two studies focused on forest stress within a single vegetative season. Specifically, Barta et al. (2021) utilised 14 Sentinel-2 images from April and November 2018, while Mandl et al. (2023) analysed 10 Sentinel-2 images from March to October 2020. Both studies focused on detecting early signs of bark beetle infestation, intentionally limiting their analyses to one vegetative season to refine their methodologies.

2.2.5 Application of S2 time series for forest stress monitoring

The 25 articles reviewed have been grouped based on the core methodology they used to detect forest stress from S2 time series images. Three main categories have been identified:

- Trend analysis
- Anomaly/change detection
- Machine learning

In the following section, the approaches used in the various studies are discussed in detail.

The trend analysis category included all articles that primarily focused on analyzing time series of different vegetation indices (hereafter VIs) for detecting trends related to changes in forest health and vigour. Nine of the 25 articles in this review fall into this category: Barka et al., (2018), Navarro et al. (2019), Puletti et al. (2019), Lastovicka et al. (2020), De Petris et al. (2021), Descal et al. (2023), Mandl and Lang (2023), Binh et al. (2024) and Raza et al. (2024)

Raza et al. (2024) analyzed NDVI time series from S2 images to study the spatial and temporal evolution of mangrove health decline in Pakistan. Their key innovation was using pixel-based nonparametric Sen's slope estimation on mangrove NDVI rasters, combined with the Mann-Kendall trend test to assess the significance of trends in mangrove health.

Navarro et al. (2019) introduced the use of cumulative distribution functions to determine optimal thresholds for stress detection. Moreover, the authors implemented the Vegetation Condition Index (VCI) which is a pixel-wise normalization of NDVI against historical patterns, that account for potential natural variability in vegetation indices due to factors such as seasonality and climate, and therefore enabling a more robust discrimination between healthy and stressed trees. Similarly, De Petris et al. (2021) proposed the Normalized Vegetation Vigour Index (nVVI) which transforms standard NDVI measurements into a trend analysis tool by incorporating phenological metrics and multi-year patterns. This allowed it to process NDVI data through several steps including seasonal integration and trend analysis, providing a way to assess tree vigour decline over time rather than relying on direct comparisons of NDVI or other vegetation indices.

Mandl and Lang (2023) take a step further by verifying the spectral trajectories of VIs derived from Sentinel-2 data. The authors identify “candidate pixels” using SIAM™ (Satellite Image Automatic Mapper) software which performs semantic enrichment of Sentinel-2 satellite data. This creates a pre-selection/pre-classification of pixels that show spectral changes consistent with potential bark beetle infestation. Therefore, only pixels that are both identified as potential candidates and show appropriate VIs change values are classified as infested. This approach demonstrated higher accuracy and a reduction in false positives compared to analyses that used only VIs. This was explained by the fact that the pre-selection step captures not only subtle spectral variations, but also changes in canopy biophysical and biochemical properties during infestation, as the semantic process considers a wider range of spectral bands (Blue, Green, Red, NIR, SWIR), unlike traditional VIs that typically consider fewer bands simultaneously.

Finally, only two studies focused on analysing the long-term trends of plant traits for detecting forest stress, instead of using the more traditional VIs. Barka et al. (2018) developed a method to assess forest health using Sentinel-2 satellite data, focusing on LAI mapping. This study analysed the

changes in the spatio-temporal patterns of LAI using an empirical approach based on VIs including the Normalized Difference Infrared Index (NDII), Disturbance Index, and, in particular, the Wetness component of Tasseled Cap transformation (TWC). The analysis, conducted over the period from 2016 to 2018, aimed to assess forest health. Binh et al. (2024) investigated the quantitative estimation of mangrove functional traits in southern Vietnam using Sentinel-2 time series. Unlike Barka et al. (2018), the study directly estimated from S2 images plant traits by combining the PROSAIL leaf-to-canopy radiative transfer model with Gaussian Processes Regression (GPR). Key plant traits such as the Effective Leaf Area Index (LAI), Leaf Chlorophyll Content (Cab), Leaf Water Thickness (Cw), and Leaf Dry Matter (Cm) were estimated. LAI and Cab showed higher retrieval accuracy compared to Cw and Cm. The resulting maps highlighted seasonal variations and long-term trends in mangrove health.

Another key approach identified in the analyzed articles is the change/anomaly detection methodology. This approach detects deviations or outlier patterns in forest vitality by comparing spectral index values from specific periods (when a stress event occurred) with a reference baseline that represents healthy forest conditions. Anomalies are typically defined using specific thresholds. The following 10 studies adopted anomaly/change detection as a core methodology for detecting forest stress using Sentinel-2 (S2) time series images: Gomez et al. (2020), Low et al. (2020), Hislop et al. (2023), Mandl and Lang (2023), Marinelli et al. (2023), Arthur et al. (2024), Lange et al. (2024), Jamali et al. (2024) and Müller et al. (2024).

For instance, Gómez et al. (2020) applied this approach to detect bark beetle infestations in 2019 by comparing monthly NDVI values from the affected year with a baseline derived from NDVI data from 2015–2018. Similarly, Hislop et al. (2023) applied the Normalized Burn Ratio (NBR) to detect canopy damage caused by drought and fire. They established a monthly baseline NBR period (2016–2018) for each pixel and converted NBR values to z-scores relative to this baseline. Pixels with z-scores below defined thresholds were flagged as "disturbed," indicating anomalous conditions.
Müller et al. (2024) also investigated drought-induced health decline in forests using a similar approach, but focused on daily time series of observations through the application of the Phenofit r package that applies interpolation techniques to evaluate values for missing days. The authors calculated a three-day moving average for the reference period (2015-2017) from different vegetation indexes, including the best performing normalized Multiband Drought Index (NMDI). Subsequently, they calculated the percentage difference between the drought period (2018) and the reference period value, and established a minimum absolute change threshold of 0.1% between consecutive days to indicate the early detection of drought stress.

Arthur et al. (2024) used a specialized vegetation index called SWIR Continuum Removal vegetation index (SWIRcr), which combines three S2 bands, one near-infrared and two shortwave infrared bands, to detect early signs of bark beetle stress in trees. Their methodology involved modeling healthy forest behavior based on S2 data from 2016-2017 using harmonic functions, and identifying potential infestations when observations exceeded 1.7 times the normal threshold across two consecutive measurements. Lange et al. (2024), differently from the previous work, developed a method to account for species-specific responses to stress, while mitigating the influence of inter-annual climatic variations through phenology correction. They introduced the Forest Condition Anomaly (FCA) index, which detects forest stress across Germany from 2016 to 2022 by analyzing deviations from expected spectral patterns. The method establishes reference conditions using percentile-based statistics of reflectance values derived from Sentinel-2 bands sensitive to chlorophyll content (band 5, 705 nm), leaf structure (band 8a, 865 nm), and water content (band 11, 1610 nm). To incorporate phenological variations, they adjust reference time series using green-up and senescence dates extracted from NDVI data, ensuring that inter-annual variations in vegetation timing are not misinterpreted as stress signals. Stress detection involves quantifying deviations from these references, which are then combined into the FCA index using a weighted principal component analysis. A threshold of FCA = -0.15 was set to identify stress, with increasingly negative values indicating higher stress or disturbance levels.

Jamali et al. (2024), introduces an innovative approach to detecting European spruce bark beetle infestations, different from traditional pixel-based methods. The research implements a novel kernel-based methodology that analyses 3×3 pixel clusters using four different vegetation indices derived from Sentinel-2 satellite imagery, with NDVI emerging as the most reliable indicator. Time-series of the coefficient of variation (CV) were calculated and fed to a change detection algorithm called Detecting Breakpoints and Estimating Segments in Trend (DBEST) that allowed them to identify significant changes in forest health over time.

In the context of this review, 7 studies were identified that employed machine learning techniques as their core methodology to detect forest areas affected by disturbances. These predominantly relied on pixel-based classification approaches to distinguish between healthy and stressed regions using machine learning models. The works grouped in this category include: Guzmán et al. (2023), Konigh et al. (2023), Bárta et al. (2021), Brun et al. (2020), Candotti et al. (2022), Mantas et al. (2022) and Schiller et al. (2024).

Brun et al. (2020) and Barta et al. (2021) employed similar straightforward approaches for identifying forest stress and disturbance using Random Forest classification. Both works developed robust classification models through extensive manual selection of training pixels with Brun et al.

(2020) labeling over 300,000 pixels and Barta et al. (2021) labeling 95,000 pixels, representing disturbed and healthy areas.

Brun et al. (2020) focused on NDVI-based detection, incorporating ten time-series statistics as predictors, including averages, extrema, change points, and temporal trends, achieving an overall accuracy of 90% in distinguishing between healthy and stressed forests. Barta et al. (2021) tested a broader range of inputs, analyzing nine spectral bands and six VIs derived from Sentinel-2 data. Tasselled Cap Wetness (TCW) index and VIs incorporating red, SWIR and Red-edge spectral bands proved to be the most sensitive in detecting progressing infestation. Similarly, Canedotti et al. (2022) investigated ten different indices and confirmed the effectiveness of TCW, together with indices incorporating the SWIR and Red-edge regions, achieving high accuracy in distinguishing stressed forests, bark beetle-infested stands, and areas affected by windthrow damage. Also König et al. (2023) highlighted the superior performance of indices incorporating Sentinel-2 red-edge bands, particularly the Chlorophyll Red Edge Index (CRE) and the Normalized Difference Red Edge Index 1 (ND1), which were most effective in distinguishing healthy from infested forest plots. Schiller et al. (2024) used transformer-based deep learning models to detect forest disturbances from Sentinel-2 time series data. The model that used only satellite bands outperformed the others, detecting disturbances as small as 40m² within 100m² pixels. The models were validated through spatial block cross-validation across different regions.

2.2.6 Conclusion

The systematic literature review, which spans from 2018 to 2024, highlights the increasing use of Sentinel-2 data for forest stress monitoring, particularly in Europe. The research predominantly focuses on coniferous forests, especially those dominated by Norway spruce. Three primary methodologies for detecting forest stress using Sentinel-2 time series imagery are identified: trend analysis, anomaly/change detection, and machine learning.

Trend analysis involves evaluating temporal changes in forest health by analysing time series of vegetation indices (VIs). Studies using this method have employed techniques like Sen's slope estimation and Mann-Kendall trend test, cumulative distribution functions for threshold determination, and normalized indices like VCI and nVVI to account for natural variability. Advanced approaches involve integrating spectral trajectories of VIs with semantic enrichment of satellite data, leading to higher accuracy in stress detection. Moreover, some studies have shifted from traditional VIs to directly estimating plant traits like LAI, Cab, Cw, and Cm from Sentinel-2 images using radiative transfer models and Gaussian Processes Regression.

Anomaly/change detection identifies deviations in forest vitality by comparing spectral index values from stress events to a baseline representing healthy conditions. Studies using this approach establish baselines and employ techniques like z-scores, percentage difference calculations, and specialized VIs like SWIRcr and FCA to detect anomalies. Some researchers have incorporated daily time series using interpolation techniques to enable early detection of stress. Innovative methods also include kernel-based analysis of pixel clusters and change detection algorithms like DBEST to identify shifts in forest health.

Machine learning techniques, primarily pixel-based classification, distinguish between healthy and stressed forest areas. The studies have identified used typically Random Forest classification, or more advanced deep learning algorithms, and tested different spectral bands and VIs derived from Sentinel-2 data for achieving the best possible performances for spotting stressed forest plots.

Trend analysis has emerged as a valuable methodological approach for identifying patterns of stress and vigour decline. Its primary advantages include ease of application and the absence of requirements for complex computational methods or advanced modelling processes. This approach is particularly effective in detecting severe processes with substantial impacts. However, its main limitation is the potential to overlook subtle stress signatures that might be missed when relying solely on trend tracking.

By contrast, anomaly detection offers the potential to appreciate more subtle patterns of change by analysing deviations from normal spectral patterns, allowing for the identification of early signs of forest stress before clear declining trends appear. This is particularly valuable for detecting insect infestations or disease outbreaks where early intervention is crucial. Moreover, anomaly analysis can account for natural seasonal variations in spectral signatures, distinguishing between normal phenological changes and changes related to stress conditions. Additionally, anomaly detection enables the setting of specific numerical or spectral thresholds to define stress levels. These thresholds act as markers or boundaries that help categorize the severity of the stress, providing an objective analysis rather than relying on subjective observations. However, in the context of Sentinel-2 data analysis, this comes with some limitations as the baseline of “normal condition” can be constructed only from 2016, as there are no S2 images available before this date. This weakens the reliability of the baseline condition for comparison, as historical data are missing, therefore potentially leading to a misinterpretation of the amplitude of change.

Concerning classification methodologies, although they can accurately detect forest stress, they often require complex computational processes and advanced modelling techniques. Moreover, these methods rely on prior knowledge of areas affected and unaffected by stress conditions to define a training dataset for effectively training the classification algorithms. Acquiring such training data

typically involves extensive and resource-intensive field campaigns, which may not always be feasible. In contrast, anomaly detection and trend analysis do not require specific model training, offering a more practical and accessible solution for stress identification, particularly when field data are limited or unavailable.

3. Monitoring functional traits of complex temperate forests using Sentinel-2 data during a severe drought period

Abstract

[1] Forest ecosystems are crucial for preserving biodiversity and providing ecosystem services. The Ticino Park is a temperate mixed forest, one of the few natural ecosystems in northern Italy, which is facing increasing natural and anthropogenic disturbances exacerbated by climate change. Remote sensing is a cost-effective tool for the indirect estimation of forest status. However, it has typically relied on indirect proxies that often have coarse spatio-temporal resolution. This study investigates the possibility of deriving high temporal resolution time series of forest traits to identify drought-induced anomalies and relate them to differences in forest type and environmental factors. Sentinel-2 images from 2017 to 2022 were analysed, with 2022 being characterised by a severe drought. Leaf area index (LAI), canopy chlorophyll content (CCC), and canopy water content (CWC) were retrieved from Sentinel-2 time series through the S2 Toolbox and validated using measurements collected during an intensive field campaign in 2022. A positive and statistically significant correlation was found for all traits. The best results were obtained for LAI (R^2 = 0.75, nRMSE = 11.49%) and CCC (R^2 = 0.82, nRMSE = 13.56%), while slightly worse results were obtained for CWC (R^2=0.64, nRMSE=8.84%). The accurate retrieval of LAI, CCC and CWC enabled the analysis of the temporal and spatial variations of the daily standardised anomalies (DSA). CCC reached the most negative DSA values, highlighting its higher sensitivity in detecting the effects of water shortage compared to CWC and LAI. The statistical analysis showed that DSA was linked to forest types. Pine and black cherry exhibited the highest stress response, while hygrophilic black alder and chestnut were the least impacted. These results highlight the species-specific responses to drought and the importance of incorporating species information in forest monitoring. The developed methodology provides a cost-effective approach for monitoring forest status and supporting effective management strategies.

---

1 The content of this chapter has been published in Science of the Total Environment as Savinelli, B., Panigada, C., Tagliabue, G., Vignali, L., Gentili, R., Fassnacht, F. E., Padoa-Schioppa, E., Rossini, M. (2024). Monitoring functional traits of complex temperate forests using Sentinel-2 data during a severe drought period. Science of the Total Environment, 957, 177428

3.1 Introduction

To date, the Earth's global average temperature has risen by approximately 1.5°C above pre-industrial levels, with projections estimating a further global increase of 1.5 to > 4°C by the end of the century (IPCC, 2023). Human activities, particularly the emission of greenhouse gases, are the main driver of climate change, which is leading to a significant increase in both the frequency and severity of extreme weather events, such as summer heatwaves and droughts (IPCC, 2023; Grillakis et al., 2019).

Drought is a complex climatic condition characterised by low precipitation and high temperatures, with potentially detrimental effects on forests, which can result in tree mortality and thus changes in composition and structure (Allen et al., 2010; Vitasse et al., 2019; Kannenberg et al., 2020). In 2022, Western Europe and the Mediterranean region experienced an unprecedented severe and prolonged drought, with major socio-ecological impacts (Faranda et al., 2023). Record-breaking negative values of the Standardised Precipitation Evapotranspiration Index (SPEI) were recorded, indicating a persistent low water availability, which also affected the forests in the region. Water deficit in forests can alter plant physiological processes and growth, and in the most severe cases lead to widespread tree mortality as a result of water stress (Adams et al., 2017). In order to implement effective forest management plans and increase the resilience of forests, it is crucial to enhance our ability to detect and track the effects of water stress on forest ecosystems to better understand how different forest types and species react to water stress. However, collecting related data is challenging, particularly in view of the expected exponential increase of extreme weather events across extensive areas which are hard to monitor in a timely fashion using field data only.

Remote sensing is widely recognised as a cost-effective tool for monitoring forest vitality (Trumbore et al., 2015; Wang and Gamon, 2019). It provides temporally and spatially continuous data, allowing the estimation and mapping of vegetation properties and vigour at different spatio-temporal scales. Recent studies have demonstrated the potential of remote sensing to assess the functional condition, diversity and vulnerability of vegetation ecosystems (Brodrick and Asner, 2017; Rodríguez-González et al., 2017; Chen et al., 2022, Le et al., 2023). However, the majority of remote sensing studies have primarily focused on detecting tree mortality caused by extreme disturbance events, such as pest outbreaks and wildfires (e.g., Lausch et al., 2013; Rodman et al., 2021). Conversely, detecting signs of vegetation health decline due to drought stress has been less successful, typically relying on indirect proxies that often have coarse spatial and temporal resolution (Brun et al., 2020).

The Normalized Difference Vegetation Index (NDVI), Enhanced Vegetation Index (EVI) and similar vegetation indices are commonly used to estimate vegetation vitality. However, these indices

have limitations when it comes to early detection or monitoring of the progression of water stress in plants (Le et al., 2023). In fact, vegetation indices typically do not directly measure physiological changes in plants, but instead assess variations in tree greenness as a proxy for vegetation condition, which lacks immediate and/or direct detection of water-stress symptoms (Anderegg et al., 2019; Le et al., 2023).

One approach to improve the detection of plant water stress from remote sensing is to focus on direct and continuous monitoring of functional traits related to tree physiological status and structure, in order to gain a comprehensive understanding of changes in forest ecosystem functioning over time.

Leaf area index (LAI), canopy chlorophyll content (CCC) and canopy water content (CWC) are key indicators of plant health and physiological processes (Panigada et al., 2010; Wang et al., 2019; Darvishzadeh et al., 2019; Campos-Taberner et al., 2018). Leaf area index (LAI), defined as single-sided leaf area per ground-area, describes the geometric structure of plant canopies; short-term reductions of LAI can be an indicator of stress coping mechanism of trees which may shed a part of their leaves to optimise water use and reduce transpiration. However, prolonged defoliation may indicate the onset of tree mortality as a consequence of carbon deficit (McDowell et al., 2008; Galiano et al., 2011; Pollastrini et al., 2019). CCC (leaf chlorophyll content per LAI) measures the total canopy chlorophyll content. Its decrease is indicative of chlorophyll degradation, which may signal stress-related physiological processes like chlorosis, often preceding tree mortality (Jiang et al., 2020; Pontius et al., 2020). CWC (leaf water content per LAI) is defined as the total amount of water in the canopy foliage. It is an indicator of the tree physiological condition as it supports crucial plant functions such as light absorption and growth (Metcalfe et al., 2008), and can therefore be an indicator of drought effects on vegetation (Asner et al., 2016; Brodrick et al., 2019; García-Haro et al., 2020). LAI, CCC and CWC can all be estimated using multispectral satellite data such as those collected by the Sentinel-2 constellation.

Sentinel-2 consists of two twin satellites, Sentinel-2A (S2A) and Sentinel-2B (S2B), launched on 23 June 2015 and 7 March 2017, respectively. Both are equipped with identical sensors detecting 13 spectral bands, covering the visible, near-infrared (NIR), and short-wave infrared (SWIR), with a spatial resolution ranging from 10 to 60 m. The global revisiting time of less than five days and the swath width of 290 km ensure frequent and extensive coverage, making Sentinel-2 particularly useful for time series analysis and forest monitoring (Drusch et al., 2012). The ability to retrieve dense image time series allows for detailed tracking of vegetation state changes over time, facilitating effective and accurate monitoring of forest ecosystem health.

The open-source Sentinel Application Platform (SNAP) software includes a biophysical processor tool that applies an artificial neural network (ANN) to automatically estimate LAI, CCC and CWC

from Sentinel-2 multispectral images. The derived functional traits may have a significant potential for vegetation monitoring, due to their straightforward retrieval process and the fine spatial and temporal resolution of Sentinel-2 data. However, the accuracy of these products has been poorly tested in temperate forests. Furthermore, to the best of our knowledge, previous studies have not applied these products in the form of a time-series analysis to capture forest responses to drought.

This study focuses on the temperate mid-latitude forest ecosystems of the Ticino Regional Park, a mixed forest located along the Ticino River in the Po Plain. The main aim is to analyse the functional responses of different forest types as observed by the spectral changes detected in Sentinel-2 data during the 2022 exceptional drought event in northern Italy (Faranda et al., 2023).

The derived LAI, CCC and CWC from 2017 to 2022 were used to determine functional trait anomalies as indicators of vegetation response to drought conditions. In addition, forest environmental characteristics and species composition were analysed to investigate if and how they influence the plant physiological response to stress events, and the corresponding spectral changes observed by Earth Observation satellites. This information is fundamental for understanding the spatial and temporal impacts of drought, as different plant species and environmental factors influence vegetation strategies to cope with drought (Volaire et al., 2018; Forner et al., 2018). Understanding how different forest types respond to drought and how this response is manifested in the satellite-signal is a crucial requirement for developing a meaningful forest monitoring system based on satellite data.

With the overarching aim to develop a remote sensing-based system to monitor the functional state of forests, the specific objectives of this study are:

1. to validate the LAI, CCC and CWC functional traits retrieved by the biophysical processor of the S2 Toolbox using ground measurements in a mixed forest ecosystem;
2. to analyse S2 time series (2017-2022) to identify drought-induced anomalies in plant traits and relate them to species' ecology and local environmental conditions;
3. to assess the spatial and temporal response of the Ticino forests to the extreme drought experienced by northern Italy in 2022.

3.2 Material and Methods

3.2.1 Study area

The study was carried out in the Ticino Regional Park in Italy (45°44′ N, 8°84′ E). It covers an area of 91.1 Kha, where natural woodland (22 Kha) and agricultural land (47 Kha) coexist in one of the most urbanised areas in Europe (Figure 1).

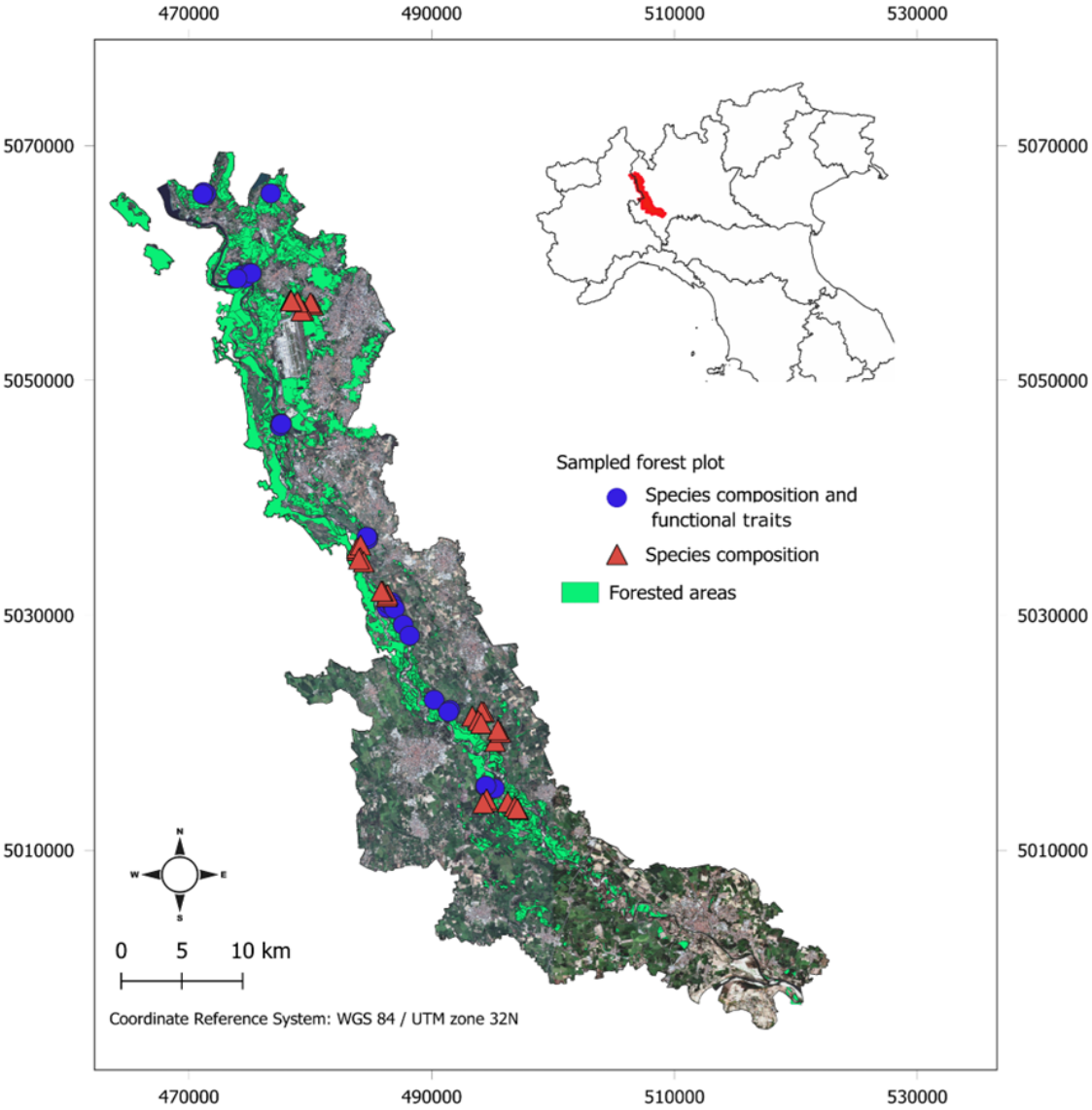

Figure 1. Map of the Ticino Regional Park. The forested areas are shown in light green. The blue dots are the forest plots where leaf sampling, LAI and species composition data were collected, the red triangles are the forest plots where only the species composition data were recorded. The top right map shows the location of the study area in northern Italy in red.

The Park is one of the largest remaining natural areas in the Po Valley, representing a unique refuge for native vegetation. With its long and narrow shape, the Park acts as a fundamental ecological corridor linking the Alps with the Apennines of central Italy. Because of its importance for the

preservation of biodiversity, the Ticino Park has been included in the UNESCO-MAB Biosphere Reserves. It is characterised by a moderate increase of elevation in the northern part, which contributes to the high diversity of habitats and plant species. The Ticino temperate mixed forests in the northern part are mainly composed of the oak-hornbeam association, a combination of oaks (typically *Quercus robur*, but also *Q. cerris, Q. petraea* and *Q. pubescens*) and hornbeam (*Carpinus betulus*), with the presence of sweet chestnut (*Castanea sativa*) and native or alien pine (*Pinus sylvestris* and *P. rigida,* respectively), while poplar (*Populus* spp.) and alder (*Alnus glutinosa*) are common in the southern part. There is also a significant presence of invasive alien species (mainly *Prunus serotina, Q. rubra*, and *Robinia pseudoacacia*), which occur mixed with native plants or in almost monospecific stands.

3.2.2 Field data collection and laboratory analysis

An extensive field campaign was carried out from June to September 2022, during which data were collected from 63 plots of 30×30 m^2 in homogeneous forest sites (Figure 1). The plots had a minimum distance of 150 metres away from one another, and were selected to be as representative as possible of the main forest types and structures found in the park. In each plot, information was collected on the composition and abundance of plant species at tree, shrub and herbaceous levels.

Secondly, each forest plot was assigned to a forest type based on plant dominance and composition (Del Favero, 2002). The forest types identified were:

a. hygrophilic black alder (dominance of *Alnus glutinosa*);
b. meso-hygrophilic oak (dominance of *Quercus robur* and *Alnus glutinosa* with sporadic presence of *Populus nigra* and *Carpinus betulus*);
c. meso-hygrophilic oak-white hornbeam (dominance of *Q. robur* and *C. betulus,* with sporadic presence *A. glutinosa* and *Prunus padus*);
d. mesophilic oaks (dominated by oaks *Q. robur*, *Q. cerris*, and *Q. rubra*);
e. mixed deciduous (mixed tree species of broadleaf, maily: *Q. robur, Q. rubra, Populus nigra, P. canescens, P. tremula, U. minor, R. pseudoacacia* and *P. serotina*);
f. open xerophilic oak (dominated by *Q. robur,* and frequent *Cytisus scoparius* in the shrub layer);
g. black cherry (almost monospecific forest of *Prunus serotina)*;
h. chestnut (dominance of *Castanea sativa*, sporadic presence of *P. sylvestris*);
i. pine (*Pinus rigida* and *P. sylvestris*).

In addition to species composition data, leaf and canopy functional traits were collected from 31 plots in June and July 2022. Subsequently, in September 2022, a subset of 19 of the 31 plots initially sampled were revisited (for a total of 50 plots where forest traits were analysed) (Tagliabue et al., 2023). This approach allowed us to evaluate the effectiveness of the adopted satellite-based trait estimation method across multiple forest types and two different moments of the vegetative phase.

The forest functional traits measured were leaf area index (LAI), leaf chlorophyll content (LCC), and leaf water content (LWC).

The geographic coordinates of each plot were recorded at its centre using a high-precision GPS device (Garmin GPSMAP 66 sr, Olathe, USA). To delineate the 30×30 m^2 plots, we measured and marked the sides of the square accordingly. LAI was measured in the field through digital hemispherical photos taken with a Canon EOS M50 MARK II camera (13 up-looking and 9 down-looking images) following a regular grid. LAI measurements were always collected in diffuse light conditions during the central hours of the day to ensure illumination consistency (Chianucci and Cutini, 2012). Mean LAI values were calculated using the CAN-EYE software (https://www6.paca.inrae.fr/can-eye/). In the stands with overstory LAI < 1.5 m^2/m^2, the total LAI was calculated as the sum of the overstory and understory LAI. Whereas, to quantify LCC and LWC, sunlit leaves were collected with a slingshot from the top of the canopy of the dominant tree species in each plot (3 trees per species and at least 12 leaves per tree, 650 leaves in total). The leaves were immediately placed in sealed plastic bags and kept in a cooler until transported to the laboratory, where they were stored at −80 °C until the chlorophyll analysis was performed. Leaf level traits were obtained from destructive measurements performed on leaf disks obtained using a 0.635 cm diameter leaf punch. For each sampled tree, 217 in total, two sets of three Eppendorf tubes filled with 12 leaf disks each were prepared. The first set of three Eppendorf tubes was used for LWC analysis. The fresh and dry (after oven-drying at 80 °C for 48 h) weight of the leaf disks was measured using an analytical balance with a sensitivity of 0.0001 g. The LWC (g cm^{-2}) was calculated according to the equation: $LWC = (Weight_{fresh} - Weight_{dry}) / Area_{tot}$. The second set of Eppendorf tubes was frozen and stored at −80 °C until the LCC analysis was conducted. For LCC quantification the methodology described in Tagliabue et al. (2022) was followed.

The weighted mean of both LWC and LCC for each plot was estimated by multiplying the LCC and LWC average values of each species by its percentage in each plot. Next, the weighted means of LCC and LWC for each plot were multiplied by the corresponding LAI to obtain the CCC and CWC.

3.2.3 Meteorological data and SPEI computation

Drought conditions within the Ticino Park Forest were assessed using the Standardised Precipitation Evapotranspiration Index (SPEI) (Vicente-Serrano et al., 2010). This index examines the water balance between the amount of precipitation (PR) and predicted evapotranspiration (PET), the latter calculated from monthly maximum and minimum temperatures.

The index was derived using the 'SPEI' R package, incorporating data from two different sources, 1) high-resolution (30arcsec) global CHELSA (Climatologies at high resolution for the earth's land surface areas) database (Karger et al., 2017, 2020, 2021), which covers the period from 1980 to 2018 and 2) observations from six different ARPA (Regional Agency for the Protection of the Environment) meteorological stations located throughout the park, which cover from 2019 to 2022.

The combined use of these two databases was necessary due to their specific constraints: the ARPA meteorological station data lacked the extensive historical range required for accurate SPEI calculation (typically a minimum of 30 years), while the CHELSA database did not provide data beyond 2018. Monthly SPEI values were calculated and then aggregated over 3 and 6-month intervals (SPEI3 and SPEI6 respectively), to capture the progressive accumulation of water deficits. SPEI3 is more sensitive to short-term changes in precipitation and evapotranspiration and is therefore more suitable for highlighting differences between months. Conversely, SPEI6 captures medium-term trends and is more suitable for identifying longer-term trends.

This study considers SPEI data from the period 2017 to 2022, which coincides with the time frame of the analysed S2 images. The classification of drought severity follows the scheme proposed by Li et al. (2015), in which 7 classes are proposed based on the SPEI value: extremely wet (≥ 2.00), very wet (2.00 to 1.49), moderately wet (1.50 to 0.99), near normal (1.00 to -0.99), moderately dry (-1.00 to -1.49), severely dry (-1.50 to -1.99) and extremely dry (≤ -2.00). SPEI values below -1.00 identify a drought event.

3.2.4 Forest types characterization

The field data on plant species composition were used to determine the Ellenberg Indicator Values (hereafter EIVs) (Ellenberg, 1974; Pignatti et al., 2005; Tichý et al., 2023) for each of the 63 forest plots. EIVs assign a functional role to each plant species as a biological indicator of a specific environmental factor, attributing a numerical value to each plant species according to it. Six EIVs were calculated for each of the 63 forest plots: light radiation (L), heat (T), climate continentality (C), soil moisture (M), soil reaction (R) and nutrients (N) (Pignatti et al., 2005).

In each plot, the percentage of alien species out of the total number of species was calculated. Elevation data for each forest plot were available at a 5×5 m^2 resolution. They were obtained from

the Digital Terrain Model (DTM) of the Lombardy Region Geoportal (https://www.geoportale.regione.lombardia.it/ricerca).

3.2.5 S2 Imagery processing and S2 Toolbox Biophysical Processor products

A total of 240 cloud-free Sentinel-2 (hereafter S2) Level 2A multispectral images, from 2017 to 2022, centred on the Ticino Forest were automatically downloaded, processed, and resampled to 10 m pixel size using the 'Sen2r' R package (Ranghetti et al., 2020). The 2016 S2 images were not included due to their limited availability throughout the year.

The biophysical processor of the S2 Toolbox, embedded in the Sentinel Application Platform (SNAP) software, was applied to retrieve LAI, CCC and CWC from S2 images (Weiss and Baret, 2016). The trait retrieval algorithm is based on a hybrid approach based on an artificial neural network (ANN). By using a pre-trained neural network, functional traits can be estimated for each pixel of the selected S2 image. The training database for the ANN was generated using a combination of the PROSPECT leaf and SAIL canopy radiative transfer models, which simulates the top of canopy reflectance as observed with S2 over the most common vegetation types (Weiss and Baret 2016; Xie et al., 2019).

3.2.5.1 Validation of functional trait maps

The accuracy of the LAI, CCC and CWC maps generated by the biophysical processor of the S2 Toolbox was evaluated by comparing the ground data measured in the 50 forest plots sampled during the 2022 field campaigns with the satellite-estimated values extracted from the corresponding 50 squares of 30×30 m^2. Goodness-of-fit statistics, such as root mean square error (RMSE), normalised RMSE (nRMSE) (i.e., RMSE/range of measured values) and the coefficient of determination (R^2) were evaluated.

To minimise the temporal mismatch between field data collection and S2 overpasses over the study area, three S2 cloud-free images, as close as possible to each sampling date (maximum 10 days of difference), were selected for the functional trait validation: 20/06/2022, 10/07/2022 and 18/09/2022.

3.2.6 Functional traits time series

The temporal behaviour of the forest traits in each plot was analysed using the 'sen2rts' R package (Ranghetti et al., 2021). The sen2rts R package was created to provide a method for processing and analysing S2 time series in the context of crop dynamics and phenology studies. In this work,

however, it was applied to extract and process the S2 time series of LAI, CCC and CWC in a natural forest context. In detail, the workflow was as follows:

1. Raw time series of LAI, CCC and CWC values were extracted from the S2 images (240 S2 images for each functional trait, from 2017 to 2022, centred on the Ticino Park) for each forest plot. Specifically, the average of each forest plot (3×3 pixels) was estimated for every available date (Supplementary materials, Figure S1a);
2. Smoothed time series were obtained by applying a three-iteration Savitzky-Golay filter to remove discontinuity. This step permits the removal of clear temporal breaks, such as sudden sharp drops often caused by low quality points (Figure S1b);
3. For winter months (specifically from DOY (Day-Of-Year) 335 to DOY 56 of the following year), the values were replaced by the value corresponding to 5% of the distribution of the entire time series. This adjustment helps to eliminate the noise introduced by winter environmental conditions, such as snow, while reflecting the naturally low level of plant traits during the senescence period (Figure S1b);
4. The final daily time series were generated by interpolating missing days with a spline function (Figure S1b).

3.2.7 Daily standardised anomaly detection and mapping

To assess the stress response of the Ticino Forest during the 2022 summer drought, the vegetation functional trait Daily Standardised Anomaly (hereafter DSA) was calculated. This consists of determining the deviation of LAI, CCC and CWC in a precise location (i.e. 3×3 pixel forest plot) and time from the 2017-2022 multi-year daily averages. The DSA values were calculated using the following formula (modified from Ma et al., 2023):

$$x(fs,t)' = \frac{x(fs,t) - x(fs)}{std(x(fs))}$$

x(fs, t)' is the normalised anomaly at the forest plot location (fs) at time t, x(fs, t) is the data value at the forest plot location (fs) at time t, x(fs) is the multi-year daily average at the forest plot location (fs), and std(x(fs)) is the multi-year data standard deviation at the forest plot location (fs). The inclusion of multi-year daily averages in the calculation serves as a baseline to isolate and highlight changes potentially induced by environmental stress, distinguishing them from typical seasonal variations. Subsequently, the function was adapted to calculate the DSA values at a raster level,

allowing the DSA computation for each pixel falling within the Ticino Park forested area. A daily anomaly map for LAI, CCC and CWC was generated every 7 days, from 2017 to 2022.

There are no generally accepted thresholds in the literature to distinguish between anomaly values caused by natural variation and those caused by drought-related effects on forest physiology. In this study, a DSA threshold of -0.2 for LAI, CCC and CWC was set. Thus, anomalies equal to or less than -0.2 are considered to be drought-induced negative anomalies. This threshold, although relatively less restrictive than the value used in other studies (e.g., Chen et al., 2022), was chosen due to the limited availability of historical S2 data and the occurrence of relatively milder dry spells during the 2017-2022 reference period.

3.2.8 Generalized additive models (GAMs)

To better understand the observed anomalies, the DSA values of LAI, CCC and CWC retrieved from S2 data were analysed to assess the forest's spatio-temporal response to the 2022 drought in the Ticino Park. Generalised additive models (GAMs) were used to investigate how different forest types and environmental factors are related to DSA values considering the 63 forest plots analysed. In particular, two analyses, which differ in the functional trait DSA values considered in the models, were conducted. Specifically:

1) Both negative and positive DSA of LAI, CCC and CWC across three key dates between June and October 2022 (i.e. S2 acquisitions collected on 20/06/22, 04/08/22, 08/10/22), corresponding to the early stage, peak and late water stress in the forest. The objective was to investigate which factors influenced the functional trait DSA, whether this was negative or positive. This approach allowed us to investigate the factors having a role in the presence or absence of drought-induced stress.

2) The minimum DSA of LAI, CCC and CWC recorded in 2022 vegetative season. In this analysis, only values $\leq$ -0.2 were considered, in order to investigate which factors are influencing the presence of drought-induced stress in the forest, independently of when the peak of stress was recorded.

The explanatory variables included at the plot level were forest types, 6 EIVs, elevation and percentage of alien species (% alien). The SPEI was not included in the analysis due to its coarse spatial resolution.

All GAMs analyses were performed using the mgcv R package and by applying the "REML" (restricted maximum likelihood) automated smoothing parameter option (Wood, 2011). This method is known to be robust to the effects of concurvity (a non-linear form of collinearity between

explanatory variables), as it relies on penalised likelihood estimation for fitting. However, despite the robustness of GAMs, a certain degree of concurvity can still affect the model's performance (Jbilou and El, 2012). By implementing the mgcv package concurvity functions it is possible to assess the concurvity scores for each variable. The function output examines three scenarios: worst, observed and estimated. In this work, only the observed scenario was taken into consideration (Wood, 2011). While this approach may be less restrictive, it is justified in the context of datasets constrained by limited replicates and the extent of the study area (Kelley and Tucker et al., 2022). In addition, the analysis of concurvity within our dataset was prioritised, rather than examining it over the coefficients generated by the GAM fitting process (Kelley and Tucker et al., 2022). Unlike for collinearity, there is no generally accepted threshold for concurvity. Following Nguyen and Leung (2022), a value of 0.8 was chosen. Therefore, the explanatory variables with the highest observed case concurvity were removed, and the GAM was refitted, repeating this process until all the selected variables had a concurvity value equal to or less than 0.8.

The Akaike Information Criterion (AIC) was used to compare different models and identify the one that best captured the variance in the standardised anomalies. The smaller the AIC value, the more likely it is that a given model fits the data significantly better than another.

3.3 Results

3.3.1 Forest type and environmental variable characterization

The forest plots dataset analysed within the Ticino Park comprehended a total of 63 plots distributed over 10 different forest types. The mean and standard deviation of each of the six EIVs, the elevation value, and the percentage of alien species per forest type are summarised in Table 1. The number of plots per forest type varied from a minimum of 3 to a maximum of 15, reflecting the occurrence frequency of the different forest types in the Ticino Park. The EIVs temperature (T) and continentality (C) showed minimal variation between forest types, suggesting similar base conditions due to the limited extent and local scale of the study area.

Table 1. Summary of Ellenberg Indicator Values (EIVs) and environmental variables per forest type. EIVs: light radiation (L), heat (T), climate continentality (C), soil moisture (M), soil reaction (R) and nutrients (N).

Forest type	N of plots	L	T	C	M	R	N	Elevation (m)	Alien (%)
Hygrophilic black alder	7	5.21 ± 0.30	5.41 ± 0.40	4.61 ± 0.09	6.33 ± 0.24	6.46 ± 0.32	6.44 ± 0.20	99.56 ± 16.68	17.60 ± 28.11

Chestnut	4	5.44 ± 0.55	6.37 ± 0.33	5.09 ± 0.28	5.37 ± 0.44	4.53 ± 0.67	5.25 ± 1.76	347.86 ± 43.60	8.16 ± 11.91
Meso-hygrophilic oak	3	5.23 ± 0.41	5.72 ± 0.07	4.79 ± 0.10	5.61 ± 0.36	6.09 ± 0.55	6.07 ± 0.42	78.16 ± 6.52	1.02 ± 1.77
Mesophilic oaks	15	5.45 ± 0.42	6.15 ± 0.28	4.96 ± 0.17	5.12 ± 0.49	5.81 ± 0.76	5.54 ± 0.72	97.83 ± 15.62	17.72 ± 24.05
Meso-hygrophilic oak-white hornbeam	9	5.2 ± 0.20	6.07 ± 0.22	4.68 ± 0.16	5.48 ± 0.42	6.25 ± 0.48	5.69 ± 0.55	100.90 ± 22.83	6.98 ± 12.80
Mixed deciduous	11	5.34 ± 0.32	6.27 ± 0.31	5.04 ± 0.29	5.45 ± 0.37	5.47 ± 0.94	6.11 ± 0.73	183.94 ± 72.31	37.91 ± 29.68
Pine	6	6.01 ± 0.32	6.34 ± 0.45	4.94 ± 0.27	6.03 ± 0.52	3.51 ± 0.37	3.06 ± 0.56	260.86 ± 38.29	0.00 ± 0.00
Black cherry	3	5.37 ± 0.49	6.06 ± 0.10	4.93 ± 0.21	5.10 ± 0.36	5.83 ± 0.87	5.56 ± 0.78	175.39 ± 52.31	86.17 ± 14.85
Xerophilic oak	5	6.81 ± 0.28	5.95 ± 0.09	5.09 ± 0.15	4.33 ± 0.23	6.04 ± 0.23	4.15 ± 0.44	88.00 ± 16.99	3.25 ± 7.27

In contrast, differences in elevation (ranging from 78.16 ± 6.52 to 347.86 ± 43.60 m a.s.l.) and in the EIV soil reaction (R) (from 3.51 ± 0.37 to 6.46 ± 0.32) were found according to the location of the forest types along the park. Chestnut and pine forest types had the highest mean elevation (347.86 ± 43.60 and 260.86 ± 38.29, respectively), and the lowest R value (4.53 ± 0.67 and 3.51 ± 0.3, respectively). Both types are mainly present in the northern part of the park, which is characterised by a higher elevation and more acidic soils. Conversely, the types located in the floodplain of the Ticino River had a lower mean elevation and a higher R value, indicating less acidic soils.

Nutrient availability, as indicated by the EIV nitrogen (N), also varied considerably. Pine forest type had the lowest value (3.06 ± 0.56), followed by xerophilic oak (4.15 ± 0.44) and chestnut (5.25 ± 1.76). On the contrary, the forest types located in the central and southern parts of the park, except for the xerophilic oak, had higher nutrient levels. In particular, hygrophilic black alder forests had the highest EIV N (6.44 ± 0.20), followed by mixed deciduous forests (6.11 ± 0.73) and meso-hygrophilic oak forests (6.07 ± 0.42). Hygrophilic black alder forests also had the highest moisture level (EIV M index = 6.33 ± 0.24), highlighting their adaptation to wetter and more fertile environments. The lowest EIV M index (4.33 ± 0.23) was recorded for the xerophilic oak type.

Light availability in the understorey was assessed using the EIV light radiation (L), which was higher in the pine and xerophilic oak, with values of 6.81 ± 0.28 and 5.90 ± 0.32 respectively,

suggesting that these habitats experience a greater solar ground incidence, however, in both forest types there was almost no understory. In contrast, the other type, especially the meso-hygrophilic oak-white hornbeam forests (5.2 ± 0.20) and hygrophilic black alder (5.2 ± 0.30), had a relatively lower light availability, indicating a denser canopy cover.

The prevalence of alien species varies considerably between the forest types. Black cherry showed the highest percentage (86.17 ± 14.85), as expected since this species is an invasive alien species (that was forming almost monospecific stands in some of the sampled plots), followed by mixed deciduous (37.91 ± 29.68). The other forest types had much lower percentages. No other alien invasive species were detected in the pine forests.

2.3.2 Temporal Variation of Drought Obtained from SPEI

In this study, SPEI was calculated to assess the severity and dynamics of drought at two different time scales (SPEI3 and SPEI6).

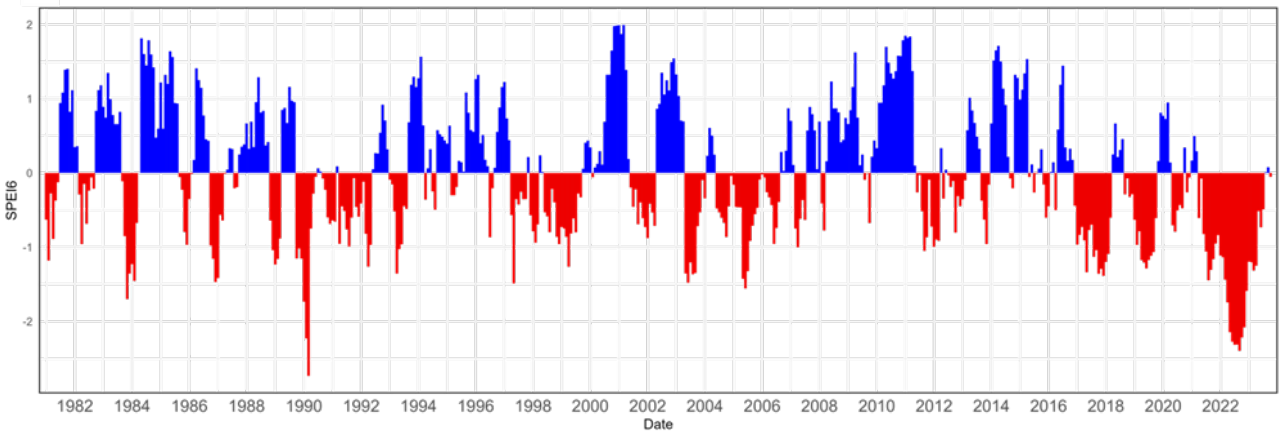

Figure 2. SPEI6 trend for the Ticino Park area from 1981 to 2022. Positive values are shown in blue and negative values in red.

The mean SPEI6 series for the Ticino Park area from 1981 to 2022 is shown in Figure 2. The data showed a clear pattern of alternating dry and wet periods, with a noticeable tendency toward more intense and longer negative SPEI values in recent years.

This trend was particularly pronounced during the 2017-2022 study period, culminating in an unprecedentedly severe and prolonged drought in the summer of 2022. There were other significant droughts over the past four decades, including those in the mid-1980s, late 1990s, and early 2000s. However, the 2022 drought event stood out for its severity and duration, with SPEI exceptionally exceeding the value of -2.00 (extremely dry condition) for several months in a row.

Looking into more detail, the 2022 SPEI (Figure S2), both SPEI3 and SPEI6 showed consistently negative values throughout 2022. It indicates an exceptionally severe drought condition for the entire year in the Ticino Park. Compared to SPEI6, SPEI3 tended to recover more quickly and showed

slightly less severe negative values, but still exceeded the threshold of severe drought (-1.50) in all spring months, reaching extremely dry conditions (-2.00) in June, July and August. On the other hand, SPEI6 displayed delayed, but more consistent and severe negative values, particularly from May onwards, where it exceeded the threshold of severely dry, reaching almost -2.50 in September. This indicates an acute accumulation of drought conditions. It appears that the medium-term drought conditions were more severe than the short-term ones, pointing to a long-term deficit in precipitation and water availability. The prolonged and acute lack of water is likely to have caused severe physiological stress in the Ticino Forest ecosystems, which has been investigated in section 3.4 of this paper.

3.3.3 Functional trait map validation

The retrieval accuracy of the functional traits maps of the Ticino Park forest derived from the S2 Toolbox was evaluated quantitatively by comparing the field-measured trait values with the S2-based estimates. A relatively high predictive power was observed in the estimation of LAI (R^2 = 0.75, nRMSE = 11.49%), CCC (R^2 = 0.82, nRMSE = 13.56%) and CWC (R^2 = 0.64, nRMSE = 28.84%). The scatter plots (Figure 3d, e) between the measured and estimated LAI and CCC values show that overall they respect the 1:1 data distribution, although a slight overestimation can be observed for high CCC values. Differently, a 2:1 relation can be observed for CWC, underlying a consistent CWC overestimation (Figure 3f). Figure 3a, 3b, 3c show an example of LAI, CCC and CWC maps of the Ticino Park forested areas, dated 20/07/2022, obtained with the S2 Toolbox.

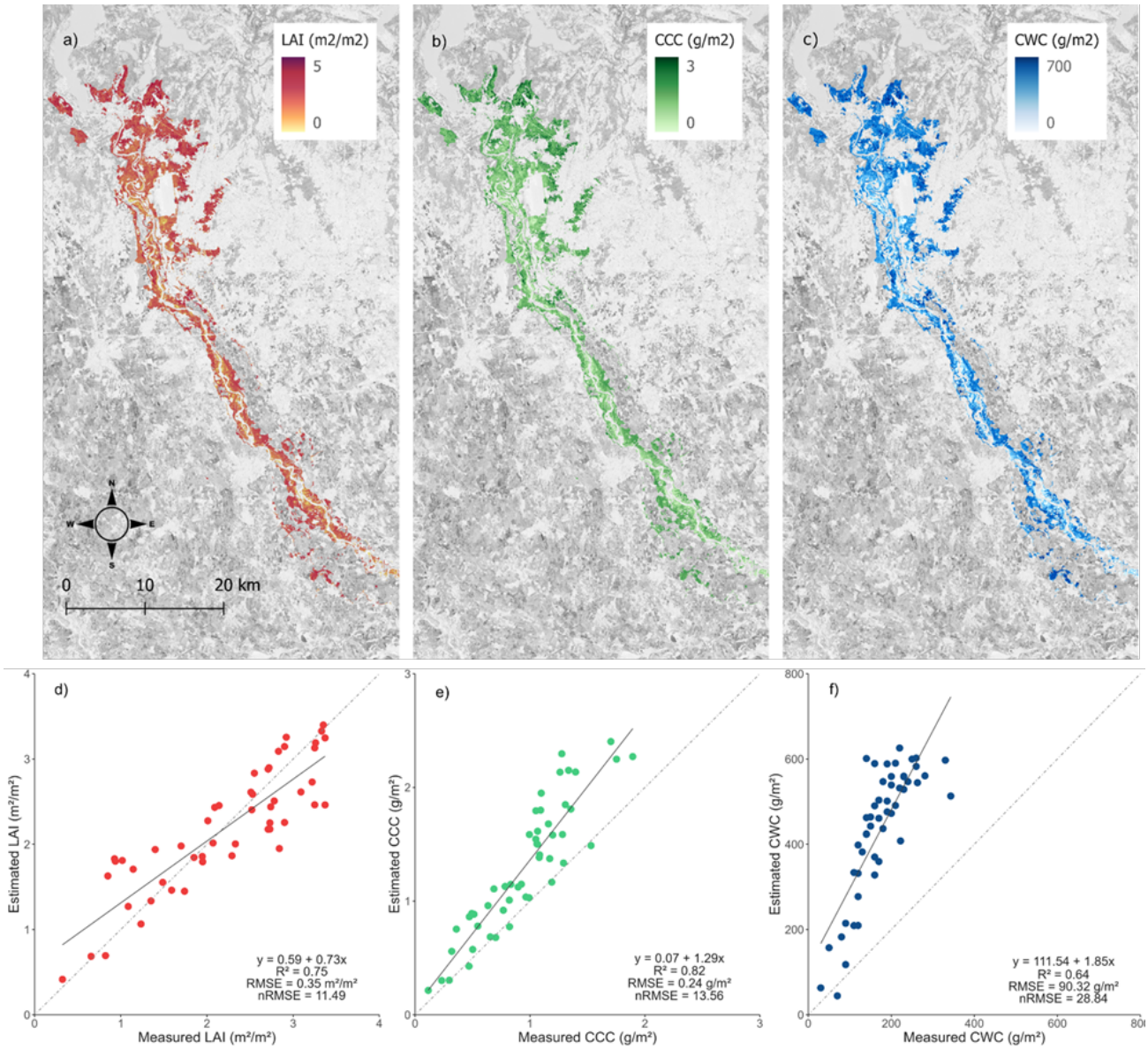

Figure 3. Ground validated maps of (a) leaf area index (LAI), (b) canopy chlorophyll content (CCC) and (c) canopy water content (CWC) (10 m resolution) from S2 images collected on 20/07/2022 (top). Scatter plots of the ground-based measurements against the estimated functional traits: (d) LAI, (e) CCC and (f) CWC (bottom). The solid lines correspond to the linear models fitted between the paired variables. The dashed lines represent the 1:1 lines.

2.3.4 Analysis of functional trait anomalies

Generalized additive models (GAMs) were employed to investigate the relationship between the functional trait anomalies and the Ticino Forest types and different environmental factors, with a focus on the 2022 drought-induced plant stress (measured as LAI, CCC, and CWC DSA). The best models selected based on the lowest AIC and the percentage of deviance explained by the model are shown in Table 2 and Table 3.

Table 2. Summary of GAM results for LAI, CCC and CWC DSA extrapolated over three different dates. Ald = hygrophilic black alder, Chest = chestnut, B. cherry = black cherry, Mix. dec = mixed deciduous, M.O.Hor = meso-hygrophilic oak-white hornbeam , M-Hyg.O = Meso-hygrophilic oak, M.O = mesophilic oaks, Xer.O = open xerophilic oak. Significance codes: '***' 0.001, '**' 0.01, '*' 0.05, '-' 0.1.

Date (Trait)	EIVs						Elev (m)	Alien (%)	Forest types									Deviance explained (%)
	L	T	C	M	R	N			Ald	Chest	B. cherry	Mix. dec	M.O. Hor	M-Hyg.O	M.O	Xer.O	Pine	
20/06/22 (LAI)							*		_		**	_				***	**	56.8%
20/06/22 (CCC)				_			***		*	**	*	**				*	***	69%
20/06/22 (CWC)				_			***		_	***						***	***	74.1%
04/08/22 (LAI)				*			***		_	**	***	**	*		***	**	***	76.6%
04/08/22 (CCC)							***			***	**	**	_		***	***	***	80%
04/08/22 (CWC)					_		***			***	**	*			***	***	***	80.5%
08/10/22 (LAI)							***			***					_	*	***	86.7%
08/10/22 (CCC)							***			***						_	***	90.4%
08/10/22 (CWC)				_			***		**	**	_	*			*	*	***	90.2%

Table 2 summarises the results of the best selected GAMs with the response variable being the anomalies recorded on specific dates (i.e. 20/06/2022, 04/08/2022, and 08/10/2022). Forest types and elevation emerged as the most common significant predictors of DSA values. Xerophile oak, pine, black cherry and chestnut were almost consistently selected as significant model predictors. However, only xerophile oak, pine and black cherry showed negative DSA values, while chestnut showed positive DSA values.

The increase in the number of forest types selected by the model from 20/06/2022 to 04/08/2022, with DSA values of mixed deciduous and mesophilic oaks also becoming significant, likely reflects the intensification of drought conditions in the Ticino Park. This led to more pronounced negative DSA values in species that are sensitive to drought stress, resulting in a clearer differentiation of

forest responses. In October, the number of forest types selected by the models decreases, as DSA values become less negative compared to August and tend slightly more towards zero (see also Figure 4). Only chestnut and pine forest types were found consistently significant in all the models, being the less (positive DSA values) and the most severely affected (maximum negative DSA values) forest types, respectively.

Concerning the other environmental factors fitted into the GAMs, soil moisture (EIV M) seems to be the variable affecting LAI anomaly the most on 04/08/2022, and to a lesser extent affecting CWC and CCC (Table 2). The pH (EIV R) showed some weak effects for CWC anomalies on 04/08/2022.

Overall, the deviance explained by the models increases over the three dates for LAI, CCC, and CWC DSA. This trend indicates a growing diversification of anomaly responses across species due to stress at the beginning, peak and end of the 2022 summer drought. The models selected for 04/08/2022 and 08/10/2022 exhibit robust performance, with percentages of explained deviance ranging from 76.6% to 91.2%, reflecting their accuracy in capturing the variation in plant trait anomalies.

Table 3. Summary of GAM results for LAI, CCC and CWC DSA extrapolated during the vegetative season, and filtered below -0.2. Ald = hygrophilic black alder, Chest = chestnut, B. cherry = black cherry, Mix. dec = mixed deciduous, M.O.Hor = meso-hygrophilic oak-white hornbeam , M-Hyg.O = Meso-hygrophilic oak, M.O = Mesophilic oaks. Significance codes: '***' 0.001, '**' 0.01, '*' 0.05, '-' 0.1, '/' not included in the model.

Date (Trait)	EIVs						Elev (m)	Alien (%)	Forest types									Deviance explained (%)
	L	T	C	M	R	N			Ald	Chest	B. cherry	Mix. dec	M.O. Hor	M-Hyg.O	M.O	Xer.O	Pine	
V. season ≤ -0.2 (LAI)				*	*					/	***	**		/	*	*	***	81.2%
V. season ≤ -0.2 (CCC)				_							***	**	_		**	**	***	78%
V. season ≤ -0.2 (CWC)				*						/	*	*		/	*	_	***	84.8%

Table 3 summarises the results of the best selected GAMs for the functional traits analysed, where the response variable considered is the maximum negative anomalies in plant traits recorded during the vegetative season. The models demonstrate a strong link between forest types and negative anomalies in all the functional traits investigated, although CCC shows a higher statistical significance level. In addition, the GAMs analysis identifies moisture (EIV M) and soil pH (EIV R) as significant factors influencing LAI anomalies, with moisture also influencing CWC anomalies and, to a lesser extent, CCC anomalies (significance of 0.1). The chestnut and mesohygrophilic oak types

were not included in the analysis of LAI and CWC models due to the absence of DSA values meeting the threshold of ≤ -0.2 (Table 3). The selected models were able to explain a substantial proportion of the variance, with percentages ranging from 78% to 84.8%, indicating the robustness of the models selected.

3.3.5 Response of the forest types to drought stress

The 2022 DSA values of LAI, CCC and CWC were computed for the 63 forest plots and extracted over different key dates (coinciding with S2 cloud free images) to show the relationship between drought-induced stress conditions and forest types over time. The CCC DSA values are shown in Figure 4. The CCC decline is evident across many of the different forest types, and in these cases is more pronounced than in LAI and CWC (Figure S3 and S4), as already evidenced by the GAMs analysis (Table 3). Conversely, LAI and CWC DSA values are less negative in the corresponding forest types and time. This suggests that CCC DSA, which reflects canopy chlorosis, may be a more sensitive indicator of drought stress compared to LAI and CWC DSA. This is particularly evident for pine (Figure 4g) and black cherry (Figure 4b), where CCC DSA reached minimum values of almost -2 and -1.5, respectively.

Forest types like hygrophilic black alder (Figure 4e), chestnut (Figure 4h) and meso-hygrophilic oak (Figure 4i) exhibited almost no signs of negative CCC DSA, indicating that the CCC values did not deviate from the multi-year daily mean value in 2022 and therefore that these forest types were not affected by the 2022 drought. The meso-hygrophilic oak-white hornbeam type (Figure 4a), experienced minor negative CCC DSA in June and August, indicating mild drought-induced stress. Conversely, xerophilic oak, mixed deciduous, mesophilic oaks displayed a sharper decline in LAI DSA values starting from June. In these forest types, the lowest CCC DSA values were observed in early August, followed by an upward trend towards zero in September. Open xerophilic oak (Figure 4c) and black cherry (Figure 4b) however continued to exhibit values slightly below zero even in September and October, suggesting prolonged stress in these forest types. Mixed deciduous (Figure 4f) and open xerophilic oak (Figure 4c) showed more variability compared to the other forest types.

The pine forest type (Figure 4g) showed median values of CCC anomalies consistently below zero. In detail, CCC anomalies decrease sharply throughout the summer, starting in July and reaching -1.5 in late August. In late August, September and October, unlike the broadleaves, pine LAI DSA values remain consistently below the CCC multi-year daily mean value, indicating a severe change in the canopy structure. The pine forest types (Figure 4g) showed the most severe and persistent signs of drought-induced forest stress.

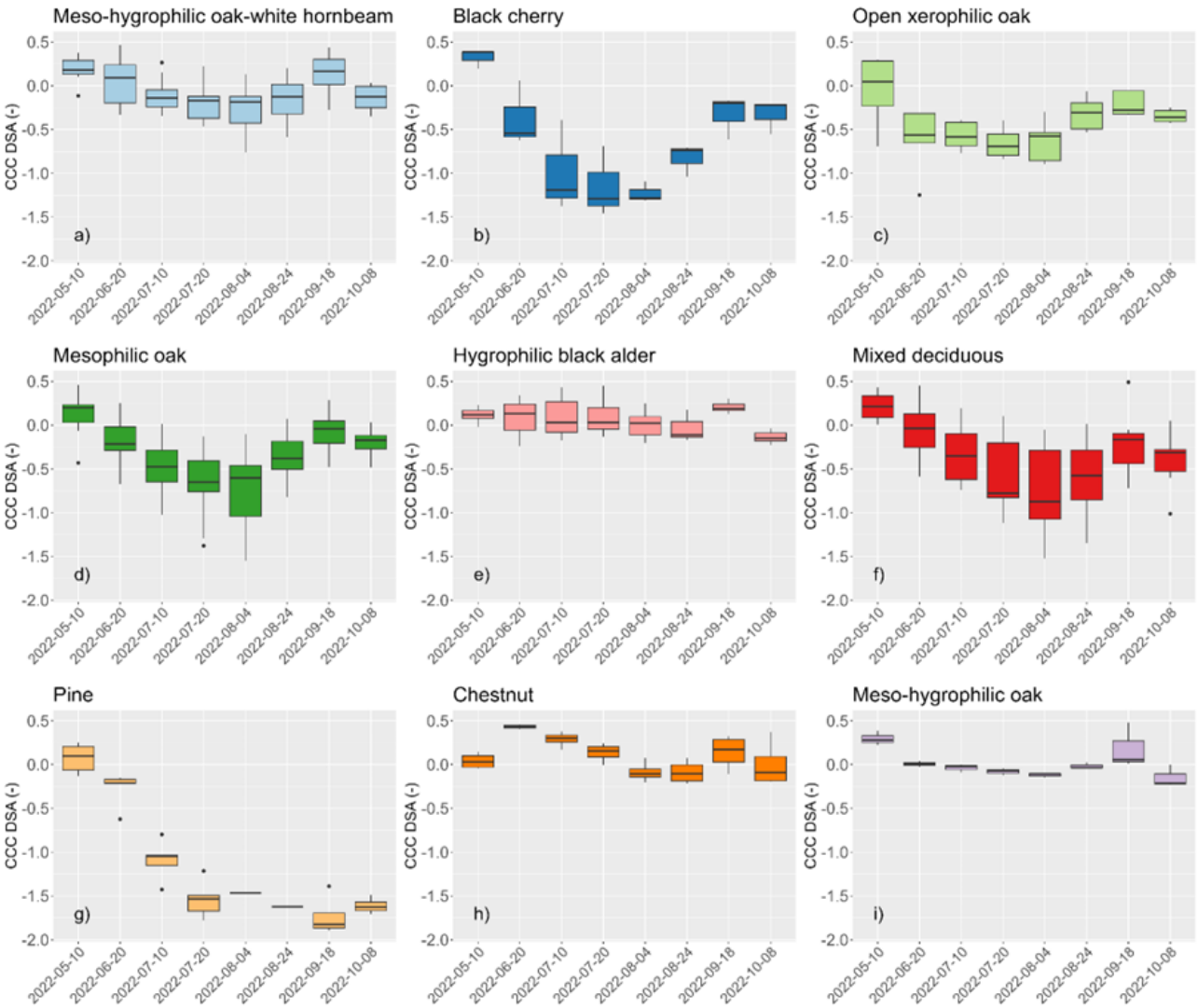

Figure 4. Box plots of canopy chlorophyll content (CCC) daily standard anomaly (DSA) values through spring, summer and autumn 2022 in the 9 different forest types.

3.3.6 Functional trait daily standardised anomalies maps

Functional trait anomaly maps provide high resolution (10 m) information on the areas of the forest interested by a decrease in functional traits compared to the average baseline from 2017 to 2022. This allows for the identification of the areas most affected by the 2022 drought event.

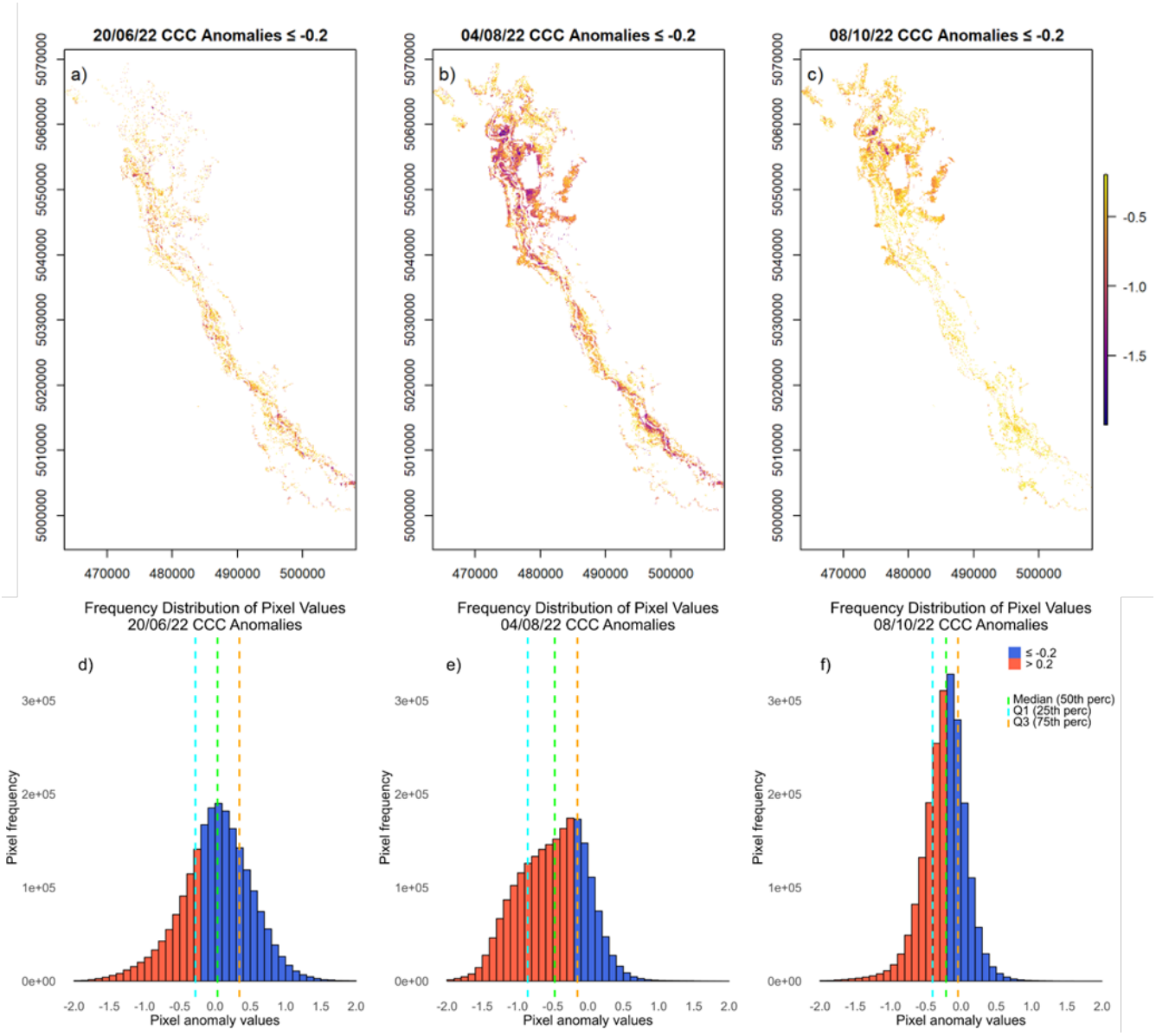

Figure 5. Spatial patterns of canopy chlorophyll content (CCC) daily standard anomaly (DSA) ≤ of -0.2 within the Ticino Forest on (a) 20/06/2022, (b) 04/08/2022 and (c) 08/10/2022 (top). Histograms of the frequency distribution of pixel values for CCC DSA on the three dates: (d) 20/06/2022, (e) 04/08/2022, and (f) 08/10/2022 (bottom).

Figure 5 illustrates the spatial distribution of CCC DSA within the forests of the Ticino Park on 20/06/2022 (Figure 5a), 04/08/2022 (Figure 5b) and 08/10/2022 (Figure 5c), capturing the early stage, peak and long-term effects of drought-induced stress in 2022, respectively (see Figure S5 and S6 for LAI and CWC maps, respectively). To highlight the areas most affected by the drought stress as the vegetative season progresses, only CCC anomalies below -0.2 are shown. On 20/06/2022, the map (Figure 5a) shows that the vegetation has a moderately negative CCC DSA throughout the park, with the exception of the northeast area, which appears less affected. The histogram of the frequency distribution of the CCC anomaly (Figure 5d) indicates that the median value of the map is close to

zero, with a relatively symmetric distribution of positive and negative anomalies. This suggests that the impact of the drought, while present, was still moderate at the time.

By 08/08/2022, the map (Figure 5b) shows a widespread sharp decrease in CCC DSA values, together with an increase in the number of pixels affected by drought-induced stress. This is confirmed by the frequency histogram (Figure 5e), which shows an increase in the frequency of pixels with negative anomalies compared to 20/06/2022. Moreover, the median value shifted to -0.5, and the majority of pixels (up to the 75th percentile) had an anomaly value of less than -0.2, indicating a widespread and detrimental impact of drought on the CCC.

The 08/10/2022 map (Figure 5c) shows a general reduction in the distribution and intensity of negative CCC DSA values in the forests of the Ticino Park compared to August. However, negative anomalies are still present, particularly in the northern part of the park, suggesting ongoing stress. The frequency histogram (Figure 5f) shows a reduction in the frequency of extreme negative and positive values. The majority of the pixels between the 25^{th} and 75^{th} percentiles have values between -0.5 and 0, with the median value around -0.25. This suggests ongoing, but less severe, drought-induced stress. However, as reported in section 3.4, this result should not be interpreted as a full recovery of the chlorophyll content in the vegetation of the Ticino Park. Instead, the shift of DSA values towards zero is likely due to the natural leaf shedding and decrease of chlorophyll content in broadleaf species, which typically begin in this period of the year. Consequently, the 2022 CCC levels align with the multi-year daily mean CCC levels. Nevertheless, the persistence of negative DSA values may indicate an early occurrence of senescence in some areas, suggesting that broadleaves species mainly in the North did not recover from the drought and went through an anticipation of senescence. Differently, the pine forest type shows no tendency for CCC DSA to return to zero after August. Instead, they remained consistently below -1, indicating persistent and severe stress (Figure 4g).

3.4 Discussion

Our study proposes a quantitative approach to effectively detect and monitor the temporal and spatial distribution of the response of a temperate mixed forest to drought-induced stress from satellite remote sensing. LAI, CCC and CWC estimates were derived from the S2 time series and multi-year daily anomalies were calculated. The anomaly values observed during a severe drought were then related to the forest type and a range of environmental variables to better understand how the satellite-observed functional response of forests is affected by these variables. The main results of this study will be discussed in the following sections.

3.4.1 Retrieval accuracy of functional traits from Sentinel-2

Good retrieval accuracies were obtained for LAI, CCC and CWC using the S2 Toolbox. CCC showed the highest accuracy, with an R^2 of 0.82 and an RMSE of 0.24 g/ m^2, closely followed by LAI, with an R^2 of 0.75 and an RMSE of 0.35 m^2/ m^2 (Figure 3d and e). For CWC, an R^2 of 0.64 and an RMSE of 90.32 g/ m^2 were obtained (Figure 3f).

Compared to other studies conducted in forest environments, our results indicate a higher prediction accuracy for both LAI and CCC. Specifically, for LAI, Hu et al. (2020) obtained in a mid-latitude temperate forest an R^2 of 0.68 and an RMSE of 0.69 m^2/ m^2, while Brown et al. (2019) reported in a deciduous broadleaf forest an R^2 of 0.54 and an RMSE of 1.55 m^2/ m^2. Furthermore, in deciduous forests, Brown et al. (2021) obtained an R^2 of 0.64 and an RMSE of 0.61 m^2/ m^2 for LAI. Regarding CCC, Brown et al. (2019) obtained a moderately accurate estimation with an R^2 of 0.52 and an RMSE of 0.79 g/m^2. Ali et al. (2020) obtained in a mixed mountain forest an R^2 of 0.66 and an RMSE of 0.35 g/ m^2. The high retrieval accuracy achieved for the S2 Toolbox derived LAI and CCC in this study can be attributed to the rigorous and diversified sampling strategy of our 2022 field campaign, as well as close canopy cover that typically allows for good retrieval accuracy with the model applied.

Specifically, leaf samples from different tree species and forest types were collected during two different phases of the vegetative season, in June and September which resulted in a wide range of LAI values which may have supported the good model accuracies. This highlights the importance of a robust dataset, where functional trait variability is maximised, for assessing trait retrieval performance.

In contrast, a consistent overestimation of CWC was observed using the S2 Toolbox processor. Figure 3f shows that almost all data points fall above the 1:1 line. A similar result was also obtained by Zhu et al. (2023), who reported a consistent overestimation of CWC across 62 wheat plots, resulting in an R^2 of 0.50 and an RMSE of 270 g/m^2 (Zhu et al., 2023, Figure 7). Indeed, the SWIR region is sensitive to the water content of plant leaves, as reported in previous studies (Fourty and Baret, 1997; Ceccato et al., 2001; Huber et al., 2014). However, the spectral resolution of the S2 instrument is not optimal for canopy water retrieval, as it has only two bands in the SWIR region and it lacks specific liquid water absorption bands at 970 nm and 1200 nm (Boren and Boschetti, 2020).

The majority of the sensor's bands are concentrated in the visible and near-infrared spectrum. This configuration makes S2 more suitable for estimating vegetation functional traits like LAI and chlorophyll content, but less effective for assessing vegetation water content. This limitation is consistent with other studies that, despite using different retrieval approaches than the S2 Toolbox,

have reported comparable performance for LAI and chlorophyll content retrieval, but found inaccurate results for vegetation water content (Tomíček et al., 2021).

It is important to note that the S2 Toolbox retrieval algorithm was not specifically optimised to retrieve functional traits in forest ecosystems. It is described as "generic", as it could be applied to different vegetation types with good performances (Weiss and Baret, 2016). The performance of forest functional trait estimation could be improved by applying a radiative transfer model (RTM) that considers forest structure parameters, as illustrated by Brown et al. (2019).

They compared the performance of the S2 Toolbox-SAIL-based retrieval algorithm with that of the Invertible Forest Reflectance Model (INFORM) optimised for the forest environment, and obtained a consistent increase in retrieval performance for both LAI and CCC. Nevertheless, the LAI and CCC retrieval accuracy obtained by Brown et al. (2019) is comparable to that obtained in the Ticino Forest applying the S2 Toolbox, which has the additional advantage of estimating functional traits in an automatic and operational way which was deemed to be more important in our study. However, it should be acknowledged that less accurate results may be obtained in forests characterised by more open canopy and in such conditions our workflow would probably benefit from alternative retrieval approaches. Moreover, we underline that the consistency of the atmospheric correction methods (sen2cor processor embedded in SNAP), sensor usage, and processing algorithms over the years 2017–2022, provides a solid basis for assuming that the retrieval accuracy obtained in 2022 should be consistent over time.

3.4.2. Drought and functional trait anomalies

The accurate retrieval of LAI, CCC and CWC enabled the analysis of the temporal and spatial variations of the functional trait DSA driven by drought stress in the Ticino Park Forest during the summer of 2022.

In our analysis, CCC reached the most negative DSA values, highlighting its higher sensitivity in detecting the effects of water shortage on vegetation functionality compared to LAI and CWC DSA. This result might have been emphasised by a slight overestimation of CCC values in the retrieval process; however, this was not the case for CWC, which consistently showed a higher degree of overestimation but was hardly sensitive to drought stress. We believe that CCC, as a product of LCC and LAI, can capture both information on vegetation plant chlorosis and canopy biomass, thus providing a deeper insight into the physiological status of plants. We therefore conclude that CCC is a more sensitive indicator for detecting drought-induced stress. This is confirmed previous findings showing the higher sensitivity of leaf chlorophyll concentration compared to LAI for assessing the condition of oak trees in the Ticino Park (Rossini et al., 2006). Conversely, the trends for LAI and

CWC DSA were similar, suggesting that the leaf water content variations are less detectable. LAI was discussed to obscure the water-related spectral variation in CWC, making it difficult to decouple the contributions of water content from those of LAI (Cohen, 1991; Riggs and Running, 1991; Colombo et al., 2008). Although water loss is typically the first detectable physiological change under drought conditions, this was not observed in our study, likely due to the lower performance in retrieving CWC with the S2 Toolbox.

Significant differences were observed in the temporal and spatial distribution of the response to drought-induced stress within the Ticino Forest during the exceptionally dry conditions of the summer of 2022. The main factor influencing differences in DSA values was the forest type. Hygrophilic black alder, chestnut and meso-hygrophilic forest types did not show negative DSA in the investigated functional traits. This can be explained considering that alder and chestnut are relatively isohydric species. Particularly, Meinzer et al. (2009), Meinzer et al. (2017) showed that alder has a high stem capacity to compensate for negative water potential due to reduced soil moisture. Moreover, chestnuts have a deep root system, which makes the species less sensitive to possible climatic stress (Marini et al., 2019). It can be assumed that the stands of these species were notably less affected by the drought since they were still able to access water resources, either by being situated in areas with more superficial water availability (small stream) or by being able to access water from deeper soil layers. In contrast, xerophilic oak, mixed deciduous, mesophilic oaks, and, above all, pine and black cherry forest type showed notably more negative DSA values for LAI, CCC and CWC, indicating a higher vulnerability or at least a stronger optical response to drought stress.

Concerning oak, our results are aligned with Panigada et al. (2010), which reported discolouration episodes in 10 different oak stands within the Ticino Park during the summer 2003 heatwave, demonstrating the susceptibility of oak species to water shortage and high temperature. Results were also confirmed by Bauweraerts et al. (2014) and Teskey et al. (2015). However, the most negative DSA values were reported in the pine and black cherry forest types. Despite both being reported to be stress tolerant species, our results highlight that extreme arid conditions can affect their health. Similar conclusions have been also reported for black cherry in Camenen et al. (2016) using a modelling approach. In particular, species distribution model projections suggest a shift in the species' habitat suitability towards northern Europe and a marked reduction in its Italian range under future climatic scenarios. In addition, since heat stress and drought stress are often interconnected, their synergistic effect can exacerbate the effects on the survival of several tree species like black cherry. Other abiotic factors can exert further negative effects on the species performance such as duration of exposure to high temperature and drought, the individual ability to tolerate or quickly acclimate, the time of the year, and the water availability.

Regarding the pine forest, the analysed forest plots of this type consisted mainly of monospecific stands of the North American alien species *P. rigida*. There is very little literature analysing the resistance of this species to drought stress in the context of mid-latitude temperate forests. However, several studies have reported the susceptibility of pine species to drought-induced mortality in different locations in Europe (Linares and Tíscar, 2010; Lévesque et al., 2014; Rosner et al., 2018; Schuldt et al., 2020; Arend et al., 2021). In addition, Puchałka et al. (2023) reported how other North American conifer alien species will contract their distribution under climate change conditions.

The analysed forest type also showed a different temporal course of the DSA of functional traits. In deciduous species, the DSA of the functional traits reached values close to zero at the end of the vegetative period. This does not indicate the recovery of forest canopy structure, chlorophyll and leaf water content late in the season because of stress relief. Rather, it reflects the fact that the functional trait values observed in 2022 are close to their multi-year mean values, which are naturally low as deciduous species begin to shed their leaves from September onwards. On the contrary, the evergreen pine forest type continues its photosynthetic activity during the autumn and winter months. Consequently, signs of stress were still detectable during October, November and December, underlining the prolonged and severe water shortage affecting the region.

The analysis clearly shows that forest type is a major driver of the optical response of the forests as observed in the satellite images. The question of whether this is directly linked to the forests' vulnerability to drought stress cannot fully be answered with the data at hand. However, our results are clearly consistent with the concept of species-specific responses to drought stress (Taiwo et al., 2020; Farooq et al., 2012) and highlight the importance of considering species information when assessing forest health and resilience. It also indicates that a forest monitoring system which does not consider species-information may be prone to misinterpreting the spatial distribution of stress-levels.

The GAM models analysis confirmed that the variability in functional traits DSA response is mainly explained by the forest types. Additionally, the GAM models indicate that elevation had a strong influence on the degree of drought stress displayed. This is a somewhat expected result given that the elevation gradient in our study area is at least partly linked to the amount of rainfall received and also to the forest type distribution. Among the other environmental factors analysed, the soil moisture and pH level were identified as additional factors influencing the forest response to water stress, however only in few of the GAM models they notably contribute to explain the variability in DSA values of the examined functional traits. Once again, this may also partly be explained by the fact that both the elevation and forest types are also linked to these two variables, with the forest type having certain preferences with respect to the site conditions.

While our results are overall plausible in accordance with field-observed stress effects, the current study is still facing some limitations. For the moment, only the drought year itself was analysed and hence this study did not account for potential cumulative drought effects which are often an important trigger for tree mortality. In addition, the functional traits multi-year daily average is currently calculated on a relatively limited number of years (from 2017 to 2022). However, as more images will become available, these methods can be further consolidated and refined. In the future, the anomaly calculation could also be based on time-series data from selected years which did not show severe SPEI anomalies. This could potentially further increase the sensitivity of the work-flow as in the current study, an additional less intense drought already occurred in the study area in 2014 (see also Figure 2).

A further very important limitation of this study is that it only documents the satellite-observed optical drought response of the examined forest types. While it is a fair working hypothesis that forests that reacted more strongly to the drought according to their satellite-observed functional response were also indeed more stressed, it is important to state that to really confirm this, additional field data from the post-drought situation is required. Given the strong variability of coping mechanisms between tree species and even within individuals of the same tree species, a strong optical response may not necessarily mean that the tree is unable to recover or even that it suffered severe damage. On the other hand, some tree species may also not show strong optical responses during the acute drought period but will only reveal the consequences of the drought in the next season.

3.5 Conclusions

This research focused on multi-year daily anomalies of key functional traits such as LAI, CCC and CWC to directly capture and measure forest drought-induced stress. LAI, CCC and CWC retrieved by the S2 Toolbox showed a good accuracy when validated through ground data, with high predictive power in the estimation of LAI and CCC, and less accurate estimation of CWC, which was consistently overestimated. The analysis of S2 time series showed that CCC was more sensitive than LAI and CWC in detecting drought induced stress. In addition, the CCC DSA anomalies were more linked to the forest type than the environmental conditions, with pine and black cherry exhibiting the highest stress. The functional traits DSA maps provided spatial and temporal patterns related to the drought-induced vegetation stress experienced by the Ticino forests in 2022. Our workflow is suitable to provide quantitative information on the functional state of forests at high spatial resolution (10 m), which are of fundamental importance for designing effective and targeted management and conservation measures.

4. Integrating Drone-Based LiDAR and Multispectral Data for Tree Monitoring

Abstract

[1] Forests are critical for providing ecosystem services and contributing to human well-being, but their health and extent are threatened by climate change, requiring effective monitoring sys- tems. Traditional field-based methods are often labour-intensive, costly, and logistically challenging, limiting their use for large-scale applications. Drones offer advantages such as low operating costs, versatility, and rapid data collection. However, challenges remain in optimising data processing and methods to effectively integrate the acquired data for forest monitoring. This study addresses this challenge by integrating drone-based LiDAR and multispectral data for forest species classification and health monitoring. We developed the methodology in Ticino Park (Italy), where intensive field campaigns were conducted in 2022 to collect tree species compositions, the leaf area index (LAI), canopy chlorophyll content (CCC), and drone data. Individual trees were first extracted from Li- DAR data and classified using spectral and textural features derived from the multispectral data, achieving an accuracy of 84%. Key forest traits were then retrieved from the multispectral data using machine learning regression algorithms, which showed satisfactory performance in estimating the LAI ($R^2 = 0.83$, RMSE = 0.44 m^2 m^{-2}) and CCC ($R^2 = 0.80$, RMSE = 0.33 g m^{-2}). The retrieved traits were used to track species-specific changes related to drought. The results obtained highlight the potential of integrating drone-based LiDAR and multispectral data for cost-effective and accurate forest health monitoring and change detection.

1 The content of this chapter has been published in Drones as Savinelli, B., Tagliabue, G.,., Vignali, L., Garzonio, R., Gentili, R.., Padoa-Schioppa, E., Panigada, C., Rossini, M. (2024). Monitoring functional traits of complex temperate forests using Sentinel-2 data during a severe drought period. Science of the Total Environment, 957, 177428

4.1 Introduction

Maintaining and expanding forest resources is crucial for sustainable development, biodiversity conservation and the provision of essential ecosystem services, including climate mitigation through carbon storage and the provision of goods essential for human well-being (Krieger et al., 2001). However, forest ecosystems face increasing threats from economic pressures, natural hazards, and human-induced disturbances, exacerbated by climate change (Achard et al., 2012; Seidl et al., 2017). In this context, accurate data are essential for the development of targeted forest management strategies aimed at the improvement and long-term conservation of forest ecosystems. Traditional field-based monitoring methods involving in situ data collection are often labour-intensive, costly, logistically challenging, and generally limited to small-scale applications (Guo et al., 2022). As a result, remote sensing has proven to be a viable way to implement forest monitoring on a large scale, enabling the cost- and time-effective acquisition of different vegetation properties, especially structural data (Tang et al., 2015; Wang et al., 2019). Among the remote sensing technologies, drones are gaining popularity due to their ability to efficiently collect high-spatial-resolution data, their ease of use, low operational cost, versatility in hosting different sensors, and high-intensity data collection (Tang et al., 2015; Gini et al., 2018). Drones can be employed in a wide range of applications, like forest inventory, species mapping, and biophysical properties estimation at different scales, from forest landscapes to individual trees and leaves (Torresan et al., 2017; Guimarães et al., 2020). However, despite the advances in drone technology, challenges remain in optimising data processing techniques and methodologies for effective forest monitoring (Shahbazi et al., 2014; Tang et al., 2015; Wallace et al., 2016).

This study aims to advance methods and data processing techniques for drone-based forest monitoring by integrating Light Detection and Ranging (LiDAR) and optical sensors, which together can provide complementary information on forest structure and biophysical properties.

LiDAR technology has become an important tool for assessing and characterising forest ecosystems (van Leeuwen et al., 2010; Toivonen et al., 2023). LiDAR generates high-resolution three-dimensional (3D) point clouds that can provide detailed information on forest structure, including canopy height models, crown density, biomass, and other morpho-functional parameters essential for effective forest management (e.g., Wallace et al., 2016; Chen et al., 2022).

In parallel, multispectral optical cameras can provide other valuable data by measuring vegetation reflectance at different wavelengths. Traditionally, vegetation indices like the NDVI (Normalised Difference Vegetation Index), the EVI (Enhanced Vegetation Index), and other similar vegetation indices are frequently utilised as a proxy of plant health (Rogers et al., 2018). However, these do not

provide a direct measurement of physiological changes in plants; rather, they evaluate variations in tree greenness as an indicator of vegetation health, which does not allow for the immediate or direct identification of plants' physiological states (Anderegg et al., 2019; Le et al., 2023). To overcome this limitation, the retrieval and monitoring of specific plant traits, such as the leaf area index (LAI) and canopy chlorophyll content (CCC) are essential in forest ecosystem monitoring, as they can provide a more direct insight into the physiological status of trees (Myneni et al., 1997; Campos-Taberner et al., 2018; Darvishzadeh et al., 2019).

The LAI, which measures the total leaf area per unit ground area, expresses the forest photosynthetic capacity, canopy structure, and tree productivity (Chen et al., 1992). Similarly, CCC reflects the chlorophyll content of plants, which is essential for photosynthesis and provides an indication of plant health and nutrient status (Gitelson et al., 2005). Both the LAI and CCC are directly related to tree structure and functioning, making them essential metrics for assessing vegetation health and understanding how vegetation responds to environmental change and stressors (Myneni et al., 1997; Campos-Taberner et al., 2018; Darvishzadeh et al., 2019; Wang et al., 2019). Despite their importance, only a few studies have investigated the possibility of retrieving the LAI and CCC from drone-based multispectral sensors in forest ecosystems, e.g., (Singh et al., 2023; Kopacková-Strnadová et al., 2021)

With the overall goal of demonstrating how drones can properly support effective forest monitoring, we conducted a study in 2022 in the Ticino Forest (Northern Italy) aiming to achieve the following objectives:

- Detect individual trees within a natural broadleaf forest using LiDAR drone point cloud data;
- identify tree species by applying object-based classification techniques to multispectral drone imagery;
- retrieve plant traits (i.e., LAI and CCC) from multispectral imagery using machine learning algorithms;
- analyse vegetation trait changes in the Ticino Regional Park Forest during the 2022 summer drought by examining the multifactorial interactions between species-specific responses and microclimatic variability.

By addressing these objectives, this study will provide insights into how drone-based technologies can advance forest monitoring and management practices.

4.2 Materials and Methods

4.2.1. Study area

This study was carried out in the "La Fagiana" Nature Reserve in Magenta (MI), located in Ticino Regional Park, Italy (Figure 1). The park has a total area of 91,800 ha, of which 22,000 ha is the natural forest. It belongs to the Ticino Val Grande Verbano Biosphere Reserve (UNESCO — Man and Biosphere Programme), one of the largest natural riverside parks in Europe. Ticino Regional Park plays a key role in preserving biodiversity in one of the most urbanised areas in Europe. It represents a unique refuge for autochthonous vegetation and constitutes a fundamental ecological corridor between the Alps and the Apennines. The Ticino temperate mixed forests are dominated by oaks (typically English oak, *Quercus robur* L.) and white hornbeam (*Carpinus betulus* L.), with a more scattered presence of black alder (*Alnus glutinosa* L.), sweet chestnut (*Castanea sativa* Mill.), pines (*Pinus* spp.), and allochthonous invasive species such as black cherry (*Prunus serotina* Ehrh.) and black locust (*Robinia pseudoacacia* L.). The forest of "La Fagiana" is largely dominated by the presence of English oak, white hornbeam, and black locust. The reserve includes areas characterised by different microclimatic conditions: xerophilic (red shaded area in Figure 1), mesophilic (yellow shaded area in Figure 1), and meso-hygrophilic (green shaded area in Figure 1). Each of them was classified based on plant species composition, density, and tree habits. The xerophilic area is characterised by the sporadic presence of English oak, which, due to the low soil moisture availability, exhibits shorter heights and different growth habits compared to trees of similar age in the mesophilic and meso-hygrophilic areas. The mesophilic area is characterised by the prevalence of English oak, while the meso-hygrophilic one is composed primarily of the English oak–white hornbeam association (Del Favero, 2002). The Ticino Forest experienced an unprecedented severe and prolonged drought in the summer of 2022, with detrimental impacts on vegetation health (Faranda et al., 2023; Gharun et al., 2024).

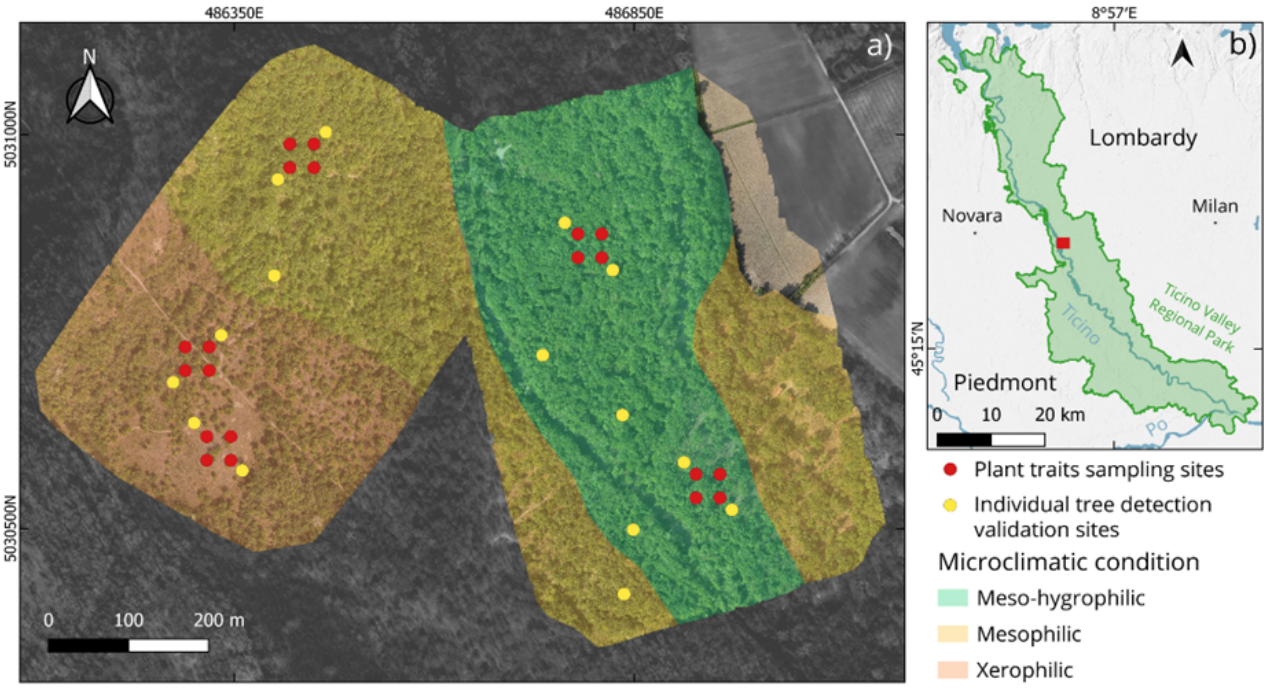

Figure 1. (**a**) RGB image of the "La Fagiana" nature reserve. The red dots indicate the centre of the sites (15 m × 15 m) where the plant traits were sampled, and the yellow dots are the centre of the validation sites (30 m × 30 m) for the individual tree detection. The shaded areas indicate the three main forest areas classified according to the microclimatic condition of the forest: meso-hygrophilic (green), mesophilic (yellow), and xerophilic (red). The Google satellite image of the area in grey scale is used as the basemap. (**b**) The extension of Ticino Park in Northern Italy (green polygon) and the location of the Fagiana area (red polygon).

4.2.2 Field plant trait data collection

In the summer of 2022, plant traits were sampled within two time windows: 21–22 June (1st campaign) and 7–8 September (2nd campaign). The field measurements were collected in the correspondence of five sampling sites of ~30 m × 30 m. The sampling sites were geo-located with a Garmin GPSMAP 66sr (Garmin Ltd., Schaffhausen, Switzerland) and are shown as red squares in Figure 1a. The LAI was estimated through digital hemispherical photos in correspondence of 4 subplots (~15 m × 15 m) for each sampling site. In each subplot, we acquired 5 up-looking digital hemispherical photos (i.e., centre and corners of each subplot) with a Laowa 4 mm f/2.8 fish-eye lens (Venus Optics, Hefei, China) mounted on a Canon EOS M50 Mark II (Canon Inc., Tokyo, Japan). The LAI of the overstory was then calculated using the CAN-EYE software v6.4.95 (https://www6.paca.inrae.fr/can-eye, accessed on 10 October 2024). We processed one subplot at a time and obtained a mean and standard deviation for each subplot, for a total of 20 LAI values in both June and September 2022 (n = 40).

The LCC was obtained from destructive measurements conducted on leaf disc samples. In each site, for each species recognised as dominant, we collected samples from three different trees. From each tree, we sampled 12 leaves from different sunlit branches pulled down with a slingshot from the

top of the canopy. Three pigment extractions, i.e., twelve 0.635 cm diameter leaf discs each, were conducted from twelve leaves. In total, we sampled 56 trees, which included 31 English oaks (372 leaves, 93 pigment extractions), 13 white hornbeams (156 leaves, 39 pigment extractions), and 12 black locusts (144 leaves, 36 extractions). The methodology used for the sample preparation is described in (Tagliabue et al., 2022). The concentrations of chlorophyll a (Chla) and b (Chlb) were then determined by spectrophotometry (V-630 UV-VIS, Jasco, Pfungstadt, Germany) in a 100% methanol extract at 665.2 and 652.4 nm, respectively, while turbidity was checked by measuring absorbance at 750 nm. Chla and Chlb concentrations were calculated using the extinction coefficients proposed by (Lichtenthaler & Buschmann, 2001). The LCC (μg cm^{-2}) was calculated according to Equation (1):

$$LCC = \frac{(Chl_a + Chl_b)}{Area_{tot}} \quad (1)$$

The LCC values of the single trees were aggregated at the sampling site level by weighting for the abundance of the corresponding species. The CCC of each sampling site was then calculated according to Equation (2):

$$CCC = LAI \times LCC \quad (2)$$

4.2.3 Drone data collection

The drone surveys were conducted using a DJI Matrice 300 RTK (DJI Ltd., Shenzhen, China) mounting different payloads (Table 1): a LiDAR DJI Zenmuse L1 sensor (DJI Ltd., Shenzhen, China), a high-resolution RGB camera Zenmuse P1 (DJI Ltd., Shenzhen, China), and a multispectral MAIA S2 camera (SAL Engineering S.r.l., Russi, Italy; EOPTIS, Trento, Italy; Fondazione Bruno Kessler, Trento, Italy).

Table 1. Summary of the sensors and technical details of the drone acquisitions performed in the Ticino Park in 2022.

Drone Platform	DJI Matrice 300 RTK		
	DJI Zenmuse L1	DJI Zenmuse P1	MAIA S2
Dates of Acquisition	28/04/22	28/04/22	01/07/22 and 31/08/22
Flight Height	80 m	120 m	110 m
Point Cloud Density	459 point/m^2	-	-
Ground Sampling Distance (GSD)	-	1.5 cm	5.5 cm
Acquisition Speed	5 m/s	10 m/s	6 m/s
Side Overlap	50%	70%	70%
Forward Overlap	80%	80%	90%

The DJI Zenmuse L1 laser scanner combines data from an RGB sensor and the IMU unit in a stabilised 3-axis gimbal, providing a true-colour point cloud from the RGB sensor. The L1 laser scanner has a beam divergence of 0.28° (vertical) × 0.03° (horizontal) and a maximum of 3 registered reflections. It can operate at a maximum distance of 450 m at 80% reflectivity (190 m at 10% reflectivity) with a recording speed of 480,000 points/second for multiple return acquisition (240,000 points/second for single return). It has a horizontal and vertical system accuracy of 10 cm and 5 cm per 50 m, respectively, and a distance measurement accuracy of 3 cm per 100 m. The DJI Zenmuse P1 camera was used to acquire data for photogrammetric processing. The sensor is a 45 Mpixel CMOS with a size of 35.9 × 24 mm and a pixel size of 4 μm, capable of taking photos with a resolution of 8192 × 5460 pixels. In this study, the camera was mounted with the DL 35 mm F2.8 LS ASPH lens. Detailed information on the L1 and P1 cameras can be found in (Štroner et al., 2021). L1 and P1 flights were performed with a vertical gimbal pitch of −90° (i.e., nadiral) at an altitude of 80 m and 120 m above ground, respectively. LiDAR acquisition results in a point cloud density of 459 points/m^2, while a ground sampling distance of 1.5 cm was obtained for RGB imagery. DJI Pilot software was used for the acquisition, following a single-grid flight pattern with a constant height relative to the take-off point. The flat terrain ensured a constant pixel size and point density in the model without the use of a terrain adaptive flight.

MAIA S2 is composed of an array of nine monochromatic sensors, each with a 1.2 Mpixel resolution (pixel resolution: 1280 × 960, pixel size: 3.75 × 3.75 μm) and their relative pass-band filters. The sensors have the same central wavelength and bandwidth as the first nine bands of the ESA Sentinel-2 multispectral instruments (Nocerino et al., 2017) and acquire data simultaneously using global shutters, allowing synchronised multi-band measurements in a single shot. The sensors have a horizontal and vertical field of view of 35 and 26 degrees, respectively, with a fixed focal

length of 7.6 mm. The system is equipped with a GNSS receiver to record the position and time of each camera shutter activation. The shutter speed was set to automatic mode to minimise motion blur, aiming for 20% exposure. To accurately estimate the reflectance factor, the incoming radiation was measured simultaneously with the multispectral acquisition and in the same bands using a cosine incident light sensor (ILS) mounted on top of the DJI Matrice 300 RTK. The ILS features a GNSS receiver which allowed the ILS and MAIA S2 shots to be synchronised using the GPS time to produce reflectance images with the incoming radiation measured at the exact time of each MAIA S2 acquisition. The images were acquired following a single-grid flight pattern at a constant altitude of 110 m above ground, resulting in a ground sampling distance of 5.5 cm.

The DJI Matrice 300 RTK has a vertical and horizontal hovering accuracy (i.e., manufacturer's declared values) of ±0.1 m in D-RTK mode (Czyza et al., 2023). Drone GNSS receivers implementing the Network Real-Time Kinematic (NRTK) technique were used in the study areas as GNSS signals and mobile network coverage were available. Štroner et al. (2021) conducted full-scale tests on the DJI Zenmuse L1 sensor, demonstrating a positioning accuracy better than the manufacturer's claim, with a precision of 3.5 cm in all directions. Reference (Karolos et al., 2024) combined the use of LiDAR and multispectral data for forest biodiversity measurements by using the initial georeferencing provided by the GNSS systems. LiDAR and RGB drones with Real-Time (RTK) or Post-Processing Kinematic (PPK) georeferencing systems were tested by (Gómez-Gutiérrez et al., 2024). These authors showed that these technologies have potential in hard-to-reach areas (e.g., forest) and produce unbiased point clouds, being the most cost-effective method. According to the previous study, we considered the georeferencing accuracy provided by the NRTK systems to be adequate for our study, and the co-registration or manual alignment of the drone products (i.e., LiDAR point cloud, RGB and MAIA orthophotos) was not necessary.

4.2.4 LIDAR data acquisition and processing

The LiDAR point cloud data were acquired with a DJI Zenmuse L1 mounted on a DJI Matrice 300 RTK in April 2022 for individual tree detection (ITD) and segmentation (ITS). The flight plan settings are shown in Table 1.

Raw point cloud (Figure 2a) data were first optimised using DJI Terra software (DJI Ltd., Shenzhen, China), manually cleaned from noise and outliers with CloudCompare (Girardeau-Montaut, 2016) and then processed in the R environment using "lidR", "rLidar", and "ForestTools" packages (Silva et al., 2017; Plowright, 2018; Roussel et al., 2020). Those packages are widely used to process point cloud data in forestry applications (Hardenbol et al., 2023). The ground point classification (Figure 2b) was performed using a progressive morphological filter (PMF) described

by (Zhang et al., 2003). After point ground classification, a 1 m resolution digital terrain model (DTM) was generated (Figure 2c) using an Inverse distance weighting (IDW) method. The point cloud was normalised (Figure 2d) to create a canopy height model (hereafter CHM). The CHM was generated using point-to-raster (P2R) algorithms, which consist of creating a grid and assigning each pixel the elevation of the highest point it belongs to; in our case, we set the CHM resolution grid to 0.2 m. An IDW method was used to interpolate "empty pixels". Although some authors suggest smoothing the CHM with filters (e.g., Gaussian filter, median filter) prior to crown delineation, our preliminary test showed that smoothing decreased the accuracy of delineation; this issue was also noted by (Hastings et al., 2020). In addition, the CHM smoothing could also affect tree height (Mielcarek et al., 2018). For these reasons, we decided not to smooth the CHM. For the ITD (Figure 2e), a local maximum filter (LMF) described by Popescu and Wynne (2013) was applied to the CHM. According to previous studies, we chose a circular shaped window (Gao et al., 2022) with a 5 m diameter and a minimum height of 2 m.

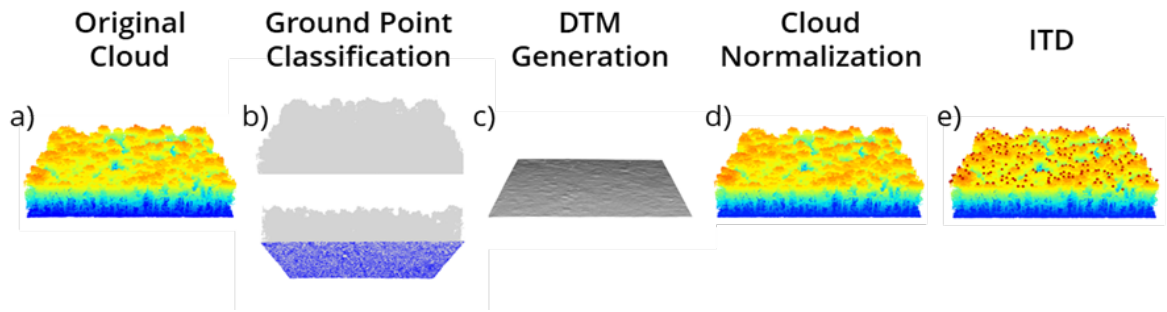

Figure 2. Illustration of the LiDAR data processing workflow. DTM = digital terrain model, ITD = individual tree detection.

For the ITS, many segmentation algorithms are described in the literature (Hastings et al., 2020; Ma et al., 2022) showing high accuracy especially for coniferous forests, while, for deciduous forests, there is still a need for further research, as no widely accepted method has yet been established. We used a marker-controlled watershed (MCWS) method for ITS (Meyer and Beucher, 1990). The markers used to guide the segmentation process were treetops determined by previous ITD. To avoid the tree edges overlapping, shadowing, and possible geometric shifts between LiDAR and MAIA products, we decided to use circular regions of interest (ROI) of 4 m diameter centred on the treetop instead of crown polygons for the classification step, which required the most rigorous training definition. Crown polygons were used only for mapping purposes.

Reference data for the ITD included field observations and photo-interpretations of 15 square 30 m × 30 m plots distributed across the study area (Figure 1a), as in (Mohan et al., 2021). A detected tree was considered matched if the distance between the treetop to the reference tree (treetop/trunk)

was less than 2.5 m. To evaluate the detection accuracy, which is assumed to be point accuracy (Zhen et al., 2016), the recall (r), precision (p), and F-score (F) equations from (Goutte & Gaussier, 2005; Sokolova et al., 2006) were calculated according to Equations (3) – (5):

$$r = \frac{TP}{TP + FN}, \tag{3}$$

$$p = \frac{TP}{TP + FP}, \tag{4}$$

$$F = \frac{2rp}{r + p}. \tag{5}$$

where TP is the number of treetops correctly detected, FN is the number of trees not detected, and FP is the number of extra trees (commission error). r measures the number of trees detected, p is the fairness of detected trees, or precision, and F is the harmonic mean of r and p, thus representing the overall accuracy. All these indices range from 0 to 1. The higher the F value, the better the accuracy of tree detection.

4.2.4.1.RGB and Multispectral Imagery Processing

Drone-based RGB imagery of our study area was acquired on the same date as LiDAR data with a DJI Zenmuse P1 sensor (DJI Ltd., Shenzhen, China) mounted on a DJI Matrice 300 RTK. Sensor characteristics are shown in Table 1. High-resolution imagery was used to verify the position of trees and to identify tree species. The flight patterns were designed in DJI Pilot GUI, (see Table 1 for the main settings). All acquired imagery was processed using Drone2Map software (ESRI, Redlands, CA, USA) to generate two orthomosaics (i.e., one for each flight) with a spatial resolution of 1.5 cm. Drone-based multispectral imagery was acquired using a MAIA S2 multispectral camera. Multispectral image processing followed Rossini et al. (2023). The raw MAIA S2 imagery underwent geometric and radial distortion correction using MultiCam Stitcher Pro (SAL Engineering S.r.l., Russi, Italy). The software, which is integrated with the MAIA, allows the images from each band to be co-registered into a single multispectral image with precise pixel-to-pixel alignment. Pseudo-reflectance was calculated for each pixel as the ratio of the radiance measured by the MAIA S2 to the incident solar radiation measured by the ILS in each spectral channel. The pseudo-reflectance images were then imported in Agisoft Metashape v1.7.2 (Agisoft, St. Petersburg, Russia) to produce the multispectral orthomosaic. The empirical line method (Smith and Milton, 1999) was finally applied

to the pseudo-reflectance orthomosaic to obtain at-ground multispectral reflectance using the calibration coefficients described in Rossini et al. (2023)

4.2.5 Dataset Preparation for Classification

An object-based classification was performed on the multispectral image collected in July 2022. In total, 190 trees were selected, representing the most common tree species in the study area: 80 English oaks, 80 white hornbeams, and 30 black locusts. The number of samples per species reflects the proportion of each species in the study area. The locations of trees in this area were originally collected by GPS and manually improved using the high-resolution RGB orthomosaics.

For each treetop location, a circular ROI of 4 m in diameter was defined and used to extract the spectral and textural features used as input to the random forest classifier.

Regarding the texture features, a grey level co-occurrence matrix (GLCM) was calculated in ENVI 5.6.1 (NV5 Geospatial Solutions Inc., Broomfield, CO, USA) on the red and NIR bands of the multispectral orthomosaic using a 5 × 5 pixel-size window, and the following features were extracted: mean, variance, homogeneity, contrast, dissimilarity, entropy, second moment, and correlation.

The classification was performed with the Random Forest classifier. It is an ensemble classifier that utilises a set of classification and regression algorithms (CARTs) to make a prediction (Breiman, 2001). The classification result (the response) is determined by a majority vote for each tree (Belgiu and Drăgu, 2016). In the last few years, RF has become widely used in several remote sensing applications (Belgiu and Drăgu, 2016; Ma et al., 2021; Liu et al., 2021). Thereby, the RF classifier was chosen to classify the tree species in “La Fagiana” Forest in the Ticino Park Valley. The training set was composed of 133 randomly selected trees. After the training phase, the RF algorithm was applied to the output of the segmentation, consisting of a polygon per tree crown with associated average spectral and textural features extracted from the MAIA S2 data.

The RF classification was performed using the R package “randomForest” (Liaw and Wiener, 2002), one of the most used RF implementations (Belgiu and Drăgu, 2016). According to Lawrence et al. (2006), the parameter Ntree was set to 500, and Mtry used for each node was the square root of the total number of input variables. The accuracy of the tree species classification using MAIA multispectral images was assessed through the confusion matrix (CM), by calculating the overall accuracy (OA), Kappa coefficient (k), producer’s accuracy (PA), and user’s accuracy (UA) (Story and Congalton, 1986).

4.2.6 Plant trait retrieval workflow

4.2.6.1. Machine Learning

Plant trait retrieval was performed using a machine learning approach developed using a broader forest dataset of LAI and CCC field measurements coupled with hyperspectral data acquired by the PRISMA spaceborne sensor (Cogliati et al., 2021). The dataset consists of 50 paired field and spectral data (n = 50) and was collected in Ticino Park over a considerably larger area that could not be covered by the drone flights (Tagliabue et al., 2023). This allowed a wide range of conditions in terms of forest microclimatic conditions, structures and condition to be included in the training dataset. The PRISMA spectra were resampled to the MAIA S2 bands (Figure 3), and several State-of-the-Art machine learning regression algorithms (MLRAs) were tested within the Automated Radiative Transfer Model Operator (ARTMO) machine learning regression algorithm toolbox (Caicedo et al., 2014; Verrelst et al., 2011). The MLRA tested included: Gaussian Processes Regression (GPR), Support Vector Regression (SVR), Partial Least Squares Regression (PLSR), Neural Networks (NNs), and Random Forest (RF).

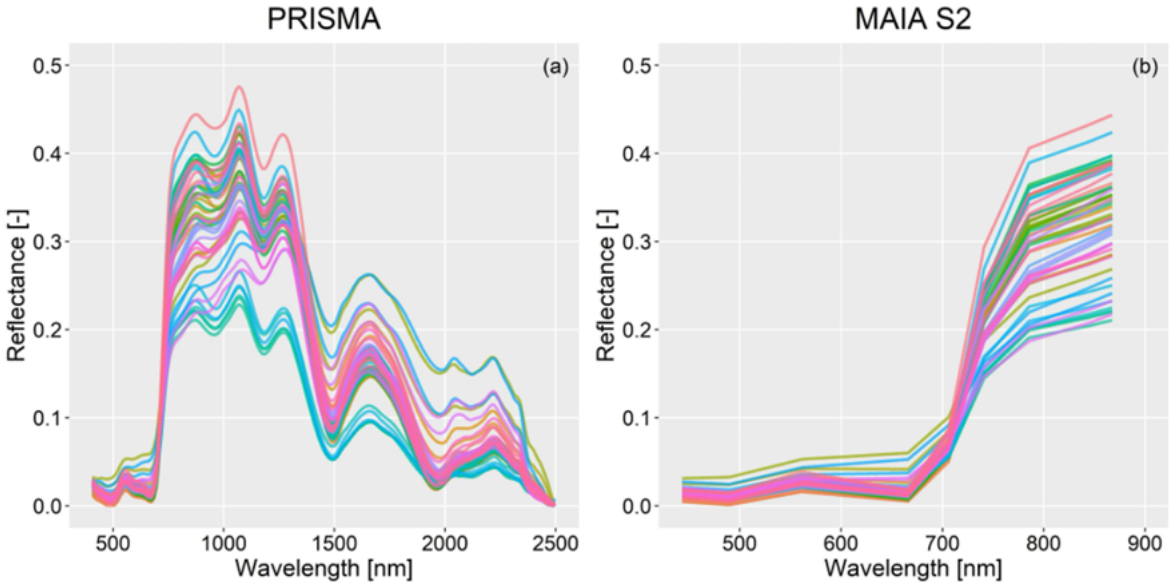

Figure 3. (**a**) Hyperspectral reflectance spectra collected by the PRISMA satellite in correspondence of the sampling sites where the field data were collected (n = 50); (**b**) PRISMA spectra resampled to the MAIA S2 spectral bands and used for the training of the machine learning regression algorithms (n = 50).

The MLRA models were cross-validated using a k-fold cross validation strategy (k = 6), and the model performance was evaluated in terms of standard goodness-of-fit statistics: coefficient of determination (R^2), root mean square error (RMSE), normalised RMSE (nRMSE) (i.e., RMSE/range

of measured values), bias (i.e., mean of estimated values—mean of measured values), and relative bias (rbias) (i.e., bias/mean of measured values) between measured and estimated values. The developed models were then applied to the real MAIA S2 spectra collected in Ticino Park and validated against the independent field dataset collected in the Fagiana Forest near simultaneously the drone overpasses and described above (n = 40). To produce the drone-based maps, the MLRA models that provided the best results for the LAI and CCC were applied to the segmentation output, consisting of a polygon per tree crown with the associated average MAIA S2 spectrum. The maps were generated for the MAIA S2 images collected on both 1 July 2022 and 31 August 2022.

3.2.5.2. Analysis of plant traits

A statistical analysis was carried out to test whether the retrieved traits (i.e., the LAI and CCC) differed based on three factors: forest microclimatic condition, species, and time. The latter was tested to analyse whether the drought that occurred in the summer of 2022 had an effect on the LAI and CCC, considering that plants in the Ticino Park normally enter the senescence phase towards late October. Instead, here, we tested the differences between the values obtained from the drone images taken in early (1 July 2022) and late (31 August 2022) summer. The analysis was performed using a three-way analysis of variance (ANOVA). Where results were significant, a post hoc Tukey test was performed to test the significance of the differences between pairs of group means. Both tests were performed in R 3.6.3.

4.3 Results and Discussion

4.3.1 Individual Tree Detection

The implementation of ITD from LiDAR data gave satisfactory results for the 236 trees analysed. The overall recall rate (r) was 0.73, ranging from 0.53 to 1, the overall precision rate (p) was 0.74, also ranging from 0.53 to 1, and the overall F-score was 0.74, with a range from 0.55 to 1 (Table 2). These metrics indicate a robust performance for tree detection. Higher F-scores were obtained in stands with lower tree density and reduced canopy overlap, while denser canopies and greater crown overlap resulted in lower F-scores. This trend is common in deciduous mixed forests, where complex crown shapes and vertical structures can reduce the detection accuracy (Hastings et al., 2020; Zhen et al., 2016). The lower accuracy of some plots may be linked to the use of an LMF to define the treetop, which can lead to overcounting in trees with complex canopy structures, such as in oak–hornbeam forests, where it is often not straightforward to identify a single crown centre treetop

(Tanhuanpää et al., 2016; Huang et al., 2018). Furthermore, in dense forest stands with a closed canopy, crown overlap further complicates the search for and the correct identification of local maxima (Vauhkonen et al., 2012; Yang et al., 2019).

Table 2. Individual tree detection (ITD) accuracy from LiDAR. TP = number of correctly detected treetops, FN = number of trees not detected, FP = number of extra trees (commission error).

Site ID	Ground-Truth/Photointerp.	ITD	TP	FN	FP	Recall Rate (r)	Precision Rate (p)	F-Score (F)
1	7	8	7	0	1	1	0.875	0.933
2	21	20	15	6	5	0.714	0.75	0.731
3	9	9	9	0	0	1	1	1
4	16	17	9	7	8	0.562	0.529	0.545
5	19	16	14	5	2	0.737	0.875	0.8
6	5	7	4	1	3	0.8	0.571	0.667
7	16	17	13	3	4	0.812	0.765	0.788
8	16	16	9	7	7	0.562	0.562	0.562
9	15	14	8	7	6	0.533	0.571	0.552
10	19	18	15	4	3	0.789	0.833	0.811
11	20	23	16	4	7	0.8	0.696	0.744
12	17	13	10	7	3	0.588	0.769	0.667
13	16	18	13	3	5	0.812	0.722	0.765
14	26	21	20	6	1	0.769	0.952	0.851
15	14	17	11	3	6	0.786	0.647	0.709
Total	236	234	173	63	61	0.733	0.739	0.736

Our accuracy results were achieved by testing many processing parameter combinations, such as local maxima window size (3, 5, and 7 m diameter) and filtering (e.g., Gaussian). In fact, the choice of point cloud processing parameters, such as CHM resolution (Miraki et al., 2021), filtering method (Mielcarek et al., 2018), size and shape of the local maxima window (Gao et al., 2022; Lisiewicz et al., 2022), and segmentation algorithm used (Ma et al., 2022; Zaforemska et al., 2019) strongly influence the ITD accuracy.

Our results are consistent with similar studies conducted in structurally complex mixed forests. Reference (van Leeuwen et al., 2010) reported an average F-score of 0.66 ± 0.01 using a similar algorithm in a mixed broadleaved forest. The higher accuracy achieved in our study might have been determined by the use of an unprocessed CHM, which, according to (Mielcarek et al., 2018), is more reliable than the smoothed CHM because of the more accurate reproduction of the crown shapes. Ref. (Ma et al., 2022) achieved, in mixed natural forest plots, an r of 0.72–0.85, a p of 0.58–0.51, and an

F-score of about 0.64 using a local maximum algorithm. Notably, the stands analysed by Ma et al., (2022) are made up of a mixture of deciduous and coniferous species, a feature that simplifies the treetop identification process and therefore probably determines the higher precision of tree identification in some stands compared to our results. This was also the case of (Mohan et al., 2021). They applied a similar workflow to mixed plots dominated by longleaf pine (*Pinus palustris*) and turkey oak (*Quercus laevis* Walter), achieving an F-score of 0.86. Their higher tree detection performance is likely due to the inclusion of both deciduous and evergreen coniferous species. In fact, coniferous species are generally easier to detect and distinguish due to their characteristic conical crown shape, which makes treetop identification easier compared to broadleaved trees (Hastings et al., 2020; Ma et al., 2022). Moreover, as highlighted by (Zhen et al., 2016), most segmentation algorithms assume a conical crown structure, thus ensuring better results when applied to coniferous species. On the contrary, tree identification for deciduous forests is still an open challenge, as there is no widely accepted and accurate method.

In addition to the species composition, variations in ITD accuracy can be linked to other ecological factors such as canopy closure (Sterenczak, 2013; Gao et al., 2022; Ma et al., 2022). Gao et al. (2022) tested different LM window sizes in forest types with different density conditions, finding that the optimal LM window size is highly species- and density-specific, significantly influencing detection accuracy (F-scores = 0.82–0.91). In our study, we used a single LM window size across all species and canopy density conditions due to the presence of mixed-species plots in our study area, which likely explains our comparatively lower accuracy. Zaforemska et al., (2019) achieved an r of 0.85, a p of 0.70, and an F-score of 0.77 in a mixed plot dominated by sycamore (*Acer pseudoplatanus* L.) and English oak using an MCWS algorithm. Overall, the better F-score value may be related to the number of reference trees used, which was significantly lower than ours.

4.3.2 Classification of forest species

The random forest classification achieved a high overall accuracy of 84% and a Kappa coefficient of 0.74 (Table 3). Black locust was classified with 100% accuracy, while some misclassification occurred between white hornbeam and English oak (PA = 75% and 88%, respectively) due to their higher spectral similarity. The algorithm was trained with 133 tree crown objects and validated with 57 tree crown objects. The resulting drone-based species map (Figure 4) illustrates the spatial distribution of English oak, white hornbeam, and black locust.

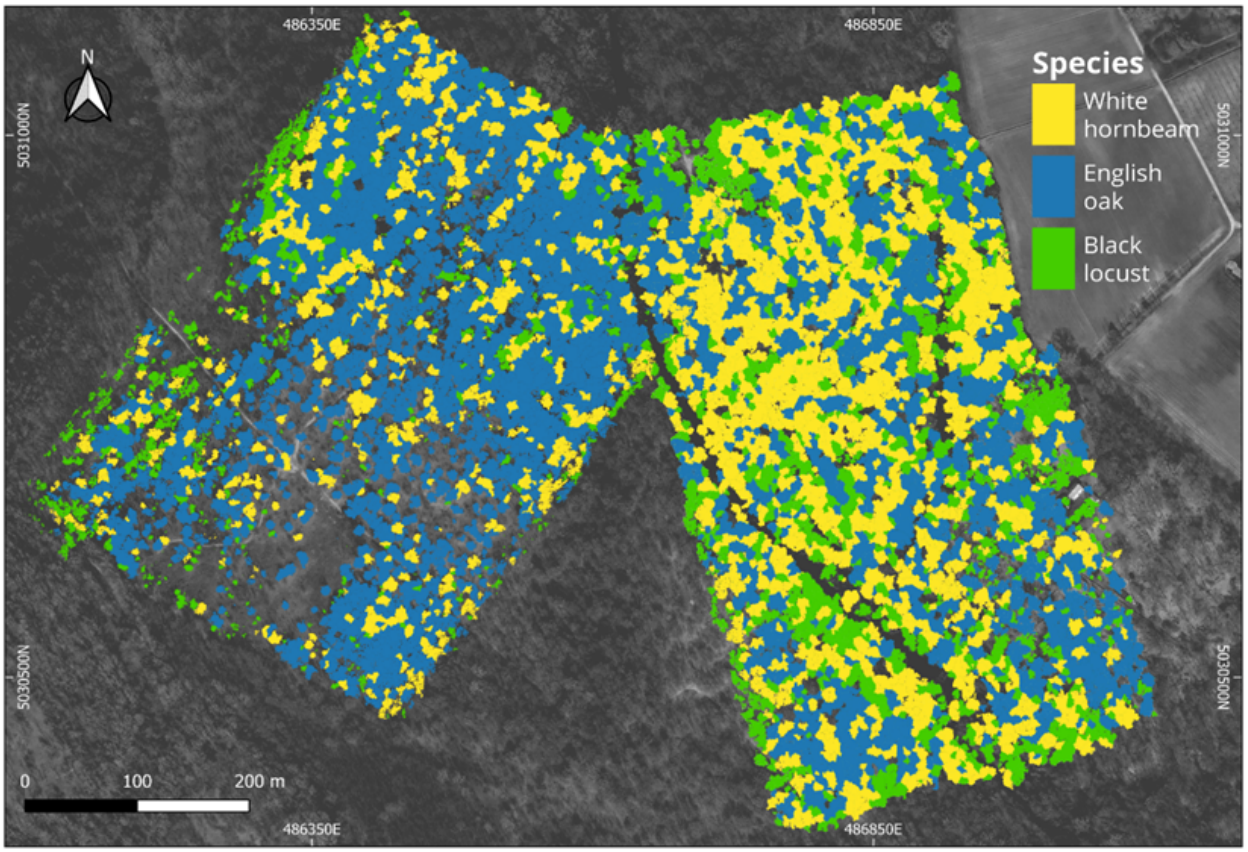

Figure 4. Drone-based classification of the tree species in the Fagiana Forest obtained from the MAIA S2 multispectral sensor using a random forest classifier. The Google satellite image of the area in grey scale is used as the basemap.

Table 3. Accuracy of random forest (RF) classification of three tree species based on 133 trees for training and 57 independent trees for validation. PA = Producer Accuracy; UA = User Accuracy; k = Kappa coefficient; and OA = Overall Accuracy.

		Reference				
	Class	**White hornbeam**	**English oak**	**Black locust**	**Total**	**UA**
Classification	**White hornbeam**	18	3	0	21	0.86
	English oak	6	21	0	27	0.78
	Black locust	0	0	9	9	1
	Total	24	24	9	57	**OA** = 0.84
	PA	0.75	0.88	1		**k** = 0.74

Comparing our results with other studies is not so straightforward due to differences in the number of species classified, training size, and the different features taken into consideration. However, examining comparable research on object-based tree species classification reveals several factors likely contributing to the high accuracy in our study.

Firstly, the inclusion of textural metrics in addition to spectral features in our classification process likely enhanced accuracy. For instance, our classification accuracy was slightly higher than similar studies that did not incorporate textural metrics, such as (Franklin & Ahmed, 2017), who

reported 78% accuracy with four species. Similar findings were reported by Mishra et al. (2018) (73% of accuracy), Xu et al. (2020) (64.85% of accuracy), Sivanandam and Lucieer, (2022) (77% of accuracy), and Gini et al. (2018) (78% of accuracy) who consistently observed improved results when texture-based metrics were included in the classification process. Secondly, the fact that MAIA S2 is one of the multispectral sensors with the highest number of spectral channels likely contributed to our improved classification performance compared to studies that used lower-resolution sensors, such as (Franklin and Ahmed, 2017; Mishra et al., 2018)

However, our accuracy was lower compared to studies focusing on conifer species. Franklin and Ahmed, (2017) reported a user accuracy of 87% in a coniferous forest using multispectral drone images. Immitzer et al., (2012) achieved 95% accuracy and a Kappa coefficient of 0.95 in an RF classification in a temperate forest, where two of the four species were coniferous, using the eight spectral bands of the WorldView-2 satellite (comparable to those of the MAIA sensor used in this study). In general, conifers are characterised by easier tree top identification and a greater spectral differentiation between species (Zhen et al., 2016). These findings were also confirmed by (Immitzer et al., 2019), who achieved an overall species classification accuracy of 90% for conifers and 80% for broadleaves when analysing multi-temporal datasets of Sentinel-2 images.

Concerning the species distribution in our study area, Figure 4 shows how English oak is the dominant species in the xerophilic area of the Fagiana Forest (highlighted in red in Figure 1), although it is also evident that English oak density is relatively low. This likely reflects the trees' adaptation to the limited water availability. Indeed, reduced forest density increases the trees' resistance to water scarcity by minimising competition for scarce resources (Hille Ris Lambers et al., 2002).

In the mesophilic areas of the Fagiana Forest (highlighted in yellow in Figure 1), a noticeably denser English oak canopy cover can be observed (Figure 4), indicating more favourable soil moisture conditions, which also support the sporadic presence of white hornbeam (Neuhäusl, 1977). The meso-hygrophilic areas of the Fagiana Forest (highlighted in green in Figure 1) are dominated by white hornbeam trees, which, mixed with English oaks, form an oak–hornbeam association, typical of the Ticino Forest. This association is indicative of moister soil conditions, as evidenced by the taller tree and denser foliage compared to the xerophilic zones. In contrast, black locust is the least represented species, confined to distinct patches mainly along the edges of the mapped area, and with few individual trees scattered throughout the different forest microclimatic conditions (Figure 4).

3.3.3 Plant trait retrieval

The cross-validation statistics of the models calculated between the measured field data and the estimated data retrieved from the PRISMA dataset resampled to the MAIA S2 spectral configuration

(n = 50) are shown in Table 4. Overall, both the LAI and CCC showed very high performance in cross-validation. More specifically, the LAI was estimated with high accuracy with all the investigated MLRA (R^2 = 0.84–0.90, nRMSE = 8.66–11.01%), whereas CCC showed a more variable performance depending on the MLRA used (R^2 = 0.68–0.83, nRMSE = 9.17–13.08%). Among the MLRA, the kernel-based algorithms (i.e., SVR, GPR) and PLSR showed the highest predictive capacity.

Table 4. Summary of the cross-validated statistics (k = 6) calculated on the coupled measured and estimated values retrieved from the PRISMA dataset resampled to the MAIA S2 spectral configuration (n = 50) for Leaf Area Index (LAI) and Canopy Chlorophyll Content (CCC): algorithm (GPR = Gaussian Processes Regression; SVR = Support Vector Regression; PLSR = Partial Least Squares Regression; NN = Neural Networks; RF = Random Forest), coefficient of determination (R^2); root mean square error (RMSE); normalised RMSE (nRMSE), bias, relative bias (rbias).

Plant Traits	Algorithm	R^2	RMSE	nRMSE	bias	rbias
LAI	GPR	0.90	0.26 m^2 m^{-2}	8.66%	0.0108 m^2 m^{-2}	0.49%
	SVR	0.90	0.27 m^2 m^{-2}	8.81%	0.0059 m^2 m^{-2}	0.27%
	PLSR	0.90	0.28 m^2 m^{-2}	9.04%	0.0113 m^2 m^{-2}	0.51%
	NN	0.85	0.33 m^2 m^{-2}	10.69%	0.0125 m^2 m^{-2}	0.57%
	RF	0.84	0.34 m^2 m^{-2}	11.01%	0.0032 m^2 m^{-2}	0.15%
CCC	GPR	0.68	0.23 g m^{-2}	13.08%	0.0370 g m^{-2}	3.89%
	SVR	0.83	0.16 g m^{-2}	9.17%	−0.0051 g m^{-2}	−0.54%
	PLSR	0.83	0.17 g m^{-2}	9.33%	0.0084 g m^{-2}	0.88%
	NN	0.79	0.19 g m^{-2}	10.69%	−0.0488 g m^{-2}	−5.13%
	RF	0.70	0.22 g m^{-2}	12.22%	0.0153 g m^{-2}	1.61%

The goodness-of-fit metrics calculated between the field dataset collected near-simultaneously the drone acquisitions and the drone-based retrievals obtained by applying the developed MLRA models to the MAIA S2 spectra (n = 40) are shown in Table 5. As expected, the results obtained using an independent validation dataset are slightly worse than those obtained in cross-validation on the PRISMA dataset resampled to the MAIA S2 spectral resolution. Still, both the LAI and CCC were accurately estimated. GPR, SVR, and PLSR showed the highest predictive capacity for both the LAI (R^2 = 0.81 – 0.83, nRMSE = 14.18 – 16.39%) and CCC (R^2 = 0.79 – 0.80, nRMSE = 22.45 – 27.7%). Using the fully independent dataset and the actual MAIA S2 data, all models showed a slight to moderate tendency to overestimate compared to the field data (rbias = 4.8 – 43.23%), especially for CCC. The scatter plots showing the measured and estimated values obtained from the MAIA S2 sensor for the LAI and CCC are shown in Figure 5 and Figure 6, respectively.

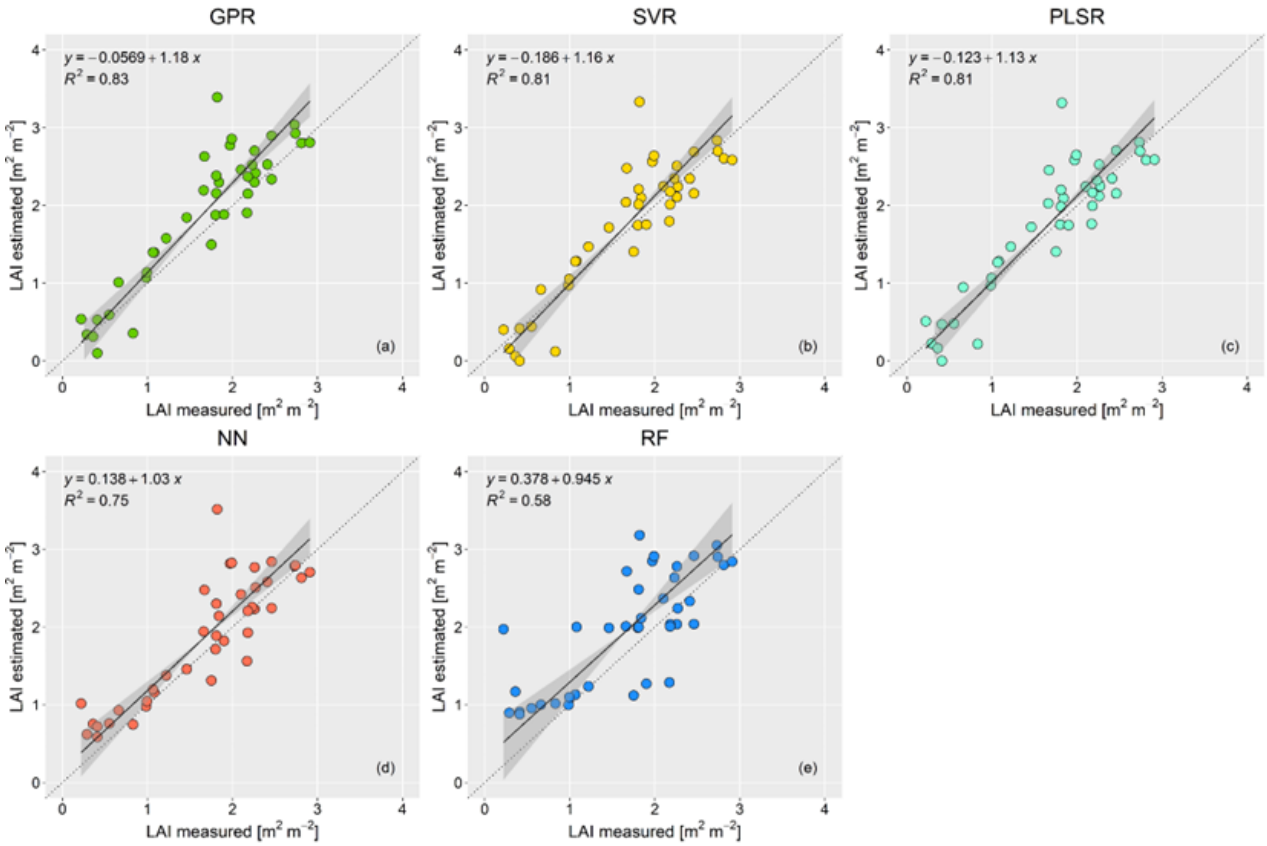

Figure 5. Scatter plots showing the measured and estimated leaf area index (LAI) values obtained from the MAIA S2 sensor with different machine learning regression algorithms: (**a**) Gaussian processes regression (GPR); (**b**) support vector regression (SVR); (**c**) partial least squares regression (PLSR); (**d**) neural network (NN); and (**e**) random forest (RF). The grey shaded areas indicate the confidence intervals (0.95) of the regression lines (solid lines) using reduced major axis (RMA) regression. The dotted line represents the 1:1 line.

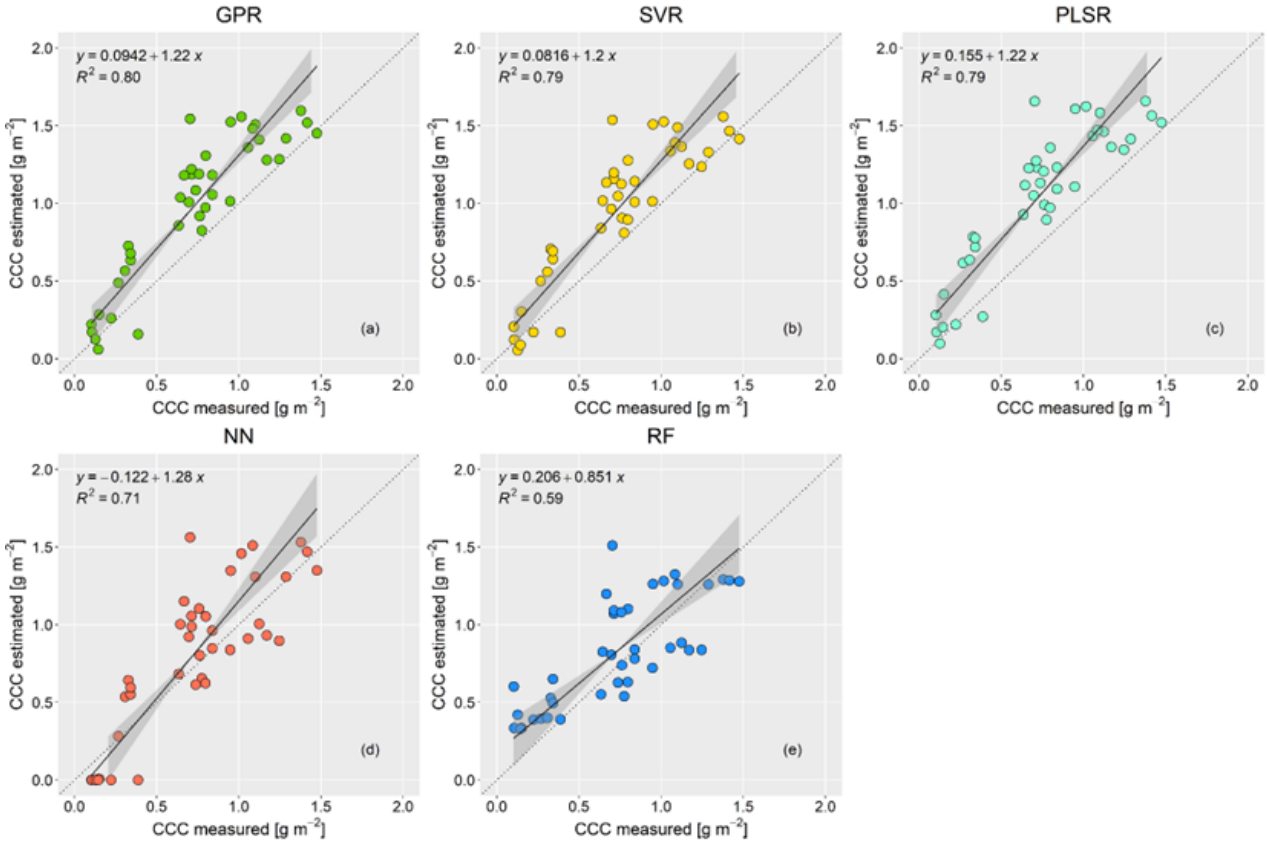

Figure 6. Scatter plots showing the measured and estimated canopy chlorophyll content (CCC) values obtained from the MAIA S2 sensor with different machine learning regression algorithms: (**a**) Gaussian processes regression (GPR); (**b**) support vector regression (SVR); (**c**) partial least squares regression (PLSR); (**d**) neural network (NN); and (**e**) random forest (RF). The grey shaded areas indicate the confidence intervals (0.95) of the regression lines (solid lines) using reduced major axis (RMA) regression. The dotted line represents the 1:1 line.

Table 5. Summary of the statistics calculated on the coupled measured and estimated values retrieved from the MAIA S2 sensor (n = 40) for leaf area index (LAI) and canopy chlorophyll content (CCC): algorithm (GPR = Gaussian processes regression; SVR = support vector regression; PLSR = partial least squares regression; NN = neural network; RF = random forest), the coefficient of determination (R^2), root mean square error (RMSE), normalised RMSE (nRMSE), bias, and relative bias (rbias).

Plant Trait	Algorithm	R^2	RMSE	nRMSE	bias	rbias
LAI	GPR	0.83	0.44 m^2 m^{-2}	16.39%	0.24 m^2 m^{-2}	14.35%
	SVR	0.81	0.39 m^2 m^{-2}	14.36%	0.08 m^2 m^{-2}	4.80%
	PLSR	0.81	0.38 m^2 m^{-2}	14.18%	0.09 m^2 m^{-2}	5.34%
	NN	0.75	0.44 m^2 m^{-2}	16.53%	0.20 m^2 m^{-2}	11.74%
	RF	0.58	0.59 m^2 m^{-2}	22.00%	0.29 m^2 m^{-2}	17.12%
CCC	GPR	0.80	0.33 g m^{-2}	24.02%	0.26 g m^{-2}	35.10%
	SVR	0.79	0.31 g m^{-2}	22.45%	0.23 g m^{-2}	31.03%
	PLSR	0.79	0.38 g m^{-2}	27.70%	0.32 g m^{-2}	43.23%
	NN	0.71	0.27 g m^{-2}	19.95%	0.08 g m^{-2}	11.57%
	RF	0.58	0.27 g m^{-2}	19.84%	0.10 g m^{-2}	13.41%

Overall, the results obtained in this study are promising towards the development of effective and consolidated retrieval schemes for the estimation of forest traits using drone-based sensors. The LAI and CCC were accurately estimated using an effective approach based on an MLRA trained on a reasonable amount of data, which could be easily applied to similar conditions or updated by adding more training samples to extend its applicability. Previous studies using drone data to estimate plant traits have mainly focused on crops, e.g., (Singhal et al., 2019; Abdelbaki et al., 2021; Chakhvashvili et al., 2022; Narmilan et al., 2022), while only a few studies have dealt with forests (e.g., Kopacková-Strnadová et al., 2021; Singh et al., 2023). The literature reports promising results in the retrieval of leaf or canopy chlorophyll content using a look-up table (LUT) or MLRA-based approaches. Zhang et al., (2024) used a hybrid approach based on radiative transfer simulations coupled with an artificial neural network to estimate the LCC and CCC of apple orchards from DJI Phantom 4 multispectral data, achieving an R^2 of 0.73 and 0.79 and RMSE of 6.63 and 28.48 μg cm^{-2}, respectively. Narmilan et al. (2022) used the same sensor to estimate the LCC of sugarcane using the MLRA applied on vegetation indices, with R^2 = 0.68 – 0.98. Chakhvashvili et al. (2022) used MicaSense Dual multispectral data to retrieve the LCC and CCC of maize using an LUT-based approach, obtaining RMSE = 3.74 – 4.92 μg cm^{-2} and RMSE = 33.1 μg cm^{-2}, respectively. Such results are in line with ours (R^2 = 0.80, RMSE = 0.33 g m−2, nRMSE = 24.02%), though we targeted a forest canopy which adds complexity to the retrieval because of the structure. In these ecosystems, previous studies have found contrasting results: Kopacková-Strnadová et al. (2021) estimated the LCC of Norway spruce from Parrot Sequoia data with moderate accuracy (R^2 = 0.45 – 0.49), while Singh et al. (2023) achieved very good results in retrieving the LCC of Himalayan pine from MicaSense RedEdge data using an LUT-based approach (R^2 = 0.94, RMSE = 6.20 μg cm^{-2}).

The retrieval of the LAI is often reported to be more challenging, especially in complex canopies with mixed sunlit and shaded pixels (Chakhvashvili et al., 2022; Zhang et al., 2024). The presence of shadows, rows, and varying leaf angles in fact confounds the signal, posing difficulties in the accurate quantification of the LAI. Chakhvashvili et al. (2022) obtained an RMSE of 0.61 – 0.7 m^2 m^{-2} in the estimation of the LAI of maize, which has a more complex geometry compared to turbid medium crops, and Zhang et al., (2024) achieved R^2 = 0.74 and RMSE = 0.28 m^2 m^{-2} in the retrieval of the LAI of apple orchards. In beech forests, Chianucci et al., (2016) estimated the LAI from a drone-based RGB camera with R^2 = 0.59 – 0.7. In our study, the good results obtained (R^2 = 0.83, RMSE = 0.44 m^2 m^{-2}) indicate that the problem of different lighting conditions at the high spatial resolution of the drones is probably mitigated by using the average crown reflectance instead of a pixel-based retrieval, which is in line with the findings of Kopacková-Strnadová et al., (2021).

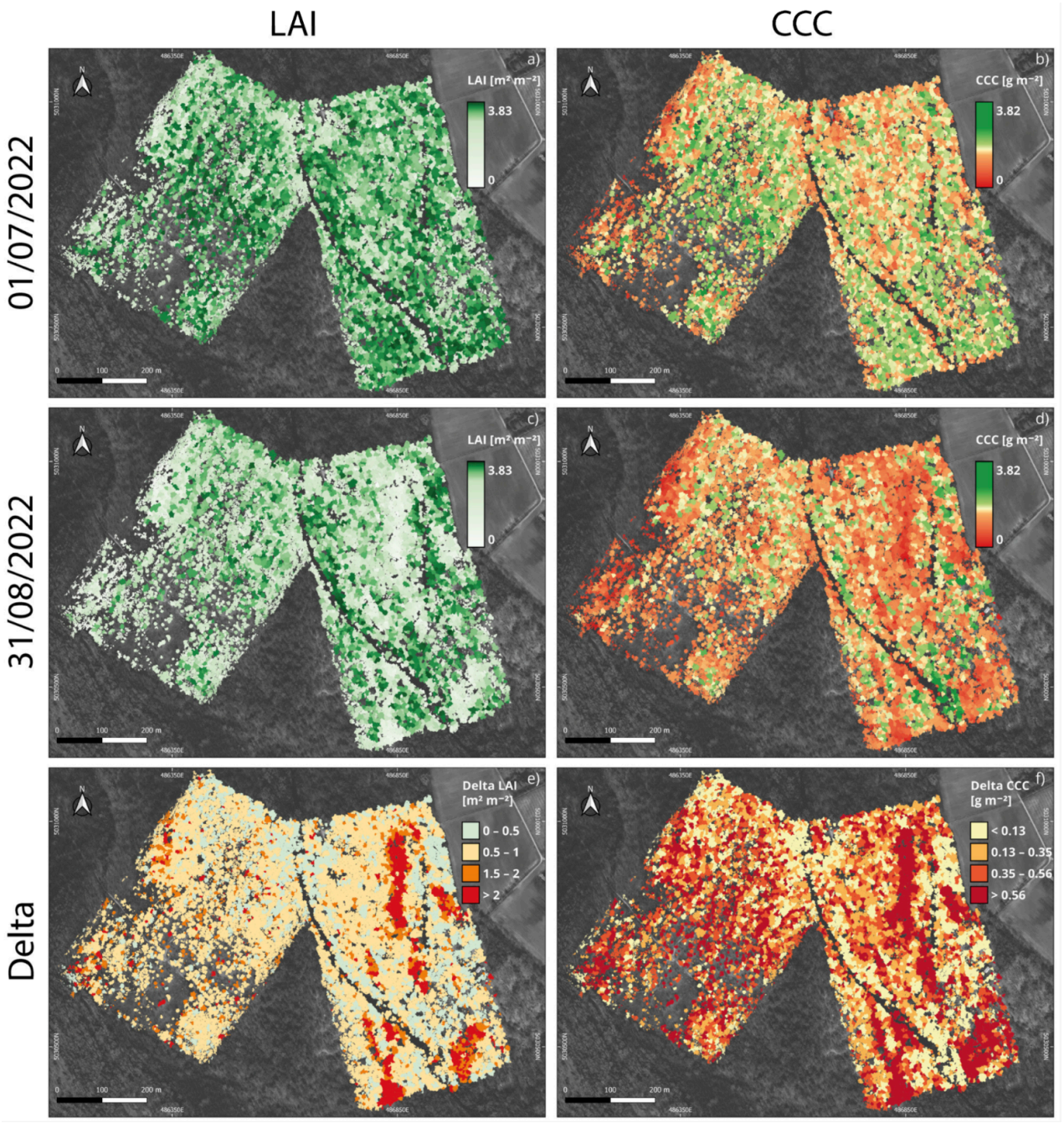

Figure 7. Drone-based maps obtained from the MAIA S2 sensor using machine learning regression algorithms: (**a**,**b**) maps of the leaf area index (LAI) and canopy chlorophyll content (CCC) obtained from drone images collected on 1 July 2022; (**c**,**d**) maps of the LAI and CCC obtained from drone images collected on 31 August 2022; and (**e**,**f**) maps of the delta LAI and CCC obtained as the difference between the LAI and CCC values retrieved from the drone images collected on 31 August 2022 and 1 July 2022.

Figure 7 shows the LAI and CCC maps of the Fagiana Forest obtained by applying the best performing MLRA to the MAIA S2 segmented images acquired on 01/07/22 and 31/08/22. A significant reduction in the LAI and CCC (indicative of biomass loss and chlorosis) is evident between these two dates (Figure 7e,f), likely as a result of the persistent drought of summer 2022 (Faranda et al., 2023; Gharun et al., 2024). In the Fagiana Forest, CCC exhibited a stronger decline

(Figure 7f) compared to the LAI (Figure 7e). This suggests that CCC may be a more sensitive indicator in detecting the effects of water shortage on vegetation functionality compared to the LAI. This result is consistent with previous studies showing the higher sensitivity of chlorophyll content compared to the LAI for assessing the condition of English oak trees in Ticino Park (Rossini et al., 2007; Savinelli et al., 2024).

3.3.4 Functional traits analysis

The ANOVA results showed that LAI values were significantly influenced by time, forest microclimatic conditions, and species (Table 6). The pairwise interaction between time and forest microclimatic conditions indicated a poorly significant interaction, suggesting that the LAI varies consistently through time across the three different microclimatic conditions. Differently, the pairwise interaction analysis indicated a highly significant interaction between time and species, suggesting that temporal changes in the LAI differ considerably across different species (Table 6, Figure 8a). Specifically, the Tukey post hoc test revealed a significant decrease in the LAI between 1 July 2022 and 31 August 2022 for both white hornbeam (−16%) and English oak trees (−12%). In contrast, no statistically significant change was observed for black locust during this period (Figure 8a). Notably, black locust already had a low mean LAI value in June compared to the other two species.

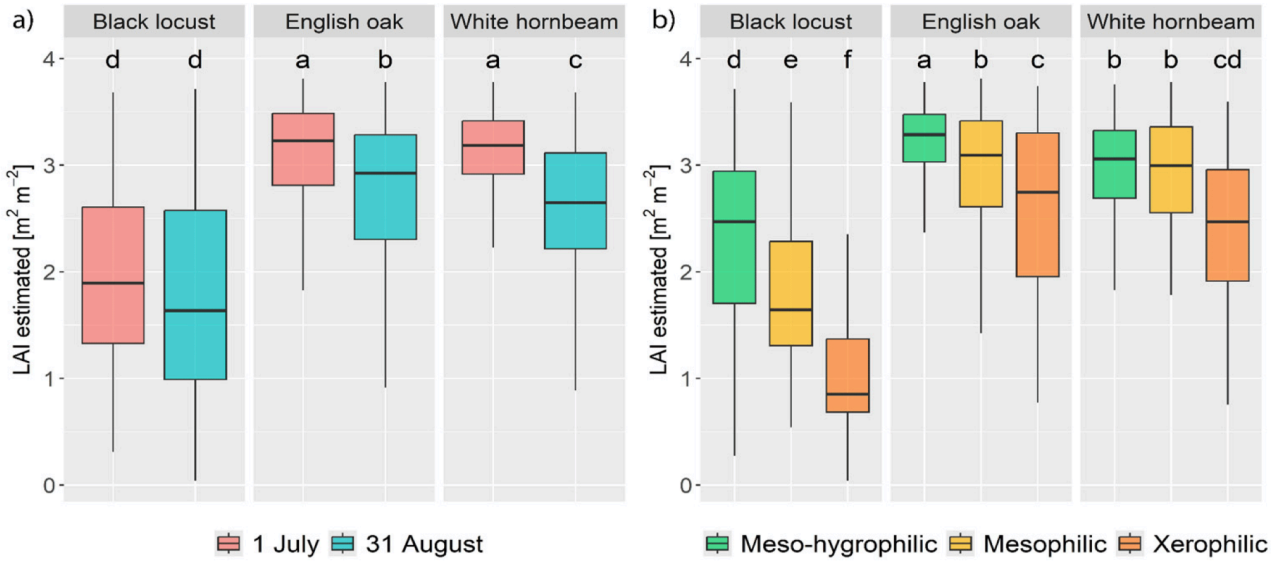

Figure 8. Boxplot of LAI against retrieval day (**a**) and forest microclimatic conditions (**b**). Different lowercase letters indicate statistically significant differences, while equal lowercase letters indicate no statistically significant difference.

Table 6. LAI results of the ANOVA test (n = 1700). Significance codes: '***' 0.001, '**' 0.01, '*' 0.05, '-' 0.1.

LAI	Df	Sum Sq	Mean Sq	F Value	Pr(>F)	Significance
Time	1	55.992	55.99	157.27	$<1 \times 10^{-16}$	***
Forest microclimatic conditions	2	99.38	49.69	139.56	$<1 \times 10^{-16}$	***
Species	2	244.65	122.32	343.58	$<1 \times 10^{-16}$	***
Time × Forest microclimatic conditions	2	2.002	1.001	2.81	0.060	-
Time × Species	2	5.42	2.71	7.61	0.0005	***
Forest microclimatic conditions × Species	4	20.65	5.16	14.50	1.20×10^{-11}	***
Time × Forest microclimatic conditions × Species	4	2.74	0.68	1.92	0.104	no
Residuals	1682	598.83	0.36			

The ANOVA analysis also revealed a statistically significant interaction between forest microclimatic conditions and species, indicating that the LAI differs significantly across various forest microclimatic conditions for the same species (Table 6, Figure 8b). For the black locust species, the LAI of the mesophilic forest is 22% lower than the meso-hygrophilic one and 55% lower when comparing the meso-hygrophilic and xerophilic environments (Figure 8b). In the case of white hornbeam, only the differences in the LAI between meso-hygrophilic and xerophilic forest were significant (with a reduction of 20%) (Figure 8b). For English oak, the differences in the LAI among the different forest microclimatic conditions were also significant, with a reduction of 7% between meso-hygrophilic and mesophilic, and a reduction of 18% when comparing the meso-hygrophilic and xerophilic forest.

The CCC analysis and, in this case, the ANOVA results, indicated that CCC values were significantly influenced by time, forest microclimatic condition, and species (**Table 7**). A significant interaction between time and species was observed, suggesting that temporal changes in CCC differ substantially between species (Table 7, Figure 9a). The Tukey post hoc test revealed a significant decrease in CCC between 1 July 2022 and 31 August 2022 for black locust (−14%), white hornbeam (−21%), and English oak trees (−18%). Similar to the LAI results, black locust had a lower initial CCC compared to the other two species (Figure 9a). However, in this case, the decrease in CCC for black locust between July and the end of August was statistically significant.

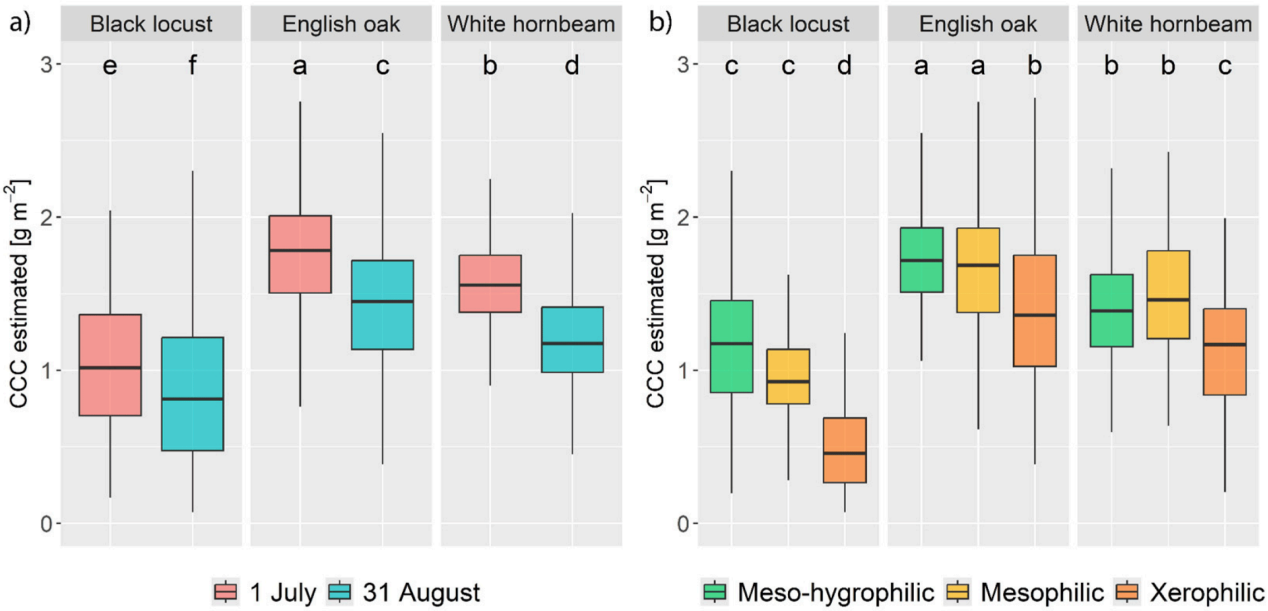

Figure 9. Boxplot of the CCC against retrieval day (**a**) and forest type (**b**). Different lowercase letters indicate statistical differences, while equal lowercase letters indicate no statistical difference.

Table 7. CCC results of the ANOVA test (n = 1700). Significance codes: '***' 0.001, '**' 0.01, '*' 0.05, '-' 0.1.

CCC	Df	Sum Sq	Mean Sq	F Value	Pr (>F)	Significance
Time	1	38.67959	38.67959	259.817	$<1 \times 10^{-16}$	***
Forest microclimatic conditions	2	32.07746	16.03873	107.735	$<1 \times 10^{-16}$	***
Species	2	87.68159	43.8408	294.486	$<1 \times 10^{-16}$	***
Time × Forest microclimatic conditions	2	0.999662	0.499831	3.35745	0.0351	*
Time × Species	2	1.867992	0.933996	6.27381	0.0019	**
Forest microclimatic conditions × Species	4	6.435499	1.608875	10.8071	1.19×10^{-8}	***
Time × Forest microclimatic conditions × Species	4	1.609187	0.402297	2.70229	0.0291	*
Residuals	1682	250.4032	0.148872			

This suggests that CCC may be a more sensitive indicator of drought-induced vegetation stress compared to the LAI. In fact, as the product between LCC and the LAI, CCC can capture information on vegetation plant chlorosis and canopy biomass, thus providing a deeper insight into the physiological status of plants.

The ANOVA analysis also revealed a statistically significant interaction between forest microclimatic conditions and species, indicating that CCC differs for the same species significantly across various forest microclimatic conditions (Table 7, Figure 9b). The Tuckey post hoc test confirmed a statistically significant difference in CCC between the meso-hygrophilic forest and xeric environments for the three species analysed (Figure 8b). In the case of black locust, the reduction in

CCC between meso-hygrophilic and xeric forest was −56%, whereas, for white hornbeam and English oak, it was −18%.

Overall, both white hornbeam and English oak showed a decrease in the LAI and CCC when comparing the values obtained on 1 July 2022 and 31 August 2022, thus confirming the efficiency of the drone-based estimation of functional traits to detect a drought-induced variation. This result is in line with what was observed by PRISMA in the Ticino Forest between June and early September (Tagliabue et al., 2023). Moreover, in the case of English oak, our results align with Panigada et al., (2010), who described discolouration episodes in 10 different English oak stands in Ticino Park during the 2003 summer heatwave, highlighting the susceptibility of English oak to water scarcity and high temperatures and the effectiveness of remotely sensed CCC in detecting English oak stress.

In contrast, black locust showed a less pronounced decline in functional traits between June and the end of August 2022 compared to the other two species analysed. However, it already exhibited an unusually low LAI in June, with a mean value of 1.9 m^2 m^{-2}, for a broadleaf species at the peak of the vegetative season. Field observations during the sampling campaign confirmed that black locust trees had relatively small canopies and appeared to be in poor health. This pre-existing condition could explain the lack of a significant reduction in the LAI over time, as the species was already under stress. Thus, although black locust is generally recognised for its stress tolerance, its non-significant reduction in functional traits under drought conditions in the Fagiana Forest context could be due to its compromised health, rather than a distinctive tolerance to the lack of water. Colangelo et al., (2018) reported the decline of this species in the Ticino Forest, underlying the species' vulnerability to climate change in this region. Puchałka et al. (2021) further supports this by suggesting that black locust distribution models predict its decline in Southern Europe, potentially leading to a northward range shift favoured by future warmer climatic conditions.

The drone-based functional trait retrieval effectively captured the variation in the LAI and CCC among the three analysed species within the different forest microclimatic conditions. Both LAI and CCC values were higher in the meso-hygrophilic and mesophilic forest area, compared with the xerophilic one. This reflects the general smaller tree leaf size and reduced canopy in the drier forest area, as a form of adaptation to the lower water moisture availability (Meier and Leuschner, 2008)

3.3.5 Strength and Limitations

The results of this study highlighted the importance of integrating drone-based multiple sensors, which together provided a comprehensive and accurate analysis of the Fagiana forest ecosystem. On the one hand, we obtained the precise spatial reconstruction of both forest structure and species composition. On the other hand, the proposed integrated approach allowed the accurate quantification

of forest functional traits (the LAI and CCC). The drone-based high-resolution tree-level data obtained offer valuable and detailed insights into forest structure and ecological processes, accounting for variations related to species and forest microclimatic conditions. The processing workflow was optimised for automation and based entirely on open-source software, ensuring both efficiency and accessibility. Therefore, this approach can be applied in similar contexts.

The developed methodology, by providing an automated workflow for the accurate reconstruction of forest structure and plant trait retrieval, represents an important step forward in the understanding and parameterisation of process-based ecological models for estimating the gross primary productivity of forest ecosystems, which is fundamental for assessing and predicting fluctuations in carbon storage due to inter- and intra-seasonal variations in climate variables.

Despite the promising results, certain limitations were encountered in the proposed processing workflow. Firstly, the tree detection accuracy was not always high due to challenges in segmenting complex canopies and correctly identifying treetops. To address this, advances in segmentation algorithms for broadleaf species are needed to improve the automatic identification of treetops and tree crowns. Moreover, varying the processing parameters (e.g., CHM resolution, CHM smoothing, and LM window size) according to canopy conditions (dense or sparse) and species types could further improve detection accuracy (Gao et al., 2022). Secondly, the species classification accuracy could potentially be enhanced through the use of multitemporal multispectral data (Lisein et al., 2015; Grybas and Congalton, 2021). Grybas and Congalton, (2021) demonstrated that utilising data from three different acquisition dates significantly improved species classification accuracy compared to relying on data from a single date (no further benefits were observed beyond three dates). Finally, although the plant traits were accurately quantified, the retrieval approach used has some limitations that may hinder the application of the workflow in different contexts. Data-driven approaches based on machine regression algorithms, although remarkably powerful, typically come at the expense of transferability (Wang et al., 2023; Wan et al., 2024). In addition, they can be biassed by the characteristics of the sensor used in the training phase, in this case, the PRISMA data. To broaden the applicability of the developed methodology, the use of hybrid approaches based on the combination of radiative transfer simulations and machine learning regression could be explored. However, this task is not trivial in forest ecosystems and at the high spatial resolution of drones due to the complexity of the canopy structure, which requires the use of geometric models that are difficult to parameterise and computationally expensive (Qi et al., 2017; Miraglio et al., 2020).

The proposed solution provides a relatively simple retrieval workflow, which represents a trade-off between generalisability and operability.

4.4 Conclusion

In this study, we demonstrated the effectiveness of integrating drone-based LiDAR and multispectral cameras to support forest monitoring. Specifically, our proposed method successfully detected individual trees within a dense broadleaf forest using drone-based LiDAR point cloud data, achieving high accuracy despite the inherent challenges of distinguishing broadleaf species, which are generally harder to differentiate than conifers.

The high tree detection accuracy also contributed to the strong performance of the object-based classification techniques applied to the multispectral MAIA S2 images. The classification accuracy was slightly higher than in similar studies, likely due to the inclusion of textural metrics and the higher resolution of the MAIA S2 sensor. Black locust was classified with greater accuracy compared to white hornbeam and English oak, likely due to spectral similarities between the latter species.

The retrieval of plant traits such as the LAI and CCC from multispectral imagery using machine learning models also performed well, showing high accuracy when compared to field data. The best-performing algorithm for both the LAI and CCC was GPR. The functional trait maps obtained revealed a significant reduction in the LAI and CCC in the Fagiana Forest when comparing the acquisition in July and the end of August 2022, as a consequence of the severe drought in the summer of 2022. English Oak and white hornbeam species experienced marked reductions in both traits, while black locust showed less pronounced changes, possibly due to its pre-existing poor health in Ticino Regional Park.

These results underline the effectiveness of the proposed workflow in effectively collecting information on forest structure and species composition, as well as quantitatively estimating forest functional traits. This method provides a powerful tool for forest managers to track and respond to climate impacts on diverse forest species.

5. Conclusions

5.1 Synthesis of the main results

The main objective of this thesis was to propose innovative remote sensing methodologies to advance the monitoring of forest functionality and biodiversity. We wanted to enhance our understanding of how forest ecosystems function and respond to change, taking into consideration species composition and environmental characteristic. To achieve this objective, multi-source remote sensing data collected at various temporal and spatial scales were analyzed to extract quantitative information on key plant physiological and functional traits.

First, we investigated the state of art on Sentinel-2 time series studies for the quantitative estimation and monitoring of forest stress, in order to highlight the opportunities and challenges associated with using time series for monitoring forest stress. Secondly, we develop a framework for detecting forest stresses throughout multi-year daily anomalies of key functional traits. Finally, we proposed a drone-based methodology to provide forest structure, species composition, and plant status information at tree level, integrating LiDAR and multispectral data.

These works were presented in Chapter 2, 3 and 4 of this thesis, respectively. The main outcomes of each chapter are summarised below, together with some concluding remarks and potential future perspectives of this work.

Chapter 2 presents a systematic literature review of studies using Sentinel-2 satellite data for forest stress detection. The review focuses on methodologies using high-resolution time-series imagery to detect changes in tree spectral characteristics associated with stress.

The review highlights three primary approaches used for forest stress detection:

- Trend Analysis: This method involves analysing temporal trends in spectral indices to identify gradual changes in forest health and vigour.
- Anomaly/Change Detection: This approach detects deviations from a reference baseline by comparing spectral index values from specific periods, indicating sudden changes or outlier patterns.
- Machine Learning: These techniques, including pixel-based classification, are employed to classify healthy and stressed forest areas. Studies used Random Forest or advanced deep learning algorithms and various spectral bands and vegetation indices to achieve the best performance.

The chapter concludes identifying anomaly/change detection as the most promising approach as it enables the recognition of subtle changes by examining deviations from typical spectral patterns, accounting for natural seasonal variations in spectral signatures. This is an effective method that allows the early detection of forest stress signs, before pronounced declining trends become evident.

Chapter 3 investigates the functional responses of different forest types in the Ticino Regional Park (Italy) to the severe drought of 2022. The study focuses on the analysis of Leaf Area Index (LAI), Canopy Chlorophyll Content (CCC), and Canopy Water Content (CWC) anomaly time series derived from Sentinel-2 data.

Key findings include:

- S2 Toolbox allowed for the accurate retrieval of plant traits, the best results were obtained for for LAI (R^2 = 0.75, nRMSE = 11.49 %) and CCC (R^2 = 0.82, nRMSE = 13.56 %), while slightly worse results were obtained for CWC (R^2 = 0.64, nRMSE = 8.84 %). The accurate retrieval of LAI, CCC and CWC enabled the analysis of the temporal and spatial variations of the daily standardised anomalies (DSA).
- CCC reached the most negative DSA values, highlighting its higher sensitivity in detecting the effects of water shortage compared to CWC and LAI.
- Drought related anomalies were linked to forest types, with pine and black cherry exhibited the highest stress response. Differently, hygrophilic black alder and chestnut were the least impacted.

Chapter 4 focuses on using drone-based LiDAR and multispectral data to assess forest functionality and biodiversity at a finer scale, complementing the findings of Chapter 3. The study was conducted in the "La Fagiana" Nature Reserve within the Ticino Regional Park, focusing on individual tree detection, species classification, and functional trait estimation.

The key results include:

- The integration of drone-based LiDAR and multispectral data proved effective for individual tree detection (F-score: 0.74), tree species classification (accuracy of 84%), and monitoring vegetation traits like LAI (R^2 =0.83) and CCC (R^2 =0.80).
- The tree response to the severe drought of 2022 was species-specific, demonstrating how CCC is more sensitive than LAI in detecting drought-induced stress, particularly in English oaks.
- Black locust showed pre-existing stress conditions with an unusually low initial LAI.

5.2 Concluding remarks and outlook

In this Ph.D. thesis, multiple approaches for monitoring forest across different spatial and temporal scales were evaluated and discussed. Through comprehensive analysis, we identified gaps in existing forest monitoring methodologies and developed innovative solutions to address them. The work focused on two complementary approaches: (1) developing robust time series analysis methods using daily standardized anomalies of key functional traits to detect and map forest stress distribution, and (2) establishing an integrated multi-sensor drone-based monitoring system for detailed local-scale forest characteristic assessment.

Overall, the results obtained effectively demonstrated the strength of remote sensing for monitoring forest status over time, offering a scalable, cost-effective alternative to traditional field-based methods, enabling detailed monitoring of forest health and resilience under environmental stressors. In particular, the results underlie how plant traits anomaly serves as a particularly sensitive indicator of drought stress. Moreover, it emerges how species-specific information is critical for accurate forest health assessments.

Together, the proposed approaches provide new insights into forest ecosystem dynamics and contribute to more effective management and conservation strategies.

Bibliography

Abdelbaki, A., Schlerf, M., Retzlaff, R., Machwitz, M., Verrelst, J. and Udelhoven, T., 2021. Comparison of crop trait retrieval strategies using UAV-based VNIR hyperspectral imaging. *Remote Sensing*, 13(1748). https://doi.org/10.3390/rs13091748

Achard, F. and Hansen, M.C., 2012. *Global forest monitoring from Earth observation*. Boca Raton, FL: CRC Press Taylor & Francis.

Adams, H.D., Zeppel, M.J., Anderegg, W.R., Hartmann, H., Landhäusser, S.M., Tissue, D.T., Huxman, T.E., Hudson, P.J., Franz, T.E., Allen, C.D. and Anderegg, L.D., 2017. A multi-species synthesis of physiological mechanisms in drought-induced tree mortality. *Nature Ecology & Evolution*, 1(9), pp.1285-1291. https://doi.org/10.1038/s41559-017-0248-x

Ali, A.M., Darvishzadeh, R., Skidmore, A., Gara, T.W., O'Connor, B., Roeoesli, C., Heurich, M. and Paganini, M., 2020. Comparing methods for mapping canopy chlorophyll content in a mixed mountain forest using Sentinel-2 data. *International Journal of Applied Earth Observation and Geoinformation*, 87, p.102037. https://doi.org/10.1016/j.jag.2020.102037

Allen, C.D., Macalady, A.K., Chenchouni, H., Bachelet, D., McDowell, N., Vennetier, M., Kitzberger, T., Rigling, A., Breshears, D.D., Hogg, E.H., Gonzalez, P., Fensham, R., Zhang, Z., Castro, J., Demidova, N., Lim, J.-H., Allard, G., Running, S.W., Semerci, A. and Cobb, N., 2010. A global overview of drought and heat-induced tree mortality reveals emerging climate change risks for forests. *Forest Ecology and Management*, 259, pp.660-684. https://doi.org/10.1016/j.foreco.2009.09.001

Anderegg, W.R.L., Anderegg, L.D.L. and Huang, C.W., 2019. Testing early warning metrics for drought-induced tree physiological stress and mortality. *Global Change Biology*, 25(7), pp.2459-2469. https://doi.org/10.1111/gcb.14655

Arend, M., Link, R.M., Patthey, R., Hoch, G., Schuldt, B. and Kahmen, A., 2021. Rapid hydraulic collapse as cause of drought-induced mortality in conifers. *Proceedings of the National Academy of Sciences*, 118(16), p.e2025251118. https://doi.org/10.1073/pnas.2025251118

Arthur, G., Jonathan, L., Juliette, C., Nicolas, L., Christian, P. and Hugues, C., 2024. Spatial and remote sensing monitoring shows the end of the bark beetle outbreak on Belgian and north-eastern France Norway spruce (*Picea abies*) stands. *Environmental Monitoring and Assessment*, 196(3), p.226. https://doi.org/10.1007/s10661-023-11333-y

Asner, G.P., Brodrick, P.G., Anderson, C.B., Vaughn, N., Knapp, D.E. and Martin, R.E., 2016. Progressive forest canopy water loss during the 2012–2015 California drought. *Proceedings of the National Academy of Sciences*, 113(2), pp.E249-E255. https://doi.org/10.1073/pnas.1523397113

Barka, I., Lukeš, P., Bucha, T., Hlásny, T., Strejček, R., Mlčoušek, M. and Křístek, Š., 2018. Remote sensing-based forest health monitoring systems–case studies from Czechia and Slovakia. *Central European Forestry Journal*, 64(3-4), pp.259-275.

Bárta, V., Lukeš, P. and Homolová, L., 2021. Early detection of bark beetle infestation in Norway spruce forests of Central Europe using Sentinel-2. *International Journal of Applied Earth Observation and Geoinformation*, 100, p.102335.

Belgiu, M. and Drăgu, L., 2016. Random forest in remote sensing: A review of applications and future directions. *ISPRS Journal of Photogrammetry and Remote Sensing*, 114, pp.24-31.

Binh, N.A., Hauser, L.T., Salinero-Delgado, M., Hoa, P.V., Thao, G.T.P. and Verrelst, J., 2024. Monitoring mangrove traits through optical Earth observation: Towards spatio-temporal scalability using cloud-based Sentinel-2 continuous time series. *ISPRS Journal of Photogrammetry and Remote Sensing*, 214, pp.135-152.

Bonan, G.B., 2008. Forests and climate change: forcings, feedbacks, and the climate benefits of forests. *Science*, 320(5882), pp.1444-1449.

Breiman, L., 2001. Random Forests. *Machine Learning*, 45, pp.5-32.

Brodrick, P.G. and Asner, G.P., 2017. Remotely sensed predictors of conifer tree mortality during severe drought. *Environmental Research Letters*, 12(11), p.115013.

Brodrick, P.G., Anderegg, L.D.L. and Asner, G.P., 2019. Forest drought resistance at large geographic scales. *Geophysical Research Letters*, 46, pp.2752–2760. https://doi.org/10.1029/2018GL081108.

Brun, P., Psomas, A., Ginzler, C., Thuiller, W., Zappa, M. and Zimmermann, N.E., 2020. Large-scale early-wilting response of Central European forests to the 2018 extreme drought. *Global Change Biology*, 26(12), pp.7021-7035. https://doi.org/10.1111/gcb.15360.

Brockerhoff, E.G., Barbaro, L., Castagneyrol, B., Forrester, D.I., Gardiner, B., González-Olabarria, J.R., Lyver, P.O.B., Meurisse, N., Oxbrough, A., Taki, H. and Thompson, I.D., 2017. Forest biodiversity, ecosystem functioning and the provision of ecosystem services. *Biodiversity and Conservation*, 26, pp.3005-3035.

Brovkina, O., Cienciala, E., Zemek, F., Lukeš, P., Fabianek, T. and Russ, R., 2017. Composite indicator for monitoring of Norway spruce stand decline. *European Journal of Remote Sensing*, 50(1), pp.550-563.

Bustamante, M.M., Roitman, I., Aide, T.M., Alencar, A., Anderson, L.O., Aragão, L., Asner, G.P., Barlow, J., Berenguer, E., Chambers, J. and Costa, M.H., 2016. Toward an integrated monitoring framework to assess the effects of tropical forest degradation and recovery on carbon stocks and biodiversity. *Global Change Biology*, 22(1), pp.92-109.

Caicedo, J.P.R., Verrelst, J., Munoz-Mari, J., Moreno, J. and Camps-Valls, G., 2014. Toward a semiautomatic machine learning retrieval of biophysical parameters. *IEEE Journal of Selected Topics in Applied Earth Observations and Remote Sensing*, 7, pp.1249–1259.

Campos-Taberner, M., Moreno-Martínez, Á., García-Haro, F., Camps-Valls, G., Robinson, N., Kattge, J. and Running, S., 2018. Global estimation of biophysical variables from Google Earth Engine platform. *Remote Sensing*, 10, p.1167. https://doi.org/10.3390/rs10081167.

Candotti, A., De Giglio, M., Dubbini, M. and Tomelleri, E., 2022. A Sentinel-2 based multi-temporal monitoring framework for wind and bark beetle detection and damage mapping. *Remote Sensing*, 14(23), p.6105.

Ceccato, P., Flasse, S., Tarantola, S., Jacquemond, S. and Gregoire, J.M., 2001. Detection vegetation water content using reflectance in the optical domain. *Remote Sensing of Environment*, 77, pp.22–23.

Chakhvashvili, E., Siegmann, B., Muller, O., Verrelst, J., Bendig, J., Kraska, T. and Rascher, U., 2022. Retrieval of crop variables from proximal multispectral UAV image data using PROSAIL in maize canopy. *Remote Sensing*, 14, p.1247.

Chazdon, R.L., 2008. Beyond deforestation: restoring forests and ecosystem services on degraded lands. *Science*, 320(5882), pp.1458–1460.

Chen, J.M. and Black, T.A., 1992. Defining leaf area index for non-flat leaves. *Plant, Cell and Environment*, 15, pp.421–429.

Chen, Q., Gao, T., Zhu, J., Wu, F., Li, X., Lu, D. and Yu, F., 2022. Individual tree segmentation and tree height estimation using leaf-off and leaf-on UAV-LiDAR data in dense deciduous forests. *Remote Sensing*, 14, p.2787.

Chen, Q., Timmermans, J., Wen, W. and van Bodegom, P.M., 2022. A multi-metric assessment of drought vulnerability across different vegetation types using high resolution remote sensing. *Science of the Total Environment*, 832, p.154970. https://doi.org/10.1016/j.scitotenv.2022.154970.

Chianucci, F., Disperati, L., Guzzi, D., Bianchini, D., Nardino, V., Lastri, C. and Corona, P., 2016. Estimation of canopy attributes in beech forests using true colour digital images from a small fixed-wing UAV. *International Journal of Applied Earth Observation and Geoinformation*, 47, pp.60–68.

Colangelo, M., Camarero, J.J., Ripullone, F., Gazol, A., Sánchez-Salguero, R., Oliva, J. and Redondo, M.A., 2018. Drought decreases growth and increases mortality of coexisting native and introduced tree species in a temperate floodplain forest. *Forests*, 9, p.205.

Colombo, R., Meroni, M., Marchesi, A., Busetto, L., Rossini, M., Giardino, C. and Panigada, C., 2008. Estimation of leaf and canopy water content in poplar plantations by means of hyperspectral indices and

inverse modeling. *Remote Sensing of Environment*, 112(4), pp.1820–1834. https://doi.org/10.1016/j.rse.2007.09.005.

Cogliati, S., Sarti, F., Chiarantini, L., Cosi, M., Lorusso, R., Lopinto, E., Miglietta, F., Genesio, L., Guanter, L., Damm, A. et al., 2021. The PRISMA imaging spectroscopy mission: Overview and first performance analysis. *Remote Sensing of Environment*, 262, p.112449.

Czyza, S., Szuniewicz, K., Kowalczyk, K., Dumalski, A., Ogrodniczak, M. and Zieleniewicz, Ł., 2023. Assessment of accuracy in unmanned aerial vehicle (UAV) pose estimation with the real-time kinematic (RTK) method on the example of DJI Matrice 300 RTK. *Sensors*, 23, p.2092.

Darvishzadeh, R., Skidmore, A., Abdullah, H.Y., Cherenet, E., Ali, A.M., Nieuwenhuis, W. and Paganini, M., 2019. Mapping leaf chlorophyll content from Sentinel-2 and RapidEye data in spruce stands using the invertible forest reflectance model. *International Journal of Applied Earth Observation and Geoinformation*, 79, pp.58–70. https://doi.org/10.1016/j.jag.2019.03.003

De Petris, S., Sarvia, F. and Borgogno-Mondino, E., 2021. A new index for assessing tree vigour decline based on Sentinel-2 multitemporal data. *Application to Tree Failure Risk Management*.

Del Favero, R., 2002. *I tipi forestali della Lombardia*. Cierre, Verona.

Descals, A., Verger, A., Yin, G., Filella, I. and Peñuelas, J., 2023. Widespread drought-induced leaf shedding and legacy effects on productivity in European deciduous forests. *Remote Sensing in Ecology and Conservation*, 9(1), pp.76–89.

Drusch, M., Del Bello, U., Carlier, S., Colin, O., Fernandez, V., Gascon, F., Hoersch, B., Isola, C., Laberinti, P., Martimort, P. and Meygret, A., 2012. Sentinel-2: ESA's optical high-resolution mission for GMES operational services. *Remote Sensing of Environment*, 120, pp.25–36.

Ellenberg, H., 1974. Zeigerwerte der Gefässpflanzen Mitteleuropas. *Scripta Geobotanica*, 9, pp.1–97.

FAO, 2020. The State of World's Forests, Forests, Biodiversity and People. FAO, Rome. Available at: https://www.fao.org/documents/card/en/c/cb9360en

Faranda, D., Pascale, S. and Bulut, B., 2023. Persistent anticyclonic conditions and climate change exacerbated the exceptional 2022 European-Mediterranean drought. *Environmental Research Letters*, 18, p.034030. https://doi.org/10.1088/1748-9326/acbc37

Farooq, M., Hussain, M., Wahid, A. and Siddique, K.H.M., 2012. Drought stress in plants: an overview. In: Aroca, R. (ed.), *Plant responses to drought stress: From morphological to molecular features*, Springer, Berlin, pp.1–33.

Filippa, G., Cremonese, E., Galvagno, M., Isabellon, M., Bayle, A., Choler, P., Carlson, B.Z., Gabellani, S., Morra di Cella, U. and Migliavacca, M., 2019. Climatic drivers of greening trends in the Alps. *Remote Sensing*, 11, p.2527. https://doi.org/10.3390/rs11212527

Foley, J.A., Asner, G.P., Costa, M.H., Coe, M.T., DeFries, R., Gibbs, H.K., Howard, E.A., Olson, S., Patz, J., Ramankutty, N. and Snyder, P., 2007. Amazonia revealed: forest degradation and loss of ecosystem goods and services in the Amazon Basin. *Frontiers in Ecology and the Environment*, 5(1), pp.25–32.

Forner, A., Valladares, F. and Aranda, I., 2018. Mediterranean trees coping with severe drought: Avoidance might not be safe. *Environmental and Experimental Botany*, 155, pp.529–540. https://doi.org/10.1016/j.envexpbot.2018.08.006

Fourty, T. and Baret, F., 1997. Vegetation water and dry matter contents estimated from top-of-the-atmosphere reflectance data: a simulation study. *Remote Sensing of Environment*, 61, pp.34–45. https://doi.org/10.1016/S0034-4257(96)00238-6

Franklin, S.E. and Ahmed, O.S., 2017. Deciduous tree species classification using object-based analysis and machine learning with unmanned aerial vehicle multispectral data. *International Journal of Remote Sensing*, 39, pp.5236–5245.

Galiano, L., Martínez-Vilalta, J. and Lloret, F., 2011. Carbon reserves and canopy defoliation determine the recovery of Scots pine 4 years after a drought episode. *New Phytologist*, 190, pp.750–759. https://doi.org/10.1111/j.1469-8137.2010.03628.x

Gao, T., Gao, Z., Sun, B., Qin, P., Li, Y. and Yan, Z., 2022. An integrated method for estimating forest-canopy closure based on UAV LiDAR data. *Remote Sensing*, 14, p.4317.

García-Haro, F.J., Campos-Taberner, M., Moreno, A., Torbern Tagesson, H., Camacho, F., Martinez, B., Sanchez, S., Piles, M., Camps-Valls, G. and Yebra, M., 2020. A global canopy water content product from AVHRR/Metop. *ISPRS Journal of Photogrammetry and Remote Sensing*, 162, pp.77–93. https://doi.org/10.1016/j.isprsjprs.2020.02.007

Gharun, M., Shekhar, A., Xiao, J., Li, X. and Buchmann, N., 2024. Effect of the 2022 Summer Drought across Forest Types in Europe. *EGUsphere*.

Gibson, L., Lee, T.M., Koh, L.P., Brook, B.W., Gardner, T.A., Barlow, J. et al., 2011. Primary forests are irreplaceable for sustaining tropical biodiversity. *Nature*, 478, pp.378–383.

Gini, R., Sona, G., Ronchetti, G., Passoni, D. and Pinto, L., 2018. Improving tree species classification using UAS multispectral images and texture measures. *ISPRS International Journal of Geo-Information*, 7, p.315.

Gitelson, A.A., Viña, A., Ciganda, V., Rundquist, D.C. and Arkebauer, T.J., 2005. Remote estimation of canopy chlorophyll content in crops. *Geophysical Research Letters*, 32, p.L08403.

Gómez-Gutiérrez, Á., Sánchez-Fernández, M., de Sanjosé-Blasco, J.J., Gudino-Elizondo, N. and Lavado-Contador, F., 2024. Is it possible to generate accurate 3D point clouds with UAS-LIDAR and UAS-RGB photogrammetry without GCPs? A case study on a beach and rocky cliff. *Landscape Ecology*, 39, p.191.

Gomez, D.F., Ritger, H.M., Pearce, C., Eickwort, J. and Hulcr, J., 2020. Ability of remote sensing systems to detect bark beetle spots in the southeastern US. *Forests*, 11(11), p.1167.

Goutte, C. and Gaussier, E., 2005. A probabilistic interpretation of precision, recall and F-score, with implication for evaluation. In: *European Conference on Information Retrieval*, Springer, Berlin/Heidelberg, Germany, pp.345–359.

Gouveia, C.M., Trigo, R.M., Beguería, S. and Vicente-Serrano, S.M., 2017. Drought impacts on vegetation activity in the Mediterranean region: An assessment using remote sensing data and multi-scale drought indicators. *Global and Planetary Change*, 151, pp.15–27. https://doi.org/10.1016/j.gloplacha.2016.06.011

Grabska, E., Hawryło, P. and Socha, J., 2020. Continuous detection of small-scale changes in Scots pine dominated stands using dense Sentinel-2 time series. *Remote Sensing*, 12(8), p.1298.

Grillakis, M.G., 2019. Increase in severe and extreme soil moisture droughts for Europe under climate change. *Science of The Total Environment*, 660, pp.1245–1255. https://doi.org/10.1016/j.scitotenv.2019.01.001

Grybas, H. and Congalton, R.G., 2021. A comparison of multi-temporal RGB and multispectral UAS imagery for tree species classification in heterogeneous New Hampshire Forests. *Remote Sensing*, 13, p.2631.

Guimarães, N., Pádua, L., Marques, P., Silva, N., Peres, E. and Sousa, J.J., 2020. Forestry remote sensing from unmanned aerial vehicles: A review focusing on the data, processing and potentialities. *Remote Sensing*, 12, p.1046.

Guo, Q., Zhang, J., Guo, S., Ye, Z., Deng, H., Hou, X. and Zhang, H., 2022. Urban tree classification based on object-oriented approach and random forest algorithm using unmanned aerial vehicle (UAV) multispectral imagery. *Remote Sensing*, 14, p.3885.

Hardenbol, A.A., Korhonen, L., Kukkonen, M. and Maltamo, M., 2023. Detection of standing retention trees in boreal forests with airborne laser scanning point clouds and multispectral imagery. *Methods in Ecology and Evolution*, 14, pp.1610–1622.

Hastings, J.H., Ollinger, S.V., Ouimette, A.P., Sanders-DeMott, R., Palace, M.W., Ducey, M.J., Sullivan, F.B., Basler, D. and Orwig, D.A., 2020. Tree species traits determine the success of LiDAR-based crown mapping in a mixed temperate forest. *Remote Sensing*, 12, p.309.

Hille Ris Lambers, J., Clark, J. and Beckage, B., 2002. Density-dependent mortality and the latitudinal gradient in species diversity. *Nature*, 417, pp.732–735.

Hislop, S., Stone, C., Gibson, R.K., Roff, A., Choat, B., Nolan, R.H. and Carnegie, A.J., 2023. Using dense Sentinel-2 time series to explore combined fire and drought impacts in eucalypt forests. *Frontiers in Forests and Global Change*, 6, p.1018936.

Hu, Q., Yang, J., Xu, B., Huang, J., Memon, M.S., Yin, G. and Liu, K., 2020. Evaluation of global decametric-resolution LAI, FAPAR and FVC estimates derived from Sentinel-2 imagery. *Remote Sensing*, 12(6), p.912. https://doi.org/10.3390/rs12060912

Huang, H., Li, X. and Chen, C., 2018. Individual tree crown detection and delineation from very-high-resolution UAV images based on bias field and marker-controlled watershed segmentation algorithms. *IEEE Journal of Selected Topics in Applied Earth Observations and Remote Sensing*, 11, pp.2253–2262.

Huber, S., Tagesson, T. and Fensholt, R., 2014. An automated field spectrometer system for studying VIS, NIR and SWIR anisotropy for semi-arid savanna. *Remote Sensing of Environment*, 152, pp.547–556. https://doi.org/10.1016/j.rse.2014.06.007

Huete, A.R., 2012. Vegetation indices, remote sensing and forest monitoring. *Geography Compass*, 6(9), pp.513–532.

IPCC, 2023. Climate Change 2023: Synthesis Report. Contribution of Working Groups I, II and III to the Sixth Assessment Report of the Intergovernmental Panel on Climate Change [Core Writing Team, H. Lee and J. Romero (eds.)]. *IPCC*, Geneva, Switzerland, pp.35–115. https://doi.org/10.59327/IPCC/AR6-9789291691647

Jamali, S., Olsson, P.O., Müller, M. and Ghorbanian, A., 2024. Kernel-based early detection of forest bark beetle attack using vegetation indices time series of Sentinel-2. *IEEE Journal of Selected Topics in Applied Earth Observations and Remote Sensing*.

Jbilou, J. and El Adlouni, S., 2012. Generalized additive models in environmental health: a literature review. *Novel Approaches and Their Applications in Risk Assessment*, 120, pp.2014–2016.

Jiang, Z., Zhu, L., Wang, Q. and Hou, X., 2020. Autophagy-related 2 regulates chlorophyll degradation under abiotic stress conditions in Arabidopsis. *International Journal of Molecular Sciences*, 21(12), p.4515.

Jönsson, P., Cai, Z., Melaas, E., Friedl, M.A. and Eklundh, L., 2018. A method for robust estimation of vegetation seasonality from Landsat and Sentinel-2 time series data. *Remote Sensing*, 10, p.635. https://doi.org/10.3390/rs10040635

Karolos, I.A., Bellos, K., Alexandridisale, V., Chrysafis, I., Georgiadis, H., Pikridas, C. and Mallinis, G., 2024. Advancing forest biodiversity conservation with the EL-BIOS digital twin: An integration of LiDAR and multispectral earth observation data. In: *Proceedings of the Tenth International Conference on Remote Sensing and Geoinformation of the Environment (RSCy2024)*, SPIE, Paphos, Cyprus, 8–9 April 2024, Volume 13212, pp.361–375.

Kannenberg, S.A., Schwalm, C.R. and Anderegg, W.R.L., 2020. Ghosts of the past: how drought legacy effects shape forest functioning and carbon cycling. *Ecology Letters*, 23(5), pp.891–901. https://doi.org/10.1111/ele.13485

Karger, D.N., Conrad, O., Böhner, J., Kawohl, T., Kreft, H., Soria-Auza, R.W., Zimmermann, N.E., Linder, H.P. and Kessler, M., 2017. Climatologies at high resolution for the earth's land surface areas. *Scientific Data*, 4, p.170122. https://doi.org/10.1038/sdata.2017.122

Karger, D.N., Conrad, O., Böhner, J., Kawohl, T., Kreft, H., Soria-Auza, R.W., Zimmermann, N.E., Linder, H.P. and Kessler, M., 2021. Climatologies at high resolution for the earth's land surface areas. *EnviDat*. https://doi.org/10.16904/envidat.228.v2.1

Karger, D.N., Dabaghchian, B., Lange, S., Thuiller, W., Zimmermann, N.E. and Graham, C.H., 2020. High resolution climate data for Europe. *EnviDat*, 1.0. https://doi.org/10.16904/envidat.150

Kelley, M.C. and Tucker, B.V., 2022. Using acoustic distance and acoustic absement to quantify lexical competition. *The Journal of the Acoustical Society of America*, 151(2), pp.1367–1379.

König, S., Thonfeld, F., Förster, M., Dubovyk, O. and Heurich, M., 2023. Assessing combinations of Landsat, Sentinel-2 and Sentinel-1 time series for detecting bark beetle infestations. *GIScience & Remote Sensing*, 60(1), p.2226515.

Kopacková-Strnadová, V., Koucká, L., Jelének, J., Lhotáková, Z. and Oulehle, F., 2021. Canopy top, height and photosynthetic pigment estimation using parrot sequoia multispectral imagery and the unmanned aerial vehicle (UAV). *Remote Sensing*, 13, p.705.

Krieger, D.J., 2001. *Economic value of forest ecosystem services: A review*. The Wilderness Society, Washington, DC, USA..

Lange, M., Preidl, S., Reichmuth, A., Heurich, M. and Doktor, D., 2024. A continuous tree species-specific reflectance anomaly index reveals declining forest condition between 2016 and 2022 in Germany. *Remote Sensing of Environment*, 312, p.114323.

Lastovicka, J., Svec, P., Paluba, D., Kobliuk, N., Svoboda, J., Hladky, R. and Stych, P., 2020. Sentinel-2 data in an evaluation of the impact of the disturbances on forest vegetation. *Remote Sensing*, 12(12), p.1914.

Lausch, A., Erasmi, S., King, D.J., Magdon, P. and Heurich, M., 2016. Understanding forest health with remote sensing—part I: a review of spectral traits, processes and remote-sensing characteristics. *Remote Sensing*, 8(12), p.1029.

Lausch, A., Heurich, M., Gordalla, D., Dobner, H.J., Gwillym-Margianto, S. and Salbach, C., 2013. Forecasting potential bark beetle outbreaks based on spruce forest vitality using hyperspectral remote-sensing techniques at different scales. *Forest Ecology and Management*, 308, pp.76–89. https://doi.org/10.1016/j.foreco.2013.07.043

Le, T.S., Harper, R. and Dell, B., 2023. Application of remote sensing in detecting and monitoring water stress in forests. *Remote Sensing*, 15(13), p.3360. https://doi.org/10.3390/rs15133360

Lévesque, M., Rigling, A., Bugmann, H., Weber, P. and Brang, P., 2014. Growth response of five co-occurring conifers to drought across a wide climatic gradient in Central Europe. *Agricultural and Forest Meteorology*, 197, pp.1–12.

Li, B., Zhou, W., Zhao, Y., Ju, Q., Yu, Z., Liang, Z. and Acharya, K., 2015. Using the SPEI to assess recent climate change in the Yarlung Zangbo River Basin, South Tibet. *Water (Switzerland)*, 7(10), pp.5474–5486. https://doi.org/10.3390/W7105474

Lichtenthaler, H.K. and Buschmann, C., 2001. Chlorophylls and carotenoids measurement and UV-VIS characterization by UV-VIS spectroscopy. *Current Protocols in Food Analytical Chemistry*, 3, pp.1–8.

Linares, J.C. and Tíscar, P.A., 2010. Climate change impacts and vulnerability of the southern populations of *Pinus nigra* subsp. *salzmannii*. *Tree Physiology*, 30(7), pp.795–806. https://doi.org/10.1093/treephys/tpq052

Lisein, J., Michez, A., Claessens, H. and Lejeune, P., 2015. Discrimination of deciduous tree species from time series of unmanned aerial system imagery. *PLoS ONE*, 10, p.e0141006.

Lisiewicz, M., Kamińska, A., Kraszewski, B. and Steren´czak, K., 2022. Correcting the results of CHM-based individual tree detection algorithms to improve their accuracy and reliability. *Remote Sensing*, 14, p.1822.

Liu, M., Liu, J., Atzberger, C., Jiang, Y., Ma, M. and Wang, X., 2021. *Zanthoxylum bungeanum Maxim* mapping with multi-temporal Sentinel-2 images: The importance of different features and consistency of results. *ISPRS Journal of Photogrammetry and Remote Sensing*, 174, pp.68–86.

Liaw, A. and Wiener, M., 2002. Classification and regression by randomForest. *R News*, 2, pp.18–22.

Lawrence, R.L., Wood, S.D. and Sheley, R.L., 2006. Mapping invasive plants using hyperspectral imagery and Breiman Cutler classifications (randomForest). *Remote Sensing of Environment*, 100, pp.356–362.

Löw, M. and Koukal, T., 2020. Phenology modelling and forest disturbance mapping with Sentinel-2 time series in Austria. *Remote Sensing*, 12(24), p.4191.

Ma, H., Cui, T. and Cao, L., 2023. Monitoring of drought stress in Chinese forests based on satellite solar-induced chlorophyll fluorescence and multi-source remote sensing indices. *Remote Sensing*, 15(4), p.879. https://doi.org/10.3390/rs15040879

Ma, K., Chen, Z., Fu, L., Tian, W., Jiang, F., Yi, J., Du, Z. and Sun, H., 2022. Performance and sensitivity of individual tree segmentation methods for UAV-LiDAR in multiple forest types. *Remote Sensing*, 14, p.298.

Ma, M., Liu, J., Liu, M., Zeng, J. and Li, Y., 2021. Tree species classification based on Sentinel-2 imagery and random forest classifier in the eastern regions of the Qilian Mountains. *Forests*, 12, p.1736.

Mandl, L. and Lang, S., 2023. Uncovering early traces of bark beetle induced forest stress via semantically enriched Sentinel-2 data and spectral indices. *PFG–Journal of Photogrammetry, Remote Sensing and Geoinformation Science*, 91(3), pp.211–231.

Mantas, V., Fonseca, L., Baltazar, E., Canhoto, J. and Abrantes, I., 2022. Detection of tree decline (*Pinus pinaster* Aiton) in European forests using Sentinel-2 data. *Remote Sensing*, 14(9), p.2028.

Marini, F., Battipaglia, G., Manetti, M.C., Corona, P. and Romagnoli, M., 2019. Impact of climate, stand growth parameters, and management on isotopic composition of tree rings in chestnut coppices. *Forests*, 10(12), p.1148. https://doi.org/10.3390/f10121148

Marusig, D., Petruzzellis, F., Tomasella, M., Napolitano, R., Altobelli, A. and Nardini, A., 2020. Correlation of field-measured and remotely sensed plant water status as a tool to monitor the risk of drought-induced forest decline. *Forests*, 11(1), p.77. https://doi.org/10.3390/f11010077

McDowell, N., Pockman, W.T., Allen, C.D., Breshears, D.D., Cobb, N., Kolb, T. and Yepez, E.A., 2008. Mechanisms of plant survival and mortality during drought: why do some plants survive while others succumb to drought?. *New Phytologist*, 178(4), pp.719–739.

Meier, I.C. and Leuschner, C., 2008. Leaf size and leaf area index in *Fagus sylvatica* forests: Competing effects of precipitation, temperature, and nitrogen availability. *Ecosystems*, 11, pp.655–669.

Meinzer, F.C., Johnson, D.M., Lachenbruch, B., McCulloh, K.A. and Woodruff, D.R., 2009. Xylem hydraulic safety margins in woody plants: coordination of stomatal control of xylem tension with hydraulic capacitance. *Functional Ecology*, 23(5), pp.922–930.

Meinzer, F.C., Smith, D.D., Woodruff, D.R., Marias, D.E., McCulloh, K.A., Howard, A.R. and Magedman, A.L., 2017. Stomatal kinetics and photosynthetic gas exchange along a continuum of isohydric to anisohydric regulation of plant water status. *Plant, Cell & Environment*, 40(8), pp.1618–1628.

Meroni, M., et al., 2021. Comparing land surface phenology of major European crops as derived from SAR and multispectral data of Sentinel-1 and -2. *Remote Sensing of Environment*, 253, p.112232.

Meyer, F. and Beucher, S., 1990. Morphological segmentation. *Journal of Visual Communication and Image Representation*, 1, pp.21–46.

Mielcarek, M., Sterenczak, K. and Khosravipour, A., 2018. Testing and evaluating different LiDAR-derived canopy height model generation methods for tree height estimation. *International Journal of Applied Earth Observation and Geoinformation*, 71, pp.132–143.

Miraglio, T., Adeline, K., Huesca, M., Ustin, S. and Briottet, X., 2020. Joint use of PROSAIL and DART for fast LUT building: Application to gap fraction and leaf biochemistry estimations over sparse oak stands. *Remote Sensing*, 12, p.2925.

Miraki, M., Sohrabi, H. and Fatehi, P., 2021. Individual tree crown delineation from high-resolution UAV images in broadleaf forest. *Ecological Informatics*, 61, p.101207.

Mishra, N.B., Mainali, K.P., Shrestha, B.B., Radenz, J. and Karki, D., 2018. Species-level vegetation mapping in a Himalayan treeline ecotone using unmanned aerial system (UAS) imagery. *ISPRS International Journal of Geo-Information*, 7, p.445.

Mohan, M., Leite, R., Broadbent, E., Wan Mohd Jaafar, W., Srinivasan, S., Bajaj, S., Dalla Corte, A., do Amaral, C., Gopan, G. and Saad, S., 2021. Individual tree detection using UAV-LiDAR and UAV-SfM data: A tutorial for beginners. *Open Geosciences*, 13, pp.1028–1039.

Müller, M., Olsson, P.O., Eklundh, L., Jamali, S. and Ardö, J., 2024. Response and resilience to drought in northern forests revealed by Sentinel-2. *International Journal of Remote Sensing*, 45(15), pp.5130–5157.

Myneni, R.B., Ramakrishna, R., Nemani, R. and Running, S.W., 1997. Estimation of global leaf area index and absorbed PAR using radiative transfer models. *IEEE Transactions on Geoscience and Remote Sensing*, 35, pp.1380–1393.

Narmilan, A., Gonzalez, F., Salgadoe, A.S.A., Kumarasiri, U.W.L.M., Weerasinghe, H.A.S. and Kulasekara, B.R., 2022. Predicting canopy chlorophyll content in sugarcane crops using machine learning algorithms and spectral vegetation indices derived from UAV multispectral imagery. *Remote Sensing*, 14, p.1140.

Navarro, A., Catalao, J. and Calvao, J., 2019. Assessing the use of Sentinel-2 time series data for monitoring Cork Oak decline in Portugal. *Remote Sensing*, 11(21), p.2515.

Nguyen, D. and Leung, B., 2022. How well do species distribution models predict occurrences in exotic ranges?. *Global Ecology and Biogeography*, 31(6), pp.1051–1065. https://doi.org/10.1111/geb.13482

Nocerino, E., Dubbini, M., Menna, F., Remondino, F., Gattelli, M. and Covi, D., 2017. Geometric calibration and radiometric correction of the maia multispectral camera. *International Archives of the Photogrammetry, Remote Sensing and Spatial Information Sciences*, 42, pp.149–156.

Panigada, C., Rossini, M., Busetto, L., Meroni, M., Fava, F. and Colombo, R., 2010. Chlorophyll concentration mapping with MIVIS data to assess crown discoloration in the Ticino Park oak forest. *International Journal of Remote Sensing*, 31(12), pp.3307–3332.

Pignatti, S., Menegoni, P. and Pietrosanti, S., 2005. Biondicazione attraverso le piante vascolari. Valori di indicazione secondo Ellenberg (Zeigerwerte) per le specie della Flora d'Italia. *Braun-Blanquetia*, 39, pp.1–97.

Pinto-Ledezma, J.N., Frantz, D., Townsend, P.A., Juzwik, J. and Cavender-Bares, J., 2023. Mapping oak wilt disease from space using land surface phenology. *Remote Sensing of Environment*, 298, p.113794.

Plowright, A., 2018. *R Package 'ForestTools'*. Available online: https://github.com/andrew-plowright/ForestTools (accessed on 31 January 2023).

Pollastrini, M., Puletti, N., Selvi, F., Iacopetti, G. and Bussotti, F., 2019. Widespread crown defoliation after a drought and heat wave in the forests of Tuscany (central Italy) and their recovery—A case study from summer 2017. *Frontiers in Forests and Global Change*, 2, p.74.

Pontius, J., Schaberg, P. and Hanavan, R., 2020. Remote sensing for early, detailed, and accurate detection of forest disturbance and decline for protection of biodiversity. In: Cavender-Bares, J., Gamon, J.A. and Townsend, P.A. (eds.), *Remote Sensing of Plant Biodiversity*. Springer, pp.121–154.

Popescu, S.C. and Wynne, R.H., 2013. Seeing the trees in the forest. *Photogrammetric Engineering and Remote Sensing*, 70, pp.589–604.

Puchałka, R., Paź-Dyderska, S., Jagodziński, A.M., Sádlo, J., Vítková, M., Klisz, M. and Dyderski, M.K., 2023. Predicted range shifts of alien tree species in Europe. *Agricultural and Forest Meteorology*, 341, p.109650.

Puchałka, R., Dyderski, M.K., Vítková, M., Sádlo, J., Klisz, M., Netsvetov, M. and Jagodziński, A.M., 2021. Black locust (*Robinia pseudoacacia* L.) range contraction and expansion in Europe under changing climate. *Global Change Biology*, 27, pp.1587–1600.

Puletti, N., Mattioli, W., Bussotti, F. and Pollastrini, M., 2019. Monitoring the effects of extreme drought events on forest health by Sentinel-2 imagery. *Journal of Applied Remote Sensing*, 13(2), pp.020501–020501.

Qi, J., Xie, D., Guo, D. and Yan, G., 2017. A large-scale emulation system for realistic three-dimensional (3-D) forest simulation. *IEEE Journal of Selected Topics in Applied Earth Observations and Remote Sensing*, 10, pp.4834–4843.

Quang, A.V., Delbart, N., Jaffrain, G., Pinet, C. and Moiret, A., 2022. Detection of degraded forests in Guinea, West Africa, based on Sentinel-2 time series by inclusion of moisture-related spectral indices and neighbourhood effect. *Remote Sensing of Environment*, 281, p.113230.

Ranghetti, L., Boschetti, M., Nutini, F. and Busetto, L., 2020. "sen2r": An R toolbox for automatically downloading and preprocessing Sentinel-2 satellite data. *Computers and Geosciences*, 139. https://doi.org/10.1016/j.cageo.2020.104473

Ranghetti, L., Nutini, F., Cillis, D. and Boschetti, M., 2021. A reproducible workflow to derive crop phenology and agro-practice information from Sentinel-2 time series: A case study for Sardinia cropping systems. *Planet Care from Space, AIT Series: Trends in Earth Observation*, 2, pp.133–136. https://doi.org/10.978.88944687/00

Raza, S.A., Zhang, L., Zuo, J. and Chen, B., 2024. Time series monitoring and analysis of Pakistan's mangrove using Sentinel-2 data. *Frontiers in Environmental Science*, 12, p.1416450.

Reinosch, E., Backa, J., Adler, P., Deutscher, J., Eisnecker, P., Hoffmann, K. and Oehmichen, K., 2024. Detailed validation of large-scale Sentinel-2-based forest disturbance maps across Germany. *Forestry: An International Journal of Forest Research*, cpae038.

Regione Lombardia, 2024. Geoportale Regione Lombardia. Accessed 5 Aug. 2024, https://www.geoportale.regione.lombardia.it/ricerca

Rodman, K.C., Andrus, R.A., Veblen, T.T. and Hart, S.J., 2021. Disturbance detection in Landsat time series is influenced by tree mortality agent and severity, not by prior disturbance. *Remote Sensing of Environment*, 254, p.112244. https://doi.org/10.1016/j.rse.2020.112244

Rodríguez-González, P.M., Albuquerque, A., Martínez-Almarza, M. and Díaz-Delgado, R., 2017. Long-term monitoring for conservation management: Lessons from a case study integrating remote sensing and field approaches in floodplain forests. *Journal of Environmental Management*, 202, pp.392–402

Rogers, B.M., Solvik, K., Hogg, E.H., Ju, J., Masek, J.G., Michaelian, M. and Goetz, S.J., 2018. Detecting early warning signals of tree mortality in boreal North America using multiscale satellite data. *Global Change Biology*, 24, pp.2284–2304

Rosner, S., Gierlinger, N., Klepsch, M., Karlsson, B., Evans, R., Lundqvist, S.O., Světlík, J., Børja, I., Dalsgaard, L., Andreassen, K. and Solberg, S., 2018. Hydraulic and mechanical dysfunction of Norway spruce sapwood due to extreme summer drought in Scandinavia. *Forest Ecology and Management*, 409, pp.527–540

Rossini, M., Panigada, C., Meroni, M. and Colombo, R., 2006. Assessment of oak forest condition based on leaf biochemical variables and chlorophyll fluorescence. *Tree Physiology*, 26(11), pp.1487–1496

Rossini, M., Panigada, C., Meroni, M., Busetto, L., Castrovinci, R. and Colombo, R., 2007. Monitoraggio delle condizioni della farnia (*Quercus robur* L.) nel Parco del Ticino mediante tecniche di telerilevamento iperspettrale. *For. J. Silvic. For. Ecol.*, 4, p.194

Rossini, M., Garzonio, R., Panigada, C., Tagliabue, G., Bramati, G., Vezzoli, G., Cogliati, S., Colombo, R. and Di Mauro, B., 2023. Mapping surface features of an Alpine glacier through multispectral and thermal drone surveys. *Remote Sensing*, 15, p.3429

Roussel, J.R., Auty, D., Coops, N.C., Tompalski, P., Goodbody, T.R.H., Meador, A.S., Bourdon, J.F., de Boissieu, F. and Achim, A., 2020. lidR: An R package for analysis of Airborne Laser Scanning (ALS) data. *Remote Sensing of Environment*, 251, p.112061

Savinelli, B., Panigada, C., Tagliabue, G., Vignali, L., Gentili, R., Fassnacht, F.E. and Rossini, M., 2024. Monitoring functional traits of complex temperate forests using Sentinel-2 data during a severe drought period. *Science of the Total Environment*, 957, p.177428.

Schiller, C., Költzow, J., Schwarz, S., Schiefer, F. and Fassnacht, F.E., 2024. Forest disturbance detection in Central Europe using transformers and Sentinel-2 time series. *Remote Sensing of Environment*, 315, p.114475.

Schuldt, B., Buras, A., Arend, M., Vitasse, Y., Beierkuhnlein, C., Damm, A., Gharun, M., Grams, T.E., Hauck, M., Hajek, P. and Hartmann, H., 2020. A first assessment of the impact of the extreme 2018 summer drought on Central European forests. *Basic and Applied Ecology*, 45, pp.86–103.

Seidl, R., Thom, D., Kautz, M., Martin-Benito, D., Peltoniemi, M., Vacchiano, G. and Reyer, C.P., 2017. Forest disturbances under climate change. *Nature Climate Change*, 7, pp.395–402.

Shahbazi, M., Théau, J. and Ménard, P., 2014. Recent applications of unmanned aerial imagery in natural resource management. *GIScience and Remote Sensing*, 51, pp.339–365.

Silva, C.A., Crookston, N.L., Hudak, A.T., Vierling, L.A., Klauberg, C. and Silva, M.C.A., 2017. Package 'rLiDAR'. *The CRAN Project*. Available online: https://github.com/carlos-alberto-silva/rLiDAR

Singhal, G., Bansod, B., Mathew, L., Goswami, J., Choudhury, B.U. and Raju, P.L.N., 2019. Chlorophyll estimation using multi-spectral unmanned aerial system based on machine learning techniques. *Remote Sensing Applications: Society and Environment*, 15, p.100235.

Singh, P., Srivastava, P.K., Verrelst, J., Mall, R.K., Rivera, J.P., Dugesar, V. and Prasad, R., 2023. High-resolution retrieval of leaf chlorophyll content over Himalayan pine forest using Visible/IR sensors mounted on UAV and radiative transfer model. *Ecological Informatics*, 75, p.102099.

Sivanandam, P. and Lucieer, A., 2022. Tree detection and species classification in a mixed species forest using unoccupied aircraft system (UAS) RGB and multispectral imagery. *Remote Sensing*, 14, p.4963.

Smith, G.M. and Milton, E.J., 1999. The use of the empirical line method to calibrate remotely sensed data to reflectance. *International Journal of Remote Sensing*, 20, pp.2653–2662.

Sokolova, M., Japkowicz, N. and Szpakowicz, S., 2006. Beyond accuracy, F-score and ROC: A family of discriminant measures for performance evaluation. In: *Australasian Joint Conference on Artificial Intelligence*, Springer, Berlin/Heidelberg, Germany, pp.1015–1021.

Sterenczak, K., 2013. Factors influencing individual tree crowns detection based on airborne laser scanning data. *Forest Research Papers*, 74, pp.323–333.

Story, M. and Congalton, R.G., 1986. Accuracy assessment: A user's perspective. *Photogrammetric Engineering and Remote Sensing*, 52, pp.397–399.

Štroner, M., Urban, R. and Línková, L., 2021. A new method for UAV LiDAR precision testing used for the evaluation of an affordable DJI ZENMUSE L1 scanner. *Remote Sensing*, 13, p.4811.

Tagliabue, G., Boschetti, M., Bramati, G., Candiani, G., Colombo, R., Nutini, F., Pompilio, L., Rivera-Caicedo, J.P., Rossi, M., Rossini, M. and Panigada, C., 2022. Hybrid retrieval of crop traits from multi-temporal PRISMA hyperspectral imagery. *ISPRS Journal of Photogrammetry and Remote Sensing*, 187, pp.362–377. https://doi.org/10.1016/j.isprsjprs.2022.03.014

Tagliabue, G., Panigada, C., Savinelli, B., Vignali, L., Gallia, L., Gentili, R. and Rossini, M., 2023. Exploitation of PRISMA spaceborne hyperspectral observations for improved functional trait retrievals in mid-latitude forest ecosystems. In: *IGARSS 2023-2023 IEEE International Geoscience and Remote Sensing Symposium*, pp.1261–1264.

Taiwo, A.F., Daramola, O., Sow, M. and Semwal, V.K., 2020. Ecophysiology and responses of plants under drought. In: Plant Ecophysiology and Adaptation under Climate Change: Mechanisms and Perspectives I: General Consequences and Plant Responses, pp.231–268.

Tanhuanpää, T., Saarinen, N., Kankare, V., Nurminen, K., Vastaranta, M., Honkavaara, E. and Hyyppä, J., 2016. Evaluating the performance of high-altitude aerial image-based digital surface models in detecting individual tree crowns in mature boreal forests. *Forests*, 7, p.143.

Tang, L. and Shao, G., 2015. Drone remote sensing for forestry research and practices. *Journal of Forestry Research*, 26, pp.791–797.

Teskey, R., Wertin, T., Bauweraerts, I., Ameye, M., McGuire, M.A. and Steppe, K., 2015. Responses of tree species to heat waves and extreme heat events. *Plant, Cell & Environment*, 38(9), pp.1699–1712.

Tichý, L., Axmanová, I., Dengler, J., Guarino, R., Jansen, F. and Midolo, G., 2023. Ellenberg-type indicator values for European vascular plant species. *Journal of Vegetation Science*, 34, p.e13168. https://doi.org/10.1111/jvs.13168

Toivonen, J., Kangas, A., Maltamo, M., Kukkonen, M. and Packalen, P., 2023. Assessing biodiversity using forest structure indicators based on airborne laser scanning data. *Forest Ecology and Management*, 546, p.121376.

Tomíček, J., Mišurec, J. and Lukeš, P., 2021. Prototyping a generic algorithm for crop parameter retrieval across the season using radiative transfer model inversion and Sentinel-2 satellite observations. *Remote Sensing*, 13(18), p.3659.

Torresan, C., Berton, A., Carotenuto, F., Di Gennaro, S.F., Gioli, B., Matese, A., Miglietta, F., Vagnoli, C., Zaldei, A. and Wallace, L., 2017. Forestry applications of UAVs in Europe: A review. *International Journal of Remote Sensing*, 38, pp.2427–2447.

Trumbore, S., Brando, P. and Hartmann, H., 2015. Forest health and global change. *Science*, 349(6250), pp.814–818.

van Leeuwen, M. and Nieuwenhuis, M., 2010. Retrieval of forest structural parameters using LiDAR remote sensing. *European Journal of Forest Research*, 129, pp.749–770.

Verrelst, J., Rivera, J.P., Alonso, L. and Moreno, J., 2011. ARTMO: An Automated Radiative Transfer Models Operator toolbox for automated retrieval of biophysical parameters through model inversion. In: *Proceedings of the EARSeL 7th SIG-Imaging Spectroscopy Workshop*, Edinburgh, UK, 11–13 April 2011, pp.11–13.

Vicente-Serrano, S.M., Beguería, S. and López-Moreno, J.I., 2010. A multiscalar drought index sensitive to global warming: the standardized precipitation evapotranspiration index. *Journal of Climate*, 23(7), pp.1696–1718.

Vitasse, Y., Bottero, A., Cailleret, M., Bigler, C., Fonti, P., Gessler, A. et al., 2019. Contrasting resistance and resilience to extreme drought and late spring frost in five major European tree species. *Global Change Biology*, 25, pp.3781–3792. https://doi.org/10.1111/gcb.14803

Volaire, F., 2018. A unified framework of plant adaptive strategies to drought: crossing scales and disciplines. *Global Change Biology*, 24, pp.2929–2938. https://doi.org/10.1111/gcb.14062

Vauhkonen, J., Ene, L., Gupta, S., Heinzel, J., Holmgren, J., Pitkänen, J. and Maltamo, M., 2012. Comparative testing of single-tree detection algorithms under different types of forest. *Forestry*, 85, pp.27–40.

Wallace, L., Lucieer, A., Malenovský, Z., Turner, D. and Vopˇenka, P., 2016. Assessment of forest structure using two UAV techniques: A comparison of airborne laser scanning and structure from motion (SfM) point clouds. *Forests*, 7, p.62.

Wan, L., Ryu, Y., Dechant, B., Lee, J., Zhong, Z. and Feng, H., 2024. Improving retrieval of leaf chlorophyll content from Sentinel-2 and Landsat-7/8 imagery by correcting for canopy structural effects. *Remote Sensing of Environment*, 304, p.114048.

Wang, L., Chang, Q., Li, F., Yan, L., Huang, Y. and Wang, Q., 2019. Effects of growth stage development on paddy rice leaf area index prediction models. *Remote Sensing*, 11(3), p.361. https://doi.org/10.3390/rs11030361

Wang, R. and Gamon, J.A., 2019. Remote sensing of terrestrial plant biodiversity. *Remote Sensing of Environment*, 231, p.111218.

Wang, Z., Féret, J.B., Liu, N., Sun, Z., Yang, L., Geng, S. and Townsend, P.A., 2023. Generality of leaf spectroscopic models for predicting key foliar functional traits across continents: A comparison between physically- and empirically-based approaches. *Remote Sensing of Environment*, 293, p.113614.

Weiss, M. and Baret, F., 2016. S2ToolBox Level 2 Products: LAI, FAPAR, FCOVER. Avignon: *Institut National de la Recherche Agronomique (INRA)*.

Weiss, M., Baret, F., Smith, G.J., Jonckheere, I. and Coppin, P., 2004. Review of methods for in situ leaf area index (LAI) determination Part II. Estimation of LAI, errors and sampling. *Agricultural and Forest Meteorology*, 121, pp.37–53.

Wood, S.N., 2011. Fast stable restricted maximum likelihood and marginal likelihood estimation of semiparametric generalized linear models: Estimation of semiparametric generalized linear models. *Journal of the Royal Statistical Society: Series B (Statistical Methodology)*, 73(1), pp.3–36. https://doi.org/10.1111/j.1467-9868.2010.00749.x

Xie, Q., Dash, J., Huete, A., Jiang, A., Yin, G., Ding, Y., Peng, D., Hall, C.C., Brown, L., Shi, Y. and Ye, H., 2019. Retrieval of crop biophysical parameters from Sentinel-2 remote sensing imagery. *International Journal of Applied Earth Observation and Geoinformation*, 80, pp.187–195.

Xu, Z., Shen, X., Cao, L., Coops, N.C., Goodbody, T.R., Zhong, T. and Wu, X., 2020. Tree species classification using UAS-based digital aerial photogrammetry point clouds and multispectral imageries in

subtropical natural forests. *International Journal of Applied Earth Observation and Geoinformation*, 92, p.102173.

Yang, Q., Su, Y., Jin, S., Kelly, M., Hu, T., Ma, Q. and Guo, Q., 2019. The influence of vegetation characteristics on individual tree segmentation methods with airborne LiDAR data. *Remote Sensing*, 11, p.2880.

Zaforemska, A., Xiao, W. and Gaulton, R., 2019. Individual tree detection from UAV LiDAR data in a mixed species woodland. *International Archives of the Photogrammetry, Remote Sensing and Spatial Information Sciences*, 42, pp.657–663.

Zhang, C., Chen, Z., Yang, G., Xu, B., Feng, H., Chen, R. and Yang, H., 2024. Removal of canopy shadows improved retrieval accuracy of individual apple tree crowns LAI and chlorophyll content using UAV multispectral imagery and PROSAIL model. *Computers and Electronics in Agriculture*, 221, p.108959.

Zhang, K., Chen, S.C., Whitman, D., Shyu, M.L., Yan, J. and Zhang, C., 2003. A progressive morphological filter for removing nonground measurements from airborne LiDAR data. *IEEE Transactions on Geoscience and Remote Sensing*, 41, pp.872–882.

Zhen, Z., Quackenbush, L.J. and Zhang, L., 2016. Trends in automatic individual tree crown detection and delineation—Evolution of LiDAR data. *Remote Sensing*, 8, p.333.

Zhu, J., Lu, J., Li, W., Wang, Y., Jiang, J., Cheng, T. and Yao, X., 2023. Estimation of canopy water content for wheat through combining radiative transfer model and machine learning. *Field Crops Research*, 302, p.109077.

La borsa di dottorato cofinanziata con risorse del
Programma Operativo Nazionale Ricerca e Innovazione 2014-2020 (CCI 2014IT16M2OP005),
risorse Fondo Sociale Europeo REACT-EU, Azione I.1 “Dottorati Innovativi con caratterizzazione industriale”, Azione IV.4 “Dottorati e contratti di ricerca su tematiche dell’innovazione” e Azione IV.5 “Dottorati su tematiche Green”